TECHNISCHE UNIVERSITÄT MÜNCHEN

Lehrstuhl für Bodenökologie

Modellierung des Wasserumsatzes verschiedener Baumarten in gemischten Beständen

Sebastian Bittner

Vollständiger Abdruck der von der Fakultät Wissenschaftszentrum Weihenstephan für Ernährung, Landnutzung und Umwelt der Technischen Universität München zur Erlangung des akademischen Grades eines Doktors der Naturwissenschaften genehmigten Dissertation.

Vorsitzender: Univ.-Prof. Dr. R. Matyssek
Prüfer der Dissertation:
1. Univ.-Prof. Dr. Dr. J. Ch. Munch
2. Priv.-Doz. Dr. E. Priesack (Georg-August-Universität Göttingen)
3. Univ.-Prof. Dr. F. Beese (i.R.) (Georg-August-Universität Göttingen)

Die Dissertation wurde am 05.12.2011 bei der Technischen Universität München eingereicht und durch die Fakultät Wissenschaftszentrum Weihenstephan für Ernährung, Landnutzung und Umwelt am   17.04.2012 angenommen.

Inhaltsverzeichnis

Zusammenfassung

Die vorliegende Arbeit entstand im Rahmen des DFG Graduiertenkollegs 1086 "Die Bedeutung der Biodiversität für Stoffkreisläufe und biotische Interaktionen in temperaten Laubwäldern". Es war das Ziel der Arbeit, den Wasserkreislauf von Mischwäldern mittels Computermodellen zu simulieren. Eigene Messungen und Messungen von anderen Teilprojekten des Graduiertenkollegs ermöglichten eine genaue Kalibrierung und Tests der verwendeten Ökosystemmodelle. Neben der Anwendung der Modelle und der Integration einzelner Ergebnisse vorheriger Untersuchungen des Wasserumsatzes des Untersuchungsgebietes, war die Weiterentwicklung von Funktion-Strukur-Einzelbaummodellen der Schwerpunkt dieser Arbeit. Die Beobachtungen der Einzelbaummodelle können auf den Bestand hochgerechnet werden und somit einen Beitrag zum Verständnis der Auswirkung der Baumartendiversität auf den Wasserkreislauf im Bestand liefern.

In der Modellierung von Ökosystemen können zwei Modellklassen unterschieden werden: Bestandesmodelle und Einzelbaummodelle. Bestandesmodelle wurden erfolgreich an vielen Standorten und für verschiedene Waldtypen eingesetzt. In dieser Arbeit werden Bestandesmodelle des Bodenwasserflusses (eindimensionaler Fluss nach der Richardsgleichung), der Wurzelwasseraufnahme (Feddesmodell), der Evapotranspiration (Penman-Monteith) und der Niederschlagsinterzeption (Gashmodell) auf Mischbestände erweitert und eingesetzt. Der Schwerpunkt der Bestandessimulationen der Beobachtungsperiode von 2005-2007 war die unterschiedliche Reaktion der Baumarten *Fagus sylvatica* L.*, Tilia cordata* Mill. und *Fraxinus excelsior L.* auf trockene Bodenwasserverhältnisse.

Der Großteil dieser Arbeit behandelt die Weiterentwicklung eines Funktion-Struktur-Modells des Wasserflusses innerhalb einzelner Bäume. Hierbei erforderte sowohl die Beschreibung der Baumstruktur als auch die Beschreibung der dem Wasserfluss zugrundeliegenden Prozesse die Entwicklung einer geeigneten Datenverarbeitung und eine Optimierung der Rechenzeit. Das Modell berechnet den Wasserfluss zwischen den

Feinwurzeln und den Ästen im wasserleitenden Xylem. Die Geometrie und Konnektivität der Baumkompartimente wird in einer hohen räumlichen Auflösung abgebildet. Die Zustandsvariablen des Modells beinhalten den Wassergehalt, das Wasserpotential und den Wasserfluss der einzelnen wasserleitenden Elemente. Die Bestimmung der räumlichen Position der Elemente der Baumkrone wurde durch den Einsatz eines terrestrischen Laserscanners ermöglicht. Die Aufnahmen des Laserscanners wurden mittels eines weiterentwickelten Skelettierungsalgorithmus in Modelleingangsdaten formatiert.

Die gleichzeitige Einbeziehung der Struktur und der hydrologischen Eigenschaften der Einzelbäume ermöglichte eine hohe zeitliche und räumliche Auflösung der Wasserflusssimulationen. Das Einzelbaummodell konnte den täglichen Verlauf und die Tageswerte des Stammsaftflusses abbilden. Messungen des Stammsaftflusses dienten hierbei der Überprüfung der modellierten Werte. Durch den Modellansatz können auch Wechselwirkungen zwischen einzelnen Bäumen verschiedener Arten abgebildet werden, da das Modell sowohl die gegenseitige Beschattung der Bäume als auch die Wurzelausbreitung berücksichtigt. Die hydrologischen Prozesse des Wasserflusses im Boden und in der Pflanze werden vorwiegend durch mechanistische Modelle beschrieben, wodurch die Anwendung des Modells auf andere Standorte und auf andere Baum- und Pflanzenarten ermöglicht wird.

Die Anwendung der Modelle auf den Standort Hainich konnte Biodiversitätseffekte, die in vorhergehenden Arbeiten aufgedeckt wurden, überprüfen und quantifizieren und darüber hinaus Einblicke in die Auswirkung der Biodiversität auf den Wasserumsatz geben. Die Ergebnisse des Bestandesmodells zeigen, dass sich die baumartenspezifische Reaktion auf trockene Bodenbedingungen am Standort Hainich in Trockenperioden stark auf die Bestandestranspiration und die Bodenwasserschöpfung auswirken können. Die Ergebnisse der Einzelbaummodellierung konnten zudem Unterschiede zwischen den Baumarten in der täglichen Transpiration auch an Tagen mit optimalen Bodenwasserbedingungen aufzeigen. Die simulierten Unterschiede sind hier eine Folge aus dem Zusammenspiel der Baumstruktur und der Baumphysiologie.

2

Summary

This study was conducted within the framework of the DFG research training group 1086 'The role of biodiversity for biogeochemical cycles and biotic interactions in temperate deciduous forests'. The aim of the study was to simulate the soil-plant-atmosphere water exchange of mixed forests. Using the database of the umbrella research project made a solid calibration and test of ecological computer models possible. In addition to the application of the model and the synthesis and quantification of the results of observations at the study site, the main goal of this study was to further develop individual based, functional-structural models of tree water usage. The approach of individual based, functional-structural models makes the analysis of biodiversity effects possible, when the information that is gained on single tree-level is scaled up to the entire mixed stand.

Two kinds of model types were used to describe the water cycle of the soil-plant-atmosphere system: stand-level models and single tree models. Stand-level models have been applied to a lot of sites and forest types in ecological modeling. This study contains the application of stand-level models of the soil water flow (one-dimensional soil water flow described by Richards equation), root water uptake (Feddes model), evapotranspiration (Penman-Monteith), and rainfall interception (revised Gash model) to mixed stands. The focus of the stand-level simulations of the observation period from the years 2005 to 2007 was the different reaction of the tree species *Fagus sylvatica* L., *Tilia cordata* Mill., and *Fraxinus excelsior* L. to dry soil water conditions.

A large part of this thesis is about the application and further development of a individual based functional-structural model to describe the water flow inside single trees. Both the structural side of the modeling and the functional side required the development of new data processing algorithms and an optimization of their requirements of the computational resources. The model could calculate the water flow from the roots to the fine branches along the hydraulic pathway given by the

architecture of the tree. The geometry and connectivity of the water conducting xylem was described at a high detail in the model and the model status variables contain information on the water potential and the water content of the conduit elements as well as on the flux between the elements. Here, the use of a terrestrial laser scanner made a detailed model description of the canopy architecture possible. An automatic tree skeleton algorithm to convert the laser scanner data into model input data was further developed and applied to single trees of the old-growth Hainich forest.

The combination of the structural information obtained by the terrestrial laser scans and the information on the hydraulic functional traits made a calculation of the water flow within single trees at high spatial and temporal resolution possible. The single tree model could reflect the diurnal and daily values of stem sap flux, that was additionally measured at the observation trees. The use of a canopy light regime model further exploited the information of the canopy structure and led to a high accordance of the simulated sap flux values with the measured values. The model approach enables the analysis of the interaction of single trees by including the shading and the space occupation of the roots. The model is described by physical processes of water flow, which allows the application on other stands and on other tree species.

The test of the models with a database of the Hainich study site could give insights into biodiversity effects in mixed forests and could quantify biodiversity effects that have been observed in preceding studies of the umbrella research project. The stand-level approach model results state, that the different reaction of the tree species to dry soil water condition can have an impact on the transpiration rates and the soil water exhaustion of the entire stand at periods of low volumetric soil water contents. The individual tree approach could further show differences between the species in the daily transpiration rates at days with optimal soil water conditions as a result of the interaction of physiological hydraulic traits and the geometrical structure of the trees.

1 Einleitung

1.1 Wasserkreislauf in Wäldern

Wälder haben einen wichtigen Einfluss auf viele hydrologische Ökosystemfunktionen, wie z.B. den Rückhalt von Regen- und Tauwasser, die Speicherung von Wasser und die Grundwasserneubildung [FAO, 2005, van Dijk and Keenan, 2007, Calder, 2007]. Die zweite Bundeswaldinventur [BMELV, 2004] gibt für Deutschland einen Waldanteil der Landoberfläche von 31,1% an, wovon wiederum 40,1% auf Laubbäume entfallen. Buchenreinbestände und Buchen in Mischbeständen bilden das Untersuchungsgebiet dieser Arbeit und haben in Deutschland einen Anteil von 14,8%. Aufgrund einer erwarteten höheren Anpassungsfähigkeit auf veränderte Umweltbedingungen [Pretzsch, 2005, Knoke et al., 2008] wird auf geeigneten Flächen die Ausweitung des Laubwaldanteils und insbesondere des Mischwaldanteils angestrebt [BMELV, 2004]. Es ist davon auszugehen, dass die Bedeutung von Laubbäumen in Mischbeständen in Deutschland in den nächsten Jahren zunehmen wird.

Die Wasserbilanz des Boden-Wald-Systems kann modellhaft durch Einzelprozesse beschrieben werden, die sich in Wassereingang und -ausgang, Pflanze-Boden Wasseraustausch und den Wasserfluss innerhalb der Bodens und innerhalb der Pflanze einteilen lassen. Das Boden-Wald-System erhält Wasser aus der Atmosphäre in Form von Freilandniederschlag, wobei ein Teil des Freilandniederschlags nach Kontakt mit der Baumkrone evaporiert (Niederschlagsinterzeption), und nicht zum Bodenwassereintrag beiträgt. Das Boden-Wald-System gibt Wasser durch Evapotranspiration wieder an die Atmosphäre ab. Da sich die Beschreibung des System räumlich beschränkt, führen lateraler Bodenoberflächenwasserabfluss und Versickerung aus dem betrachtetem Bodenprofil zu einem simulierten Wasseraustrag. Die Vegetation nimmt Bodenwasser über die Wurzeln auf und Wasser erreicht die Bodenoberfläche nach Kontakt mit der Vegetation als Stammabfluss und als Kronentraufe. Zudem werden Wasserflüsse innerhalb der Pflanzen und in den Bodenschichten beschrieben. An den meisten dieser modellhaften Teilprozesse ist die Vegetation direkt beteiligt. Neben dem Alter des Bestandes und der Waldstruktur beeinflusst hierbei auch die Artenzusammensetzung des Waldes den Wasserkreislauf maßgeblich, da sich die Baumarten stark in ihren hydrologischen Eigenschaften unterscheiden können.

1.1.1 Einfluss der Baumartendiversität auf den Wasserkreislauf

Vergleichende Studien kommen zu dem Ergebnis, dass die Baumartzusammensetzung gemischter Bestände die hydrologische Ökosystemfunktionen stark beeinflussen kann [FAO, 2005, Calder, 2007, van Dijk and Keenan, 2007]. Aber es ist festzustellen, dass die zugrundeliegenden Mechanismen nicht ausreichend bekannt sind. Von 31 aktuellen vergleichenden Studien, die die Auswirkung der Anzahl der Baumarten eines Standorts, im Folgenden als Baumartendiversität oder Biodiversität bezeichnet, untersuchen und in einem Übersichtsartikel von Nadrowski et al. [2010] zusammengestellt werden, behandelt nur eine einzige Arbeit die Auswirkungen auf den Wasserkreislauf [Krämer and Hölscher, 2009]. Während über die hydrologischen Eigenschaften einzelner Baumarten meist eine Vielzahl wissenschaftlicher Literatur zu finden ist, rückte die Untersuchung der Auswirkung der Baumartendiversität auf den Wasserkreislauf des Bestandes erst in den letzten Jahren verstärkt in das Blickfeld der Forstwissenschaft, wobei es bisher weiterhin wenige quantifizierende Studien gibt [Scherer-Lorenzen and Schulze, 2005, Scherer-Lorenzen et al., 2007, Leuschner et al., 2009, Nadrowski et al., 2010, Thompson et al., 2009]. Die meisten Untersuchungen zu Biodiversitätseffekten wurden in Graslandsystemen durchgeführt, da Forstsysteme schwer manipulierbar sind und längere Beobachtungszeiträume benötigen. Diese Arbeit ist Teil des Graduiertenkollegs 1086 "Die Bedeutung der Biodiversität für Stoffkreisläufe und biotische Interaktionen in temperaten Laubwäldern", das seit dem Jahr 2005 die Biodiversitätseffekte am Standort Hainich in Thüringen untersucht [Leuschner et al., 2009].

Die Konkurrenz um verfügbare Bodenressourcen und das Sonnenlicht kann zu einer Adaption der Einzelbaumstruktur [Gayler et al., 2008] und somit zu weiteren möglichen Biodiversitätseffekten führen, die sich sowohl positiv als auch negativ auf die Ökosystemfunktionen auswirken können. So wurde am Forschungsstandort Hainich eine effektivere Kronenraumbesetzung von Mischbeständen gegenüber Reinbeständen beobachtet [Frech et al., 2003, Seidel, 2011]. Der Wasserkreislauf wird durch die Kronenstruktur direkt durch die Interzeption und den Stammabfluss beeinflusst, Unterschiede von Misch- und Reinbeständen können hierbei am Standort Hainich auf den Anteil der Buche am Bestand zurückgeführt werden. So steigt der jährliche Bestandesstammabfluss mit dem Buchenanteil an und die Interzeption mit dem Buchenanteil ab, wobei die Menge des infiltrierten Bodenwassers sich nicht zwischen den Beständen unterscheidet [Krämer and Hölscher, 2009]. Die Transpirationsraten der

Blätter reagieren sensibel auf die Intensität des eingehenden Tageslichts und hängen über die räumliche gegenseitige Beschattung der Bäume auch von der Kronenstrukur ab. Hierbei wurde eine komplementäre Nutzung und eine höhere Interzeption des eingehenden Lichts durch Mischbestände beobachtet [Kelty, 1992]. Aufgrund der nichtlinearen Abhängigkeit der Transpiration vom eingehenden Licht, insbesondere aufgrund der beobachteten Sättigung der Transpiration bei hoher Lichtintensität, führt eine effizientere Lichtauslöschung in der Baumkrone aber nicht notwendig auch zu einer höheren Bestandestranspiration. Es gibt auch Hinweise darauf, dass eine starke Einzelbaumkonkurrenz die stomatäre Wasserleitfähigkeit und damit die Transpiration verringern kann [Loranty et al., 2010].

Auch im Wurzelraum sind komplementäre Raumerschließung und -nutzung in Mischbeständen von Buchen und anderen Arten belegt [Buttner and Leuschner, 1994, Rothe and Binkley, 2001, Schmid and Kazda, 2002]. Besonders für den Wurzelraum sind diese Ergebnisse aber nicht allgemein gültig, da das Durchwurzelungsverhalten der Bäume stark standortabhängig ist. So konnte am Forschungsstandort Hainich keine komplementäre Bodentiefennutzung der Feinwurzeln verschiedener Arten beobachtet werden und Mischbestände unterschieden sich in der Feinwurzelbiomasse nicht von Buchenreinbeständen [Meinen et al., 2009]. Eine Adaption der Wurzelausbreitung von Einzelbäumen an Nachbarschaftsverhältnisse konnte im Nationalpark Hainich nicht beobachtet werden. Dies kann ein Effekt der besonderen Bodenverhältnisse mit einer flachen Wurzelzone sein. Aber nicht nur über die Struktur, sondern auch über die hydraulische Eigenschaften können sich Baumarten in der Bodenwasseraufnahme unterscheiden und durch den Wettbewerb um verfügbares Bodenwasser interagieren. So wurde am Standort Hainich beobachtet, das sich die Baumarten in der Reduktion der Bodenwasseraufnahme während Trockenperioden unterscheiden [Hölscher et al., 2005, Köcher et al., 2009].

1.2 Modellierung des Wasserkreislaufs in Mischwäldern

Das Forschungsziel dieser Arbeit besteht darin, basierend auf den Beobachtungen am Standort Hainich, Biodiversitätseffekte in Mischwäldern aufgrund der unterschiedlichen Eigenschaften der Baumarten, sowie aufgrund von Einzelbaumwechselwirkungen im Computermodell abzubilden und zu analysieren. Die vorhandenen Informationen

zum Standort Hainich (siehe Kapitel Abschnitt 1.3) ermöglichen eine zuverlässige Parametrisierung der Modelle. Zugleich sollen Sensitivitäts- und Unsicherheitsanalysen die gefundenen Ergebnisse generalisieren und die Übertragung auf andere Standorte und Baumarten ermöglichen.

Messungen und Beobachtung in Mischwäldern beschränken sich meist auf einen Aspekt des Wasserkreislaufs oder einer hydraulischen Baumeigenschaft. Die Integration der einzelnen Beobachtungen zu einem Gesamtmodell der Wassernutzung ist ein wichtiger Beitrag, den die Computermodellierung zum Verständnis der Boden-Pflanze-Atmosphäre leisten kann. Hierbei ist auf die hohe Komplexität und Nichtlinearität der Wasserbilanzgleichungen hinzuweisen, die aus der Rückkopplung einzelner Teilprozesse des Wasserkreislaufs resultieren und eine Quantifizierung der Biodiversitätseffekte durch beobachtende und empirische Studien erschweren.

Modelle des Stoffumsatzes von Wäldern lassen sich in Bestandesmodelle und Einzelbaummodelle unterteilen [Porté and Bartelink, 2002]. Bestandesmodelle unterscheiden nicht zwischen einzelnen Individuen eines Bestandes, die Eingangsparameter und Ausgabevariablen beziehen sich auf den Bestand. Durch eine artenanteilsgewichtete Summe der Eigenschaftsparameter aller Baumarten, die einen Mischbestand bilden, kann hier in erster Näherung ein Mischbestand abgebildet werden. Auch Wechselwirkungsprozesse können prinzipiell in den Parametern der Bestandesmodelle berücksichtigt werden. Dies geschieht in der Regel durch die Verwendung von Messdaten aus geeigneten Mischwäldern und schränkt hierdurch eine genaue und generalisierte Modellierung ein, da Informationen oft nicht vorhanden sind und sich die Messungen meist auf die natürlichen Baumartenmischungen beschränken müssen.

Einzelbaummodelle haben ein hohes Potential, die Interaktion benachbarter Bäume abzubilden [Gayler et al., 2008]. Hierbei sind v.a. Funktion-Strukur-Modelle zu nennen, die die räumliche Struktur der Bäume beinhalten. Der Wettbewerb nach Licht, Wasser und Nährstoffen ist zum Großteil ein Wettbewerb um unter- und oberirdische Raumnutzung. Somit bietet eine detaillierte Beschreibung der Geometrie der Äste und Wurzeln ein hohes Potential, generelle Wechselwirkungen zwischen Einzelbäumen zu analysieren.

Nadrowski et al. [2010] empfehlen die Hochskalierung der Beobachtungen auf Einzelbaumebene auf den Gesamtbestand als einen vielversprechenden Ansatz der Biodiversitätsforschung. Die in dieser Arbeit verwendeten Einzelbaummodelle verfolgen diesen Ansatz, indem die modellierten Wasserflüsse der einzelnen Bäume auf

den Wasserkreislauf des Boden-Pflanze-Atmosphäre Systems hochskaliert werden. Die Ergebnisse der Kapitel 3 und 4 zeigen auch, dass eine Beschreibung auf Einzelbaumebene zudem zum Erkenntnisgewinn über die hydraulischen Eigenschaften der Baumarten beitragen kann, was für die Beschreibung von Biodiversitätseffekten grundlegend ist.

1.3 Untersuchungsgebiet - Nationalpark Hainich

Der Nationalpark Hainich in Thüringen ist der größte zusammenhängende Laubwald in Deutschland. Seit den 1960er Jahren war der Wald militärisches Sperrgebiet, und im Jahr 1997 erhielt der Hainich den Nationalparkstatus. Als Folge dessen ist der Wald in einem naturnahen Zustand, da die Bewirtschaftung in den letzten Jahrzenten minimal war [Schmidt et al., 2009]. Das Untersuchungsgebiet ist seit mindestens 200 Jahren ein Laubwald. Da in der älteren Vergangenheit verschiedene Gebiete des Waldes unterschiedlich bewirtschaftet wurden, finden sich heute neben Buchenreinbeständen auch Gebiete im Hainich, die von anderen Baumarten oder Baumartenmischungen dominiert werden [Schmidt et al., 2009].

Das Untergrundgestein im Nationalpark Hainich ist Muschelkaltk, das von einer Lößschicht unterschiedlicher Mächtigkeit bedeckt wird. Der Bodentyp (Luvisol, FAO, 1998) führt zu Stauwasser im Frühling und im Herbst, im Sommer trocknet der Boden schnell aus. Das langjährige Mittel des Freilandniederschlags der nahegelegenen Wetterstation in Weberstedt ist $590\,mm$ (1973-2004, Deutscher Wetterdienst).

1.4 Forschungsansatz und Kapitelübersicht

Die vorliegende Arbeit wurde von der DFG finanziell gefördert und ist ein Teilprojekt des Graduiertenkollegs 1086 "Die Bedeutung der Biodiversität für Stoffkreisläufe und biotische Interaktionen in temperaten Laubwäldern". Seit dem Jahr 2005 untersuchen die beteiligten Wissenschaftler die Rolle der Baumartendiversität anhand von unterschiedlich diversen Beständen im Nationalpark Hainich.

1.4.1 Flächenansatz

Im Flächenansatz der ersten Phase des Forschungsprojekt vom Jahr 2005 bis 2008 wurden zwölf natürliche quadratische Waldflächen mit der Seitenlänge von $50\,m$ ausgewählt. Die zwölf Flächen unterteilen sich in drei Diversitätsstufen (DL1, DL2, DL3). DL1 Flächen werden von Rotbuchen *(Fagus sylvatica* L.) dominiert, DL2 Flächen bestehen hauptsächlich aus Bäumen der Arten *F. sylvatica,* Linde (*Tilia cordata* Mill. und *T. platyphyloos* Scop.) und Esche (*Fraxinus excelsior* L.) und DL3 Flächen werden von den Baumarten Buche, Linde, Esche, Hainbuche (*Carpinus betulus* L.) und Ahorn (*Acer pseudoplatanus* L. und *Acer platanoides* L.) dominiert. Die Messungen des Wasserumsatzes der Flächen beinhalteten Messungen des Stammsaftflusses [Gebauer, 2010], des volumetrischen Bodenwassergehalts [Krämer and Hölscher, 2010], des Bestandesniederschlags und des Stammabflusses [Krämer and Hölscher, 2009]. Die Auswahl zufälliger Punktmesspositionen auf den Flächen ermöglichte eine Ausmittelung kleinräumiger Variabilität und gewährleistete den Vergleich zwischen den Diversitätsstufen.

In Kapitel 2 dieser Arbeit werden die Messungen des Flächenansatzes verwendet, um ein eindimensionales Boden-Pflanze-Atmosphäre Bestandesmodel zu kalibrieren und zu testen. Einzelgrößen der Wasserbilanz, wie die Interzeption, Bestandestranspiration und Evapotranspiration, sowie die zeitliche Dynamik des volumetrischen Bodenwassergehalts konnten erfolgreich reproduziert werden. Die einzelnen Teilprozesse des Wasserkreislaufs wurden in Teilmodellen berechnet und mit dem Modellpaket *Expert-N* [Engel and Priesack, 1993, Stenger et al., 1999, Priesack et al., 2001, Priesack and Bauer, 2003, Priesack, 2003] gekoppelt. Die Bodenwasserdynamik wird mittels eines eindimensionalen Bodenschichtmodells beschrieben und der Wasserfluss zwischen den Schichten wird durch die Lösung der Richards-Gleichung für den Wasserfluss in porösen Medien nach einem Ansatz des *HYDRUS* Modells bestimmt [Šimunek et al., 1998]. Die Retentionskurven des Bodenwassers werden durch die Parametrisierung nach van Genuchten [1980] beschrieben. Die Niederschlagsinterzeption wird mit dem Gashmodell [Gash et al., 1995] berechnet. Die potentielle Evapotranspiration wird mit der Grasreferenzverdunstungsmethode nach Penman-Monteith berechnet [Allen et al., 1998], und die Aufteilung in potentielle Bodenevaporation und Baumtranspiration erfolgt über den Bodenbedeckungsgrad der Flächen [Droogers, 2000]. In einem weiteren Teilmodell wird die Wurzelwasseraufnahme durch das Wasserstressmodell nach Feddes [Feddes et al., 1978] beschrieben.

Diese genaue Kalibrierung und Tests des Bodenwassermodells und des Interzeptionsmodells sind wichtige Grundlagen für die Kapitel 3 und 4. In diesen Kapiteln wird auf die Parametrisierung der Bodeneigenschaften wie der Interzeption zurückgegriffen, aber andere Einzelmodelle der Transpiration und der Wurzelwasseraufnahme verwendet. Der Forschungsschwerpunkt der Simulationen auf Bestandesebene in Kapitel 2 ist es, das Verhalten von Mischwäldern in Trockenperioden zu untersuchen. Ausgeprägte Trockenperioden werden im Hainich im Sommer beobachtet und die Reaktion der Untersuchungsbaumarten wurde in den letzten Jahren ausführlich untersucht und konnte im Modell abgebildet werden. Es wird insbesondere auf den Unterschied zwischen trockenheitstoleranten Baumarten, wie der Esche, und der trockenheitsintoleranten Buche eingegangen.

1.4.2 Clusteransatz

Der Clusteransatz der zweiten Phase des Forschungsprojekts vom Jahr 2008 bis 2011 analysiert die Ursachen von Biodiversitätseffekten. Hierfür wurden 100 Baumgruppen (Diversitätscluster) ausgewählt, die jeweils aus drei dominanten Bäumen bestehen, die sich in der Kronenschicht in direkter Nachbarschaft befinden und ein Dreieck bilden. Durch die Auswahl von Clustern, die nur aus Bäumen einer der Untersuchungsbaumarten bestehen, sowie aus Clustern, die aus drei Bäumen verschiedener Art bestehen, konnten Biodiversitätseffekte auf einer kleineren räumlichen Skala untersucht werden.

In den Kapiteln 3 und 4 werden die Wasserflüsse einzelner Clusterbäume simuliert. Der Ansatz ist hierbei, den Wasserfluss in den Wurzeln, dem Stamm und den Ästen detailliert zu beschreiben. Die Berücksichtigung der dreidimensionalen Struktur soll die Möglichkeiten des Modells erweitern, Interaktionen zwischen Einzelbäumen abzubilden. Auch die Parametrisierung der Einzelbaummodelle unterscheidet sich wesentlich von dem Bestandesmodell, da baumartenspezifische hydraulische Parameter des Xylems, der Blattspaltöffnungen und der Wurzeln im Modell verwendet werden. Kooperationen mit anderen Teilprojekten des Graduiertenkollegs ermöglichen hierbei eine genaue Parametrisierung der Modelle durch die Verwendung von *in situ* Messungen der Observablen der Baumarten.

Die Baumkronen der Untersuchungsbäume wurden mit einem terrestrischen Laserscanner aufgenommen. Diese Methode der optischen Vermessung resultiert in einer räumlich hoch aufgelösten Menge dreidimensionaler Punkte, die sich auf der

Oberfläche der Vegetation befinden. In den letzten Jahren wird die Methode des terrestrischen Laserscanners vermehrt in der Forstwissenschaft eingesetzt, hauptsächlich um strukturelle Bestandeseigenschaften zu ermitteln [van Leeuwen and Nieuwenhuis, 2010]. Eine Herausforderung des Einsatzes des terrestrischen Laserscanners in Funktion-Strukur-Modellen ist die Aufbereitung der Messdaten zu verwendbaren Modelleingangsdaten. Das Einzelbaummodell der Kapitel 3 und 4 beschreibt die Kronenarchitektur geometrisch als verbundene Einzelzylinder, deren Position aus den Laserscannerpunktwolken erst ausgelesen werden muss. Hierzu wurde ein Algorithmus zur Extraktion des Baumskeletts aus Punktwolken [Xu et al., 2007] weiterentwickelt und optimiert und erstmals in einem Funktion-Strukur-Modell eingesetzt.

Aufgrund des Nationalparkstatus des Untersuchungsgebiets war es nicht möglich, das Wurzelsystem von Untersuchungsbäumen freizulegen und zu vermessen. Die Simulation der Wurzelarchitektur konnte aber auf eine baumartenspezifisch gemessene radiale und vertikale Feinwurzelverteilung und eine Abschätzung der Feinwurzeloberfläche zurückgreifen [Meinen, 2008].

Zusätzlich wurden 15 Untersuchungsbäume (5 Buchen, 5 Eschen, 5 Linden) mit Granier-Saftflusssensoren bestückt, und das Modell an diesen Messdaten erfolgreich getestet. Die Kombination der detaillierten Struktur und der hydraulischen Eigenschaften der Baumarten in Kapitel 3 kann Unterschiede zwischen Ringporern (Esche) und Diffusporern (Buche, Linde) in der Transpirationsdynamik und in der Wasseraufnahme aufzeigen.

Kapitel 4 koppelt die Ansätze der Kapitel 2 und 3 mit einem geometrisch explizitem Lichtmodell, um die Interaktion der Einzelbäume durch gegenseitige Beschattung zu ermöglichen. Auch das Lichtmodell greift auf die Aufnahmen des Laserscanners zurück, der für das Lichtmodell zusätzliche Parametrisierungsaufwand ist gering.

1.4.3 Künstlicher Bestand junger Buchen im Gewächshaus

Das in Kapitel 4 vorgestellte Lichtmodell verwendet die Aufnahmen von Laserscannern, um eine hoch aufgelöste Einhüllende der Baumkrone zu erzeugen. Blätter und Äste werden durch Würfel (Voxel) dargestellt, die sich in ihrer Lichtdurchlässigkeit unterscheiden. Das eingehende Tageslicht wird bei Durchtritt durch die Voxel in seiner Intensität abgeschwächt und die Beschattung des Bestandes kann somit geometrisch explizit berechnet werden. Der Ansatz, eingehendes Licht mit einem Voxelabsorpti-

onsmodell zu verbinden, wurde erfolgreich in der Ökosystemmodellierung angewandt [Kimes, 1984, Cohen and Fuchs, 1987, Gastellu-Etchegorry et al., 2004, Van der Zande et al., 2009]. Wenige Arbeiten geben aber eine Fehleranalyse des Modells an, insbesondere in der Kombination mit Laserscanneraufnahmen.

Ansatz des Kapitels 5 ist es, das laserscannergenerierte Voxelmodell zu testen, sowie eine Parametersensitivitätsanalyse durchzuführen. Ein künstlicher Bestand junger Buchen wurde in einem Gewächshaus mit einem Laserscanner vermessen. Die Buchen wurden beleuchtet und die Intensitätsverteilung des photosynthetisch aktiven Lichts an der Bodenoberfläche sowie in der Krone gemessen. Das Voxelmodell wurde an diesen Messdaten unter einem wohlbekanntem Lichtregime getestet und konnte die Lichtverteilung abbilden. Des weiteren wurden Erfahrungen für die Parametrisierung und die Anwendung des Modells im Bestand (Kapitel 4) gesammelt.

Folgende in begutachteten Fachzeitschriften eingereichte, zum Einreichen vorbereitete und veröffentlichte Manuskripte sind in der vorliegenden Arbeit enthalten:

Kapitel 2 S. Bittner, U. Talkner, I. Krämer, F. Beese, D. Hölscher, E. Priesack. Modeling stand water budgets of mixed temperate broad-leaved forest stands by considering variation in species specific drought response. Agricultural and Forest Meteorology 150: 1347-1357

Kapitel 3 S. Bittner, M. Janott, D. Ritter, P. Köcher, F. Beese, E. Priesack. Using terrestrial laser scanner data for a functional-structural water flow model of three broad-leaved tree species.

Kapitel 4 S. Bittner, N. Legner, F. Beese, E. Priesack. Simulating the interaction between the canopy light regime and the hydraulic architecture of single *F. sylvatica* trees.

Kapitel 5 S. Bittner, S. Gayler, C. Biernath, J. B. Winkler, S. Seifert, E. Priesack. The perfomance of a voxel-based canopy light model based on terrestrial laser scans.

S. Bittner hat als Erstautor alle Manuskripte erstellt, die zugrundeliegenden Simulationen durchgeführt und statistisch ausgewertet, Modellentwicklung geleistet, die Messdaten aufbereitet, die Saftflussmessungen in Kapitel 3 und 4 und die Laserscanneraufnahmen in Kapitel 5 durchgeführt. Die Modellentwicklung umfasste hierbei die Implementierung des Gashmodells für Mischbestände, des Feddesmodells auf Einzelereignisbasis, die Berechnung der potentiellen Transpiration nach Penman-Monteith mit stündlichen Zeitschritten, die Erweiterung des Einzelbaumwasserflussmodells auf adulte Bäume, die Implementierung des Lösers des Gleichungssystem des Wasserflusses zwischen den leitenden Elementen nach Ross [2003], die Optimierung des Computerressourcenverbrauchs des Einzelbaumwasserflussmodells, sowie die Entwicklung der Algorithmen zur Aufbereitung der Laserscannerdaten. Der Skelettierungsalgorithmus der Laserscannerdaten wurde in Kooperation mit dem Lehrstuhl für Systemsimulation der Universität Erlangen-Nürnberg weiterentwickelt.

Literaturverzeichnis

R.G. Allen, L.S. Pereira, D. Raes, M. Smith, et al. Crop evapotranspiration-guidelines for computing crop water requirements-fao irrigation and drainage paper 56. *Irrigation and Drainage Paper No. 56. FAO, Rome, Italy*, 300, 1998.

BMELV, Bundesministerium für Ernährung, Landwirtschaft und Verbraucherschutz. 2. Bundeswaldinventur. www.bundeswaldinventur.de. 2004.

V. Buttner and C. Leuschner. Spatial and temporal patterns of fine root abundance in a mixed oak-beech forest. *Forest ecology and management*, 70(1-3):11–21, 1994.

I.R. Calder. Forests and water–Ensuring forest benefits outweigh water costs. *Forest Ecology and Management*, 251(1-2):110–120, 2007.

S. Cohen and M. Fuchs. The distribution of leaf area, radiation, photosynthesis and transpiration in a Shamouti orange hedgerow orchard. Part I. Leaf area and radiation. *Agricultural and Forest Meteorology*, 40(2):123–144, 1987.

P. Droogers. Estimating actual evapotranspiration using a detailed agro-hydrological model. *Journal of Hydrology*, 229(1-2):50–58, 2000.

T. Engel and E. Priesack. Expert-N, A building block system of nitrogen models as a resource for advice, research, water management and policy. In *Integrated soil and sediment research: A basis for proper protection*, pages 503–507. Kluwer Academic Publishers, Dodrecht, The Netherlands, 1993.

FAO. ISRIC, ISSS World Reference Base for Soil Resources. *World Soil Resources Reports*, 84, 1998.

FAO. Global forest resources assessment 2005. *FAO Forestry Paper*, 147, 2005.

R.A. Feddes, PJ Kowalik, and H. Zaradny. *Simulation of field water use and crop yield.* Pudoc, Wageningen, 1978.

A. Frech, C. Leuschner, M. Hagemeier, and D. Hölscher. Nachbarschaftsbezogene Analyse der Kronenraumbesetzung von Esche, Hainbuche und Winterlinde in einem artenreichen Laubmischwald (Nationalpark Hainich, Thüringen). *Forstwissenschaftliches Centralblatt*, 122(1):22–35, 2003.

JHC Gash, CR Lloyd, and G. Lachaud. Estimating sparse forest rainfall interception with an analytical model. *Journal of Hydrology*, 170(1-4):79–86, 1995.

JP Gastellu-Etchegorry, E. Martin, and F. Gascon. DART: a 3D model for simulating satellite images and studying surface radiation budget. *International Journal of Remote Sensing*, 25(2):73, 2004.

S. Gayler, T. E. Grams, W. Heller, D. Treutter, and E. Priesack. A dynamical model of environmental effects on allocation to carbon-based secondary compounds in juvenile trees. *Annals of Botany*, 101(8):1089, 2008.

T. Gebauer. *Water turnover in species-rich and species-poor deciduous forests: Xylem sap flow and canopy transpiration.* PhD thesis, Georg-August-Universität Göttingen, Göttingen, 2010.

D. Hölscher, O. Koch, S. Korn, and C. Leuschner. Sap flux of five co-occurring tree species in a temperate broad-leaved forest during seasonal soil drought. *Trees-Structure and Function*, 19(6):628–637, 2005.

M.-J. Kelty. Comparative productivity of monocultures and mixed-species stands. In *The Ecology and silviculture of mixed-species forests*, page 287. Kluwer Academic Publishing, Dordrecht, The Netherlands, 1992.

DS Kimes. Modeling the directional reflectance from complete homogeneous vegetation canopies with various leaf-orientation distributions. *Journal of the Optical Society of America A*, 1(7):725–737, 1984.

T. Knoke, C. Ammer, B. Stimm, and R. Mosandl. Admixing broadleaved to coniferous tree species: a review on yield, ecological stability and economics. *European Journal of Forest Research*, 127(2):89–101, 2008.

P. Köcher, T. Gebauer, V. Horna, and C. Leuschner. Leaf water status and stem xylem flux in relation to soil drought in five temperate broad-leaved tree species with contrasting water use strategies. *Annals of Forest Science*, 66(1):101–101, 2009.

I. Krämer and D. Hölscher. Rainfall partitioning along a tree diversity gradient in a deciduous old-growth forest in central germany. *Ecohydrology*, 2(1):102–114, 2009.

I. Krämer and D. Hölscher. Soil water dynamics along a tree diversity gradient in a deciduous forest in central germany. *Ecohydrology*, 3(3):262–271, 2010.

C. Leuschner, H.F. Jungkunst, and S. Fleck. Functional role of forest diversity: pros and cons of synthetic stands and across-site comparisons in established forests. *Basic and Applied Ecology*, 10(1):1–9, 2009.

M.M. Loranty, D.S. Mackay, B.E. Ewers, E. Traver, and E.L. Kruger. Competition for light between individual trees lowers reference canopy stomatal conductance: Results from a model. *Journal of Geophysical Research*, 115(G4):G04019, 2010.

C. Meinen. *Fine root dynamics in broad-leaved deciduous forest stands differing in tree species diversity.* PhD thesis, Georg-August-Universität Göttingen, Göttingen, 2008.

C. Meinen, C. Leuschner, N.T. Ryan, and D. Hertel. No evidence of spatial root system segregation and elevated fine root biomass in multi-species temperate broad-leaved forests. *Trees-Structure and Function*, 23(5):941–950, 2009.

K. Nadrowski, C. Wirth, and M. Scherer-Lorenzen. Is forest diversity driving ecosystem function and service? *Current Opinion in Environmental Sustainability*, 2(1-2):75–79, 2010.

A. Porté and HH Bartelink. Modelling mixed forest growth: a review of models for forest management. *Ecological Modelling*, 150(1-2):141–188, 2002.

H. Pretzsch. Diversity and productivity in forests: evidence from long-term experimental plots. *Forest diversity and function*, pages 41–64, 2005.

E Priesack. *FAM-Bericht 60. Expert-N Dokumentation der Modellbibliothek.* Forschungsverbung Agrarökosysteme München, 2003.

E. Priesack and C. Bauer. *FAM-Bericht 59. Expert-N Datenmanagement.* Forschungsverbung Agrarökosysteme München, 2003.

E. Priesack, S. Achatz, and R. Stenger. Parameterization of soil nitrogen transport models by use of laboratory and field data. In *Modeling carbon and nitrogen dynamics for soil management Lewis publishers*, pages 461–484. CRC Press, Boca Raton USA, 2001.

P. J. Ross. Modeling soil water and solute transport - fast, simplified numerical solutions. *Agronomy Journal*, 95:1352–1361, 2003.

A. Rothe and D. Binkley. Nutritional interactions in mixed species forests: a synthesis. *Canadian Journal of Forest Research*, 31:1855–1870, 2001.

M. Scherer-Lorenzen and E.D. Schulze. *Forest diversity and function: temperate and boreal systems.* Springer Verlag, 2005.

M. Scherer-Lorenzen, E.D. Schulze, A. Don, J. Schumacher, and E. Weller. Exploring the functional significance of forest diversity: a new long-term experiment with

temperate tree species (biotree). *Perspectives in Plant Ecology, Evolution and Systematics*, 9(2):53–70, 2007.

I. Schmid and M. Kazda. Root distribution of norway spruce in monospecific and mixed stands on different soils. *Forest Ecology and Management*, 159:37–47, 2002.

I. Schmidt, C. Leuschner, A. Mölder, and W. Schmidt. Structure and composition of the seed bank in monospecific and tree species-rich temperate broad-leaved forestsModeling soil water and solute transport - fast, simplified numerical solutions. *Forest Ecology and Management*, 257:695–702, 2009.

D. Seidel. *Terrestrial laser scanning - Appications in forest ecological research*. PhD thesis, Georg-August-Universität Göttingen, Göttingen, 2011.

R. Stenger, E. Priesack, G. Barkle, and C. Sperr. Expert-N, A tool for simulating nitrogen and carbon dynamics in the soil-plant-atmosphere system. In *NZ Land Treatment Collective Proceedings Technical Session 20: Modelling of Land Treatment Systems*, pages 19–28, New Plymouth, New Zealand, 1999.

I. Thompson, B. Mackey, S. McNulty, and A. Mosseler. Forest resilience, biodiversity, and climate change. In *A synthesis of the biodiversity/resilience/stability relationship in forest ecosystems. Secretariat of the Convention on Biological Diversity, Montreal. Technical Series*, pages 43–67, 2009.

D. Van der Zande, S. Mereu, N. Nadezhdina, J. Cermak, B. Muys, P. Coppin, and F. Manes. 3D upscaling of transpiration from leaf to tree using ground-based LiDAR: Application on a Mediterranean Holm oak (Quercus ilex L.) tree. *Agricultural and Forest Meteorology*, 149(10):1573–1583, 2009.

A.I.J.M. van Dijk and R.J. Keenan. Planted forests and water in perspective. *Forest Ecology and Management*, 251(1-2):1–9, 2007.

M.T. van Genuchten. A closed-form equation for predicting the hydraulic conductivity of unsaturated soils. *Soil Sci. Soc. Am. J*, 44(5):892–898, 1980.

M. van Leeuwen and M. Nieuwenhuis. Retrieval of forest structural parameters using lidar remote sensing. *European Journal of Forest Research*, 129:749–770, 2010.

J. Šimunek, K. Huang, and M.T. Van Genuchten. The hydrus code for simulating the one-dimensional movement of water, heat, and multiple solutes in variably-saturated media. *US Salinity Laboratory Research Report*, 144, 1998.

H. Xu, N. Gossett, and B. Chen. Knowledge and heuristic-based modeling of laser-scanned trees. *ACM Transactions on Graphics (TOG)*, 26(4):19, 2007.

2 Modeling stand water budgets of mixed temperate broad-leaved forest stands by considering variations in species-specific drought response

Sebastian Bittner, Ulrike Talkner, Inga Krämer, Friedrich Beese, Dirk Hölscher, Eckart Priesack

Modeling stand water budgets of mixed temperate broad-leaved forest stands by considering variations in species specific drought response
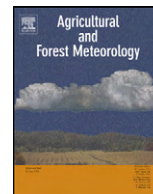
Sebastian Bittner [a,*], Ulrike Talkner [b,1], Inga Krämer [c,2], Friedrich Beese [b],
Dirk Hölscher [c], Eckart Priesack [a]

[a] Institute of Soil Ecology, Helmholtz Zentrum München – German Research Center for Environmental Health, Ingolstädter Landstraße 1, 85764 Neuherberg, Germany
[b] Department of Soil Science of Temperate and Boreal Ecosystems, University of Göttingen, Büsgenweg 2, 37077 Göttingen, Germany
[c] Department of Tropical Silviculture and Forest Ecology, University of Göttingen, Büsgenweg 1, 37077 Göttingen, Germany

ABSTRACT

This modeling study used recent observations at a temperate broad-leaved forest in Central Germany to calculate water balances of a *Fagus sylvatica* monoculture and mixed stands of *F. sylvatica*, *Tilia* spp., *Acer* spp., *Carpinus betulus*, *Fraxinus excelsior* and *Quercus robur*.

To simulate soil water flow the modeling framework Expert-N was applied which combines models that describe the physiological and hydrological processes of the plant-soil system including models of evapotranspiration (Penman–Monteith equation), interception (revised Gash model) and soil water flow (Richards equation). Measurements of rainfall partitioning, volumetric soil water content, evapotranspiration and tree transpiration provided reliable data for the parameterization and the calibration of the model for three stands of different diversity levels. They allowed to include species specific physiological (transpiration rates, response to dry soil water conditions) and structural (leaf area dynamics) characteristics.

During the 3-year long observation period 2005–2007 the mean yearly precipitation was 652 mm, the simulated mean yearly interception loss of the three observed forest stands was between 219 and 272 mm, the transpiration accounted for 197–225 mm, the forest floor evaporation for 96–104 mm, the drainage for 16–60 mm and the runoff for 13–50 mm. The calculations of the water balance were sensitive to the species composition of the forest and showed differences of rainfall interception and root water uptake between the stands. The applied stand-level model was able to simulate the water dynamics of the monospecific and mixed forest stands. It was shown that differences in drought tolerance of tree species can have a strong impact on the simulated soil water extraction during periods when available soil water is low.

© 2010 Elsevier B.V. All rights reserved.

1. Introduction

Forest structure and tree species composition have a strong influence on the water storage, retention of water and groundwater recharge in forest ecosystems (FAO, 2005; van Dijk and Keenan, 2007; Calder, 2007). Stand water dynamics are mainly determined by the functional traits of the different tree species present in the stand. The rainfall partitioning and evapotranspiration of broad-leaved tree species of Central European forests are reviewed in (Peck, 2004). It is shown that in particular observations of different tree species under similar meteorological conditions are rare and that broad-leaved tree species of Central European forests other than beech (*Fagus sylvatica* L.) have been less investigated with respect to rainfall partitioning and water uptake. One of these rare studies analyses the differences of the direct throughfall caused by different broad-leaved tree species compositions in a mixed forest stand in southern Sweden (Nordén, 1991). The throughfall was lowest for beech, followed by Norway maple (*Acer platanoides* L.), small leaved lime (*Tilia cordata* Mill.), hornbeam (*Carpinus betulus* L.), and common oak (*Quercus robur* L.) in ascending order. Sap flux studies in mixed stands have revealed differences in whole-tree water turnover among co-occurring tree species (Pataki and Oren, 2003; Granier et al., 1996; Dünisch and Morais, 2002) and in the reaction of the species to dry soil water conditions (Pataki et al., 2000; Oishi et al., 2010). In a mixed forest in Denmark, ash (*Fraxinus excelsior* L.) had half as much stemflow as beech (Dalsgaard, 2007). Moreover,

* Corresponding author. Tel.: +49 89 3187 2467; fax: +49 89 3187 3376.
   E-mail address: sebastian.bittner@helmholtz-muenchen.de (S. Bittner).
[1] Present address: Northwest German Forest Research Institute, Grätzelstraße 2, 37079 Göttingen, Germany.
[2] Present address: Leibniz Institute for Baltic Sea Research, Warnemünde, Seestraße 15, 18119 Rostock, Germany.

different timing of leafing and leaf shedding could lead to differences in interception and water uptake during spring and autumn. For example, higher throughfall is likely to occur under ash, as ash is known to get into leaves relatively late in spring.

Recent observations in a deciduous old-growth forest in Central Germany (Hainich National Park) showed differences between tree species with respect to water use and their impact on water flows. The species European beech, lime (*T. cordata* and *T. platyphyllos* Scop.), ash, hornbeam, and sycamore (*Acer pseudoplatanus* L.) were found to differ in physiological characteristics such as root water uptake (Korn, 2004), transpiration rates (Gebauer, 2010; Hölscher et al., 2005; Köcher et al., 2009) and reaction to dry soil conditions (Hölscher et al., 2005; Köcher et al., 2009). Information on the stands composed of these species was also provided by hydrological measurements such as rainfall partitioning (Krämer and Hölscher, 2009) and soil water content dynamics (Krämer and Hölscher, in press). Characteristics of the stand structure were given by observations of the fine root distribution (Meinen et al., 2009; Meinen, 2008) and leaf area index (LAI) dynamics.

Therefore, the aim of our study was to simulate the observed water balance dynamics of the Hainich stands applying a functional stand-level model by using the available information on the species specific functional traits and hydrologic stand characteristics and thereby to characterize the input of different tree species on the water balance dynamic. In a first step the model was calibrated and tested for three stands with similar soil and climatic conditions but with a different diversity level (DL) of tree species. One stand was a monoculture of beech trees and two stands were mixed stands of beech and other broad-leaved deciduous tree species.

Secondly a subsequent scenario analysis was performed to study the impact of the species composition on the water balance and in particular to analyse the effect of different root water uptake and different tree species specific reactions to dry soil water conditions. We expect this analysis to allow conclusions about how mixed stands react to changed climatic conditions and how species composition itself affects the stability and function of the whole stands under conditions of low soil water availability.

2. Materials and methods

2.1. Stand-level models

We applied the modeling framework Expert-N (Engel and Priesack, 1993; Priesack et al., 2001; Stenger et al., 1999) for the management of the input data (meteorological data, soil properties, physiological parameters) and for the coupling of single process models. The considered processes were rainfall interception, forest floor evaporation, transpiration, and soil water fluxes and the applied models included the FAO Penman–Monteith evapotranspiration model (Monteith, 1965, 1981; Allen et al., 1998), the revised Gash interception model (Gash et al., 1995) and the description of soil water flows by the Richards equation of porous media.

Model input parameters can be divided into two groups. Mean values of the stand can be derived by measuring a certain system variable (e.g., soil water content) at different positions in the stand and taking the mean of all measured values. Examples in this study were measured values of rainfall partitioning, volumetric soil water contents, and the leaf area index of the fully developed canopy. Tree species specific parameters (e.g., reaction to dry soil conditions) are weighted by the proportion of the tree species in the stand. For n different tree species with a property expressed by the parameter p_i ($i \in 1, \ldots, n$) and the species proportion c_i, the property of the whole stand p_s is calculated as a linear combination $p_s = \sum_{i=1}^{n} c_i p_i$. The water stress factor due to dry soil conditions and the transpiration

rates of the tree species were examples of this weighted mean in this study.

All model approaches are described in detail below as well as the measurements that provided the data for the parameterization and testing of the models.

2.2. Study site

The study site was located in a deciduous forest in the Hainich National Park (Thuringia, Germany. 51°N, 10°E, national park founded in 1997). European beech is the dominant tree species in large areas of the National Park, but up to 14 tree species coexist in some parts as a consequence of former management practice (Schmidt et al., 2009). In the last decades minimal forest management took place due to the military training status of the area since the 1960s. Since 1990 the site has not been managed at all, therefore the forest has a near-natural state. The selected plots represent old-growth forest stands with a closed canopy. The subatlantic climatic conditions of the plots can be considered to be the same with respect to daily temperatures, precipitation, global radiation, humidity and wind speed.

Parent rock is Triassic limestone covered with a loess layer of variable depth. The soil type is a Luvisol that dries out strongly during summer and shows stagnant properties in winter and spring (Guckland et al., 2009). The soil texture of all plots was characterized by high silt content and low sand content (silt loam to silt clay loam, Table 1). The groundwater table is found far below the rooting zone.

2.2.1. Study plots

In the forest area three study plots of 50 m × 50 m size each were selected. The maximum distance between two plots was 1.5 km. The plots were situated at 296–354 m a.s.l., slopes ranged between 2.9° and 3.2° and exposition of all plots was northeast. One monospecific stand with *F. sylvatica* and two mixed stands with a variable mixture of broad-leaved deciduous species (*F. sylvatica*, *T. cordata*, *T. platyphyllos*, *F. excelsior*, *C. betulus*, *A. pseudoplatanus*, *A. campestre*, *A. platanoides* and *Q. robur*) were analysed. The fraction of the dominating tree species was calculated by the projected crown area. The stand age of each of the three plots was between 79 and 117 years (Schmidt et al., 2009), the mean crown diameter was between 4.6 and 5.2 m. The canopy closure during summer was on average 87% (Krämer and Hölscher, 2009) and the mean leaf area index was 6.9 (Jacob et al., 2010). All stand details are based on trees with a diameter at breast height (dbh) >7 cm. Main stand characteristics are presented in Table 2.

The thickness of the loess cover was heterogeneous and varied between 60 and 120 cm (Guckland et al., 2009) at the three study plots. Soil texture in the upper mineral soil (0–30 cm) of the tree plots was characterized by high silt content (74–82%) and low sand content (<5%). The clay content varied between 14–23% at a soil depth of 0–30 cm, 15–32% at a depth of 30–40 cm and 33–41% at a depth of 40–60 cm (Table 1) depending on the depth of the illuvial Bt horizon. The mean values of the soil bulk densities were 1.1 g cm^{-3} at 0–10 cm and increased with depth to 1.5 g cm^{-3} at 40–60 cm.

The plot names follow the classification given by Leuschner et al. (2009). Overall, twelve study plots were set up and plots with similar Shannon tree diversity indices were grouped in the three diversity levels DL1, DL2 and DL3. Additionally they were assigned in preceding studies with letters a–d. For the possibility to look up the plot characteristics in cited studies, we used the same names (DL1a, DL2c and DL3a) in this study. Leuschner et al. (2009) give a detailed description of the study site and the forest biodiversity research activity in the Hainich National Park.

Table 1

Soil properties and soil hydraulic parameters. Δz depth interval, ρ_b soil bulk density, θ_s saturated vol. water content, θ_r residual vol. water content, n van Genuchten parameter, α van Genuchten parameter, and K_S saturated hydraulic conductivity.

Plot	Δz cm	Sand %	Silt %	Clay %	ρ_b g cm^{-3}	θ_s %	θ_r %	n 1	α cm^{-1}	K_S mm day^{-1}
DL1a	0–10	4.2	78.3	17.5	0.89	55	6	1.336	0.023	1150
	10–20	3.3	82.3	14.4	1.09	50	6	1.357	0.016	770
	20–30	3.6	79.6	16.8	1.42	40	7	1.276	0.017	220
	30–40	3.6	78.4	18.0	1.37	40	8	1.283	0.018	280
	40–60	1.9	65.3	32.8	1.57	38	11	1.200	0.018	50
	60–80	1.9	65.3	32.8	1.65	38	7	1.240	0.011	25
	80–100	2.0	58.0	40.0	1.62	41	15	1.200	0.070	15
DL2c	0–10	2.2	82.0	15.0	1.23	51	6	1.374	0.014	540
	10–20	2.8	82.4	14.8	1.45	46	6	1.346	0.011	220
	20–30	3.4	81.2	15.2	1.59	41	8	1.241	0.033	210
	30–40	4.7	80.2	15.2	1.49	41	7	1.218	0.032	110
	40–60	1.8	57.0	41.2	1.62	40	9	1.216	0.036	25
	60–80	2.0	58.0	40.0	1.60	40	16	1.247	0.066	25
	80–100	2.0	58.0	40.0	1.63	41	11	1.161	0.055	20
DL3a	0–10	2.6	74.6	22.8	1.05	52	9	1.314	0.037	675
	10–20	2.1	75.9	22.0	1.18	49	9	1.299	0.032	505
	20–30	2.1	74.3	23.6	1.37	48	12	1.294	0.045	500
	30–40	1.8	66.6	31.6	1.54	45	9	1.202	0.035	70
	40–60	2.1	59.5	38.4	1.44	45	17	1.394	0.091	70

2.2.2. Precipitation

The mean annual precipitation of four stations around the national park amounts to 544–662 mm (annual mean from 1961 to 1990 (DWD, 2009)). During the observation period 2005–2007 the precipitation was automatically recorded every hour at the meteorological station Weberstedt/Hainich (270 m a.s.l., 51°10′N, 10°52′E, Meteomedia, Germany). The yearly precipitation amount and the rainfall in the vegetation period differed significantly in the three observed years. The year 2005 had a typical amount of precipitation (601 mm) compared to the long-term annual mean precipitation. The year 2006 was relatively dry (518 mm) and 2007 was a year with a high amount of precipitation (838 mm). The year 2006 had a long drought period with only 28 mm precipitation from June 1st to July 27th. The precipitation in the vegetation period (May-October) was 318 mm in 2005, 239 mm in 2006 and 537 mm in 2007. The precipitation values for the dry year 2003 (388 mm) that were used in the scenario simulations in Section 3.3 were measured by CarboEurope (CarboEurope, 2009).

2.3. Soil hydraulic parameters and volumetric soil water content

The soil water flow simulations implemented in Expert-N are based on the numerical solution of the 1D Richards equation according to the approach applied in the model HYDRUS 6.0 (Šimunek et al., 1998). The water retention curves were expressed by the van Genuchten parametrization (van Genuchten, 1980). We used the software Rosetta Version 1.2 (Schaap et al., 2001) for the estimation of the saturated volumetric water content θ_s, the residual volumetric water content θ_r, the saturated hydraulic conductivity K_S and the van Genuchten parameters α and n. Rosetta needs the soil texture, soil bulk density ρ_b (Table 1) and measured

volumetric water contents at a pressure of 33 and 1500 kPa as input data for each soil horizon.

Soil texture was determined using the sieving and pipette method (Schlichting et al., 1995). In 0–10 cm soil depth the texture analysis was performed at three sampling points per stand. In 10–20, 20–30, 30–40, and 40–60 cm soil depth it was performed at single soil samples taken from soil-profile pits adjacent to the plots. In deeper soil layers the textual class was estimated and tabulated values of the clay, silt and sand content were used. At the plot DL3a the soil was parameterized to the depth of the loess layer that was just 60 cm at that plot. Soil bulk density was determined gravimetrically from three undisturbed soil cores (125 cm^3) taken from the adjacent soil-profile pits. The volumetric water contents at a pressure of 33 and 1500 kPa were determined on five undisturbed 250 cm^3 soil cores per sampling depth from the soil pits adjacent to the stands, with a suction membrane in the lower suction range (33 kPa) and a pressure membrane device in the higher suction range (1500 kPa).

At the three study plots the volumetric soil water content θ_V was measured using frequency domain reflectometry (FDR) probes (Diviner 2000 FDR sensors, Sentek Pty Ltd., Stepney, Australia) at six locations per study plot (Krämer and Hölscher, in press). The probe measures the dielectric constant across a ≈10 cm sphere of influence surrounding the sensor and at 10 cm depth intervals to a depth of 40 cm. The FDR probe was depth-specifically calibrated in the field (Krämer and Hölscher, in press) as suggested and described by the manufacturer.

2.4. Interception

The rainfall interception was simulated using the revised Gash model (Gash et al., 1995) on daily basis and on event basis. The

Table 2

Forest stands characteristics of the three study plots. 'lime': *Tilia cordata* and *T. platyphyllos*, LAI: leaf area index. Trees >7 cm dbh.

Plot	[a]LAI			Share of crown projection area				
	2005	2006 m^2/m^2	2007	Beech %	Lime %	Ash %	Hornbeam %	Sycamore %
DL1a	6.5	7.3	7.2	94	2	2	0	2
DL2c	6.6	6.5	6.2	73	14	10	0	1
DL3a	7.3	7.6	6.5	7	55	9	14	2

[a] M. Jacob, personal communication, calculated from leaf biomass collected in litter traps.

daily-basis model assumes the daily precipitation to occur at a single storm. The event basis model uses hourly precipitation amounts and assumes that two single rain events are separated by a period without precipitation during which the canopy dries. The duration of the dry period was assumed to be at least one hour according to our observations at the Hainich forest.

The Gash model needs the fraction p of rain which falls directly to the forest floor (free throughfall) as input parameter. To determine this parameter, the gap fraction g in summer and the branch cover in winter were determined by hemispherical photographs (Krämer and Hölscher, 2009). The hemispherical photographs were taken vertically upward above each rain gauge (for the measurement of the throughfall, see below). The camera (Minolta Dimage Xt, Japan) had a $185°$ fish-eye lens. Images were analysed for gap fraction in a $10°$ circular area directly above the gauges with CanEye 5.0 (INRA, 2009).

Additionally, the interception capacity S (mm) of the canopy and the mean canopy evaporation rate per mean rainfall rate $\bar{E}_C/\bar{R}$ are needed as input for the Gash model. We estimated these parameters using measured throughfall TF and gross precipitation P for single rain events during the observation period. For observed single rain events with neglectable stemflow amounts, interception I can be set to $I = P - TF$. A scatter plot $I(P)$ can be divided into a wetting part and a saturated part and be used for the mean method estimation of the Gash parameters (Klaassen et al., 1998). A linear regression of $I(P)$ for rain events high enough to saturate the canopy results in estimates for $\bar{E}_C/\bar{R}$ and S_{mean} (mm), the mean water storage capacity by using

$$I = S_{mean} + \frac{\bar{E}_C}{\bar{R}}P. \tag{1}$$

The interception capacity S is then given by

$$S = -\frac{\bar{E}_C}{\bar{R}}S_{mean}\left[\left(1 - p - \frac{\bar{E}_C}{\bar{R}}\right)\ln\left(1 - \frac{\bar{E}_C/\bar{R}}{1-p}\right)\right]^{-1}, \tag{2}$$

if $(\bar{E}_C/\bar{R} - p) < 1$.

The calibration of the interception model was tested by using measurements from the whole period 2005–2007 for which the partitioning of gross rainfall P into interception I, throughfall TF and stemflow SF has been measured (Krämer and Hölscher, 2009).

2.5. Potential evapotranspiration

The potential evapotranspiration ET_{pot} was calculated by the FAO Penman–Monteith equation (Monteith, 1965, 1981; Allen et al., 1998), which estimates the daily ET_{pot} for a hypothetical grass reference surface. The partitioning of ET_{pot} into the potential transpiration of the forest canopy and potential evaporation of the forest floor was achieved by a plant cover factor and the leaf area index (LAI [$m^2\,m^{-2}$]) of the trees. To this, the LAI of the plots was calculated from leaf biomass collected in litter traps (Jacob et al., 2010). The physiological development of the leaves in spring and autumn was interpolated such that the LAI increases from 0 to the measured value for the fully foliated canopy following a sigmoidal function of time in spring and decreased in the same way in autumn. We included species specific dates of spring leafing and shedding in fall according to measurements of transpiration rates (T. Gebauer, personal communication) and direct observations.

The daily ET_{pot} was partitioned into the daily potential transpiration T_{pot} and daily potential forest floor evaporation E_{pot} by a cover factor f (Droogers, 2000)

$$T_{pot} = fET_{pot} \tag{3}$$

$$E_{pot} = (1 - f)ET_{pot}. \tag{4}$$

2.6. Actual forest floor evaporation and root water uptake

The actual forest floor evaporation E_{act} was simulated by limiting E_{pot} by the calculated maximal water flux q_{max} (mm day^{-1}) at time t (day) from the top soil segment (Hutson and Wagenet, 1992). E_{act} is then given by

$$E_{act} = \min(E_{pot},\quad q_{max}\Delta t). \tag{5}$$

The actual transpiration T_{act} was calculated under consideration of the soil water availability and the vertical distribution of fine roots in the soil. At the depth z the root water uptake is proportional to the density $g(z)$ and to the reduction factor $r(h)$ that depends on the soil matric potential h (Perrochet, 1987; Lai and Katul, 2000). This factor includes the special edaphic situation with clay-rich soils that restrict root water uptake by low soil hydraulic conductivities and the species specific physiological reaction to dry soil conditions. The total actual transpiration was calculated by integrating the root water uptake over the depth of the rooting zone L,

$$T_{act} = T_{pot}\int_o^L g(z)r(h)dz \tag{6}$$

Note that the constraints $\int_o^L g(z)dz = 1$, $\int_o^L r(h)dz \leq 1$ and $\int_o^L g(z)r(h)dz \leq 1$ have to be met.

A non-linear vertical cumulative root distribution (Gale and Grigal, 1987) was used to describe the decrease of the fine root biomass with increasing soil depth. The cumulative root biomass fraction $y(l)$ from the surface to depth l is determined by

$$y(l) = \int_0^l g(z)dz = 1 - \beta^l, \tag{7}$$

using the parameter β which describes if the roots are mostly located in deeper soil layers or if they are distributed mostly near the surface and assuming a simple relation to describe the vertical root density distribution $g(z)$. The vertical fine root distribution in the soil was determined by taking soil samples down to a depth of 40 cm and measuring the biomass of fine roots with a diameter less than 2 mm (Meinen et al., 2009; Meinen, 2008).

The simulated values of T_{act} were then compared with the values of T_{act} that have been calculated from measurements of xylem sap flux density in the tree stem observed by Gebauer (Gebauer, 2010) using Granier heat dissipation sensors (Granier, 1985; Granier, 1987) installed on 44 trees with dbh > 10 cm on the plots DL1a, DL2c and DL3a in the years 2005 and 2006.

At the nearby Hainich site of the CarboEurope (2009) research project the latent heat flux above the canopy was measured half hourly by the eddy covariance method and the evaporation was calculated using these measurements.

3. Results and discussion

3.1. Parameterization

3.1.1. Interception

To parameterize the Gash model values of the gap fraction, the canopy storage capacity and the mean canopy evaporation rate to rainfall rate ratio are needed. The measured gap fraction of the canopy in summer was 0.11–0.16 for the three plots (Table 3) and the branch cover in winter was 0.11–0.13. The low rainfall intensities in winter (Krämer and Hölscher, 2009) and the fact that the measured interception loss in winter was about 30% and nearly as high as in summer indicated that the small rain drops of winter rain events mostly could not pass the defoliated canopy freely. Therefore, also for the defoliated canopy in winter we assumed p

Table 3
Gash interception model parameters free throughfall p, mean canopy evaporation rate per mean rainfall rate $\bar{E}_C/\bar{R}$ and interception capacity S.

Plot	p	$\bar{E}_C/\bar{R}$	S [mm]
Foliated			
DL1a	0.11	0.22 ± 0.06	1.02 ± 0.36
DL2c	0.12	0.22 ± 0.05	1.35 ± 0.43
DL3a	0.16	0.21 ± 0.04	0.45 ± 0.30
Defoliated			
DL1a	0.11	0.16 ± 0.09	0.94 ± 0.41
DL2c	0.12	0.21 ± 0.11	0.70 ± 0.60
DL3a	0.16	0.23 ± 0.11	0.59 ± 0.53

to be equal to the measured gap fraction of the canopy in summer (foliated canopy). The estimated parameters of $\bar{E}_C/\bar{R}$ and S for the foliated and the defoliated canopy for the observation periods are given in Table 3, the linear regression of $I(P)$ for the foliated plot DL1a is given in Fig. 1.

3.1.2. Transpiration and forest floor evaporation

In the winter period ($T_{act} = 0$) we could calibrate the cover factor to $f = 0.7$, such that the simulated soil water contents θ_V matched the measured values. The factor was the same for all plots during the leafless period. In the foliated period f was increased in the model due to the additional coverage of the forest floor by the foliation of tree canopies. This additional coverage was calculated for periods of fully developed LAI using the difference between the measured canopy cover in summer ($1 - g$, gap fraction g) and in winter (branch cover). In spring and fall the LAI dynamics of the different tree species were used to calculate the additional coverage of the forest soil. The values of LAI in summer varied between 6.2 and 7.6 $m^2\,m^{-2}$ between the study plots and years (M. Jacob, personal communication; Table 2).

3.1.3. Root density distribution

Data on root biomass distribution by Meinen et al. (2009) were used to parameterize the model. The fine root biomass decreased markedly with soil depth and the vertical distribution was similar between the three stands. Therefore also the values of β which were determined by the observed root distribution were similar in the different stands and varied between 0.93 and 0.94. In all plots about half of the total fine root biomass was found in the first 15 cm of the profile and more than 85% of the fine root biomass in the first 40 cm according to an extrapolation of the root distribution model.

The fine root biomass distribution was also determined for the single tree species. The fine root biomass proportion of the single tree species in the mixed stands reflected the aboveground propor-
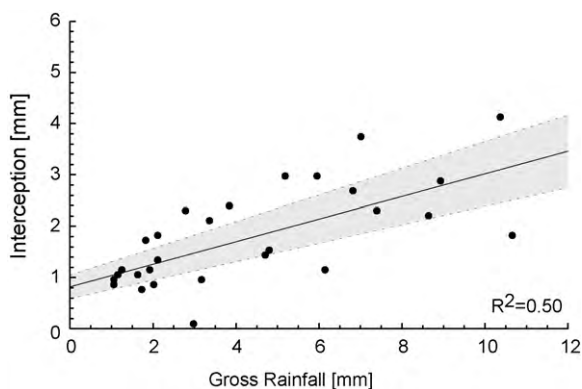

Fig. 1. Measured values of gross rainfall and interception for the parameterization of the Gash model of the foliated plot DL1a. The mean canopy evaporation rate per mean rainfall rate $\bar{E}_C/\bar{R}$ and S_{mean} are given by the slope and the y-intercept. The shadowed area shows the uncertainty range of the parameters.
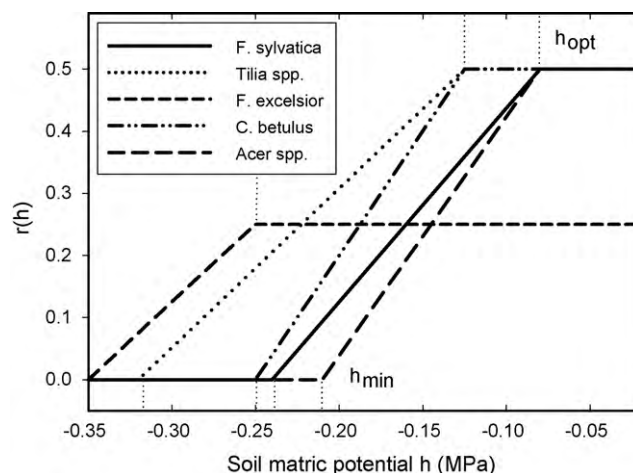

Fig. 2. Root water uptake at optimal wet soil conditions ($h > h_{opt}$) and reaction to water stress ($h < h_{opt}$). Root water uptake is reduced by the factor $r(h)$.

tion of the particular tree species in the stand. The differences in vertical root distribution were low with β between 0.91 for *Acer* spp. on DL2 and 0.94 for *F. sylvatica*. For simplicity, we did not distinguish the vertical root distribution of the single tree species in the model. We also assumed the understory to have the same composition of trees as the stand with full canopy height.

Grass and herb roots were distinguished from tree roots by their smaller diameter, non-lignified structure and lighter color. The contribution of herb roots to the total root biomass in the profile was marginal (1% in DL1a and DL2c; 4% in DL3a).

3.1.4. Root water uptake reduction factor

At optimal wet soil water conditions the water uptake reduction factor $r(h_{opt})$ was estimated by comparing the measured and simulated values of T_{act} and θ_V. Because the measured transpiration of the three sites was low (maximal measured yearly value: 158 mm) compared with other deciduous forests (Gebauer, 2010) the factor was set $r(h_{opt}) \leq 0.5$. A reason for the observed low transpiration could be the low unsaturated hydraulic conductivity of the clay-rich soils, which limit the water flow to the roots. Gebauer (2010) measured the sap flux density of five tree species and observed that at optimal wet soil water conditions the contribution of the different tree species to total stand transpiration did not reflect the proportion of the accordant species in the canopy. The transpiration rates of the ring-porous species *F. excelsior* were significantly lower than the rates of the diffuse-porous species *F. sylvatica*, *Tilia* spp., *Acer* spp. and *C. betulus*. This could be explained by the small hydroactive sapwood area of *F. excelsior* with only the youngest annual rings being involved in water transport (Gebauer et al., 2008). In our model, the differences of the species in root water uptake were parameterized according to the studies of Gebauer (2010) and Hölscher et al. (2005). The reduction factor of the diffuse-porous species was set to 0.5 for optimal soil water conditions in the model. The factor of the ring-porous species *F. excelsior* was set to 0.25.

At dry soil water conditions, the water uptake was further decreased to account for the stomatal reaction of the trees. Several stand-level forest models consider the reaction of trees to water stress and describe the effect on the total water balance (Fischer et al., 2008; Mitchell, 2005; Sen et al., 2000). We assume a linear decrease of water uptake at dry soil conditions (Fig. 2, Table 4), as this behaviour was observed for the tree species at the Hainich forest (Hölscher et al., 2005; Köcher et al., 2009).

According to the root water uptake model of Feddes et al. (1978), the root water uptake decreases linearly when the soil matric potential h is lower than the matric potential h_{opt} of an optimal

Table 4

Species specific parameters of transpiration, reaction to water stress due to dry soil water conditions, and leaf development. The root water uptake decreases linearly with a soil matric potential lower than h_{opt}. At a soil matric potential of $h < h_{min}$ the trees are not able to take up water from the soil. The reduction factor of transpiration rate at optimal wet soil conditions is given by $r(h_{opt})$.

Species	$r(h_{opt})$ 1	h_{opt} MPa	h_{min} MPa	Foliated period
Fagus sylvatica	0.5	−0.08	−0.24	05/01–10/31
Tilia spp.	0.5	−0.13	−0.32	05/08–10/25
Fraxinus excelsior	0.25	−0.25	−0.35	05/15–10/15
Carpinus betulus	0.5	−0.13	−0.25	05/15–10/15
Acer spp.	0.5	−0.08	−0.21	05/15–10/15

wet soil. For values $h > h_{opt}$ the water uptake reaches a constant maximum value. At a soil matric potential of $h < h_{min}$ the trees are not able to take up water from the soil. The reduction factor $r(h)$ can be interpreted as a water stress factor. *F. sylvatica* and *Acer* spp. respond sensitively to soil drought and show a strong reduction of water uptake. *Tilia* spp. is less sensitive to drought conditions and *F. excelsior* can deal best with dry soil conditions. No reduction of water uptake of *F. excelsior* was observed during a dry period in the study of Hölscher et al. (2005) and during the observation period of the study by Köcher et al. (2009). In contrast to the model of Feddes et al. (1978), our model parameterization did not include a decrease of the water uptake due to anaerobic conditions at very wet soil conditions.

Herbst et al. (2007) pointed out that ash shows a heterogeneous radial pattern of the sap flux density and proposed a specific calibration function for the sap flux sensors for ash. This specific calibration function would result in a higher sap flux density and thus in higher transpiration rates than the ones obtained by the commonly used calibration function. Thus the absolute values of transpiration for ash have to be regarded with caution, but the behaviour of ash at dry soil conditions remains unaffected. This uncertainty in the model calibration has a low impact on the simulated total transpiration values of the three plots, because of the low percentage of ash in the plots, but may affect the simulated values of transpiration of the scenario calculations in Section 3.3.

Moreover, three-dimensional modeling of the root architecture and the root water uptake might lead to a more complex one-dimensional water uptake reduction function (Javaux et al., 2008). A further analysis of the three-dimensional architecture of the root system therefore may lead to an improved and more realistic one-dimensional water uptake reduction function.

3.2. Simulation

3.2.1. Interception

The measured interception loss was between 21 and 41% of the gross precipitation and differences between seasons were more pronounced than between plots (Krämer and Hölscher, 2009). The
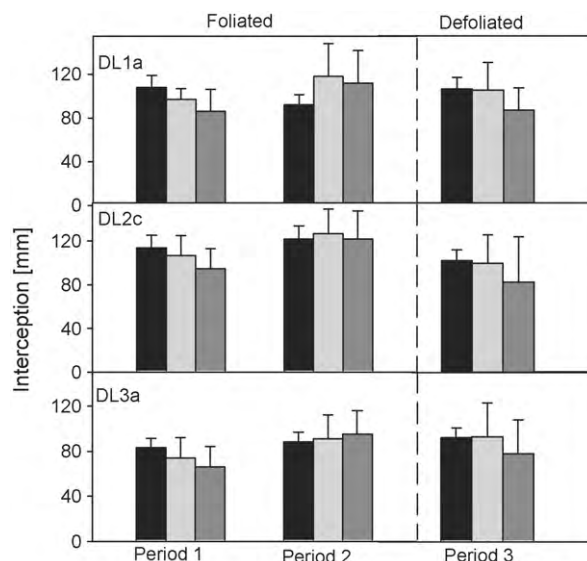

Fig. 3. Measured (black) and simulated (light gray: event basis; dark gray: daily basis) interception loss (mm) during three observation periods. Period 1: 5/19/2006–9/6/2006; period 2: 5/17/2007–8/22/2007; period 3: 12/2/2006–4/5/2007. The error bars indicate the measurement error and the model uncertainty due to the uncertainty of the parameters S and $\bar{E}_C/\bar{R}$.

measured stemflow played a minor role at all three stands and was between 0.4 and 6.2% of the gross precipitation.

The simulated values of interception were compared with the measured values in Fig. 3 for two summer periods and one winter period. The periods were defined according to the observed physiological development of the trees and represent periods fully foliated and fully defoliated canopies. The largest deviation between simulation and measurement could be observed in summer 2007 at the plot DL1a, where the measured value was 26 mm (22%) lower than the simulated value. For all other observation periods and plots the deviation between simulation and measurement was below 10%. These differences are comparable to other studies that use the revised Gash model to simulate the rainfall interception of mixed stands (Deguchi et al., 2006; Price and Carlyle-Moses, 2003). The simulated interception values were also compared with the difference of measured gross precipitation and measured values of throughfall for rainfall events with no observed stemflow ($P < 2$ mm, $I = P − TF$, Fig. 4). For single events with higher P, an estimation of the measured interception was not possible, as the stemflow for single events was not measured.

If more than one rainfall event per day occurs, the use of the Gash model at event basis can lead to higher values of rainfall interception than the model based on the daily basis. But using the model at event basis can also lead to lower interception values because rainfall events that occur over midnight are separated by the daily-basis
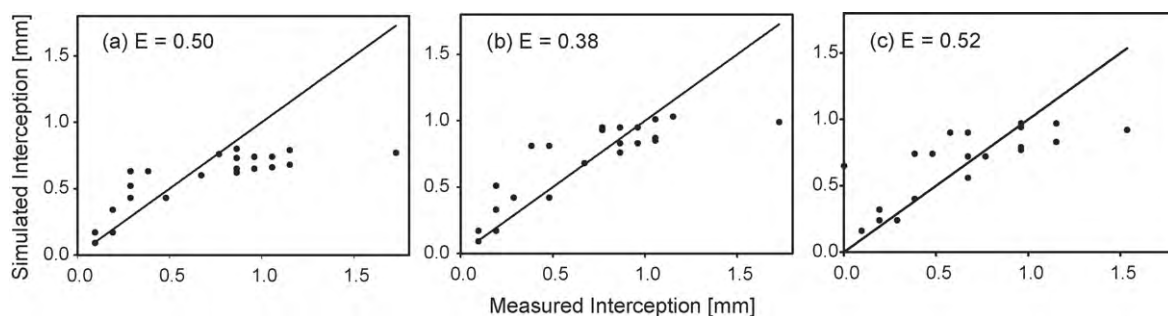

Fig. 4. Measured and simulated interception of single rainfall events for the plots DL1a (a), DL2c (b) and DL3a (c). Model efficiency E (Nash–Sutcliffe index), solid line: measured = simulated.

Table 5
Simulated yearly water balances of the years 2005–2007 at the three study plots. T_{obs} contains the observed values of transpiration by trees with dbh > 10 cm (Gebauer, 2010), T is the simulated total tree transpiration, all values in mm.

Year	Plot	T_{obs}	T	E	I	D	R	ΔS
2005 ($P = 601$)	DL1a	101	233	93	236	31	2	5
	DL2c	97	199	97	267	5	19	12
	DL3a	158	224	104	213	25	18	17
2006 ($P = 518$)	DL1a	134	208	91	223	17	3	−24
	DL2c	139	174	95	256	4	17	−27
	DL3a	128	205	97	204	16	25	−29
2007 ($P = 838$)	DL1a	–	234	102	259	133	36	73
	DL2c	–	217	106	292	40	97	84
	DL3a	–	217	112	238	107	106	57

P, precipitation; E, forest floor evaporation; I, interception; D, drainage; R, runoff; ΔS, change in soil water storage.

model but not by the event basis model. The difference between the simulation at daily basis in contrast to the event basis was rather low (4–11%) for the summer period. In winter, the simulated interception showed significantly higher (16–18%) values if calculated at event basis than at daily basis and matched the measured values better. An explanation is the low rainfall intensity in winter (Krämer and Hölscher, 2009), as the single events in winter had lower amounts of rain than the summer events and in winter usually more than one event occurred per day. Therefore, we used the Gash model on event basis for the subsequent simulation and analysis of the soil water flow and plant water uptake.

It was not possible to extract the parameters of the Gash model for the single tree species, because the number of analysed plots was too low to derive the values by statistical methods. By using the observations at 12 plots at the Hainich National Park (Krämer and Hölscher, 2009), it was also not possible to extract the influence of single tree species on the interception. In this study Krämer and Hölscher (2009) found a positive correlation of direct throughfall and a negative correlation of the stemflow with the diversity level but no significant correlation between the diversity level of the plots and the interception loss. It was also stated (Krämer and Hölscher, 2009) that the rainfall partitioning was strongly influenced by stand structural characteristics such as stand height, crown length, and crown roughness. The higher measured and simulated interception loss of the plot DL2c in comparison with the other two plots (Table 5) may be seen as an effect of non species specific stand structure (i.e. stem density) rather than stand species composition.

3.2.2. Transpiration and forest floor evaporation

The simulated yearly values of the sum of forest floor evaporation E and transpiration T (Table 5) ranged from 269 to 336 mm, the differences were higher between the years than between the different plots. The values were low compared with those of other forests (Wullschleger et al., 2001; Wullschleger and Hanson, 2006; Vincke et al., 2005a; Granier et al., 2000; Schipka

et al., 2005), but similar to the values of evapotranspiration measured by the *CarboEurope* project at a beech site with similar soil properties and similar stand age located near to our study sites (2005: 270 mm; 2006: 280 mm; 2007: 350 mm; (CarboEurope, 2009)).

The forest floor evaporation showed the highest values in April and May, when the leaves of the trees were not fully developed and the potential evapotranspiration increased. For the total year, the ratio of E to the total evapotranspiration $E/(E + T + I)$ was 0.17–0.19. For the summer periods, the fraction was 0.10–0.13. These values are similar to the values observed at deciduous forests with a LAI similar to our site by using lysimeter studies (0.10–0.20 (Kelliher et al., 1992)) or eddy flux measurements at the forest floor (0.10–0.11 (Moore et al., 1996); 0.08 (Wilson et al., 2001)).

The biomass of the herb layer increased along the tree species diversity gradient (Mölder et al., 2008). Also the thickness of the litter layer depended on the diversity level of the plots and decreased with increasing tree species diversity (Mölder et al., 2008). Thus a model separation of forest floor evaporation into components such as herb layer transpiration (Marin et al., 2000) and litter evaporation (Ogée and Brunet, 2002) might improve the description of biodiversity effects on the simulated water balance.

The simulated values of transpiration were 45–87 mm higher than the values obtained by sap flux measurements in the year 2006 (Table 5). The simulated values of water uptake must be interpreted as the transpiration of the total canopy, i.e. the trees with full canopy height plus the understory, as the model was calibrated to the measured volumetric soil water content. The differences may be explained by the contribution of the understory to the total transpiration. Also the herb layer can possibly extract high amounts of water from the soil as shown in cases of other forest types (Lüttschwager et al., 1999; Vincke et al., 2005b; Iida et al., 2009). Thus a more complex model of the forest floor that includes the competition between herbs and trees for soil water may lead to a lower value of the transpiration of the trees. A possible underestimation of the tree transpiration by the xylem flux method is also
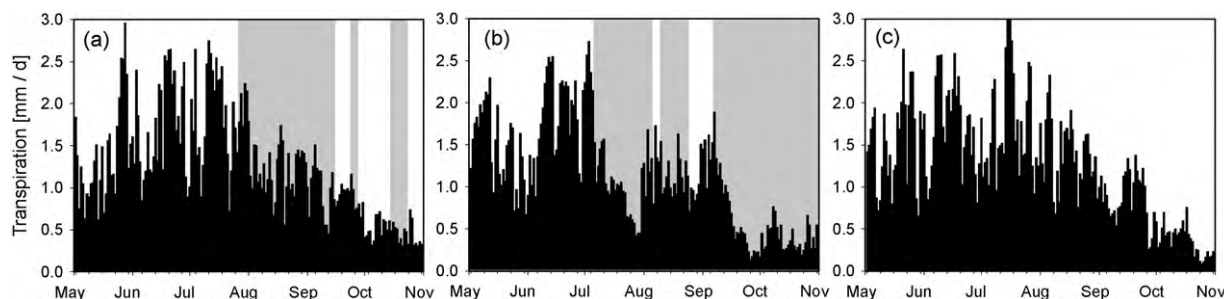

Fig. 5. Simulated daily transpiration (mm) at the beech dominated plot DL1a during the years 2005 (a), 2006 (b) and 2007 (c). The gray areas show the periods of water stress for *F. sylvatica* according to the water stress model.

discussed in a study on the soil water extraction at the study site (Krämer and Hölscher, in press).

The measured yearly transpiration values for the two beech dominated plots DL1a and DL2c in 2005 were low ($\approx$100 mm) in comparison with the third plot DL3a and the values of the year 2006. The model did not show lower values for these plots in the year 2005, the values were 199–233 mm for all the three plots. The plot DL3a had a large fraction of lime (55%), but even by parameterizing higher values of $r(h_{opt})$, h_{min}, and h_{opt} for lime the model could not reproduce the measured higher transpiration in 2005 in comparison with the beech dominated plots and maintain the lower transpiration in 2006 of the DL3a plot. Gebauer (2010) considers after-effects of the extreme drought in the year 2003 as one reason for the low transpiration values of the beech dominated plots DL1a and DL2c. Because our model did not quantify the damage of trees due to water stress, possible damages of the water stress sensitive *F. sylvatica* caused by the drought in 2003 may explain the high deviation between simulated and measured values in 2005 for the beech dominated plots DL1a and DL2c.

The daily values of simulated transpiration and the periods of water stress of the beech dominated DL1a stand are presented in Fig. 5. The year 2006 had rainless periods in June, July and September. The daily modelled transpiration rates decreased rapidly in July and September as a reaction to dry soil water conditions. This decrease was also measured by Gebauer (2010). Therefore, the model was able to describe the decrease of water uptake under dry soil conditions. In the years 2005 and 2007 longer periods without rainfall did not occur during the vegetation period. A decrease of daily transpiration values could be observed only near the end of the vegetation period and can be explained by a lower atmospheric evaporative demand.

The differently parameterized water uptake functions did not lead to strong differences between the simulated yearly transpiration rates of the three plots. One reason was the fact that the fraction of the only ring-porous species ash that was parameterized to have lower uptake rates at optimal soil water conditions was low at all three plots ($\leq$10%) and that different reactions of the tree species to water stress had an effect just within some weeks. One of these periods was July 2006, when the reduction of water uptake due to dry soil water conditions accounted for 20 mm at the plot DL1a which was 53% of the total water uptake of July 2006. At the plot DL2a the reduction was 19 mm, at the plot DL3c the reduction accounted for 13 mm. Moreover, the transpiration rates are a consequence of the overlay of the water uptake strategies with other factors such as soil water input and soil hydraulic characteristics.

At all three study plots, no indication of vertical segregation of the fine root system was observed (Meinen et al., 2009; Meinen, 2008), which indicates that a spatial complementary soil water use by the different species plays a minor role during most of the time.

3.2.3. Soil water flow and water balances

The measured values of the volumetric soil water content θ_V at soil depths of 10, 20, 30 and 40 cm in comparison with the simulated values at DL1a are shown in Fig. 6. The simulation was in accordance with the measurement with respect to the maximum and minimum soil water conditions and the seasonal changes. The model mirrored the soil water conditions of the dry year 2006 with a long drought period in summer as well as the relative wet year 2007. The model efficiency and the root mean square error for all three simulated sites can be seen in Table 6. The quality is comparable to 1D-SVAT simulations of monoculture forest stands (Hoff et al., 2002; Christiansen et al., 2010; Christiansen et al., 2006; Schwärzel et al., 2009, 2007).

The good match of simulated and measured volumetric soil water content at different depths indicates that the soil hydraulic properties are parameterized properly and that the simulated soil
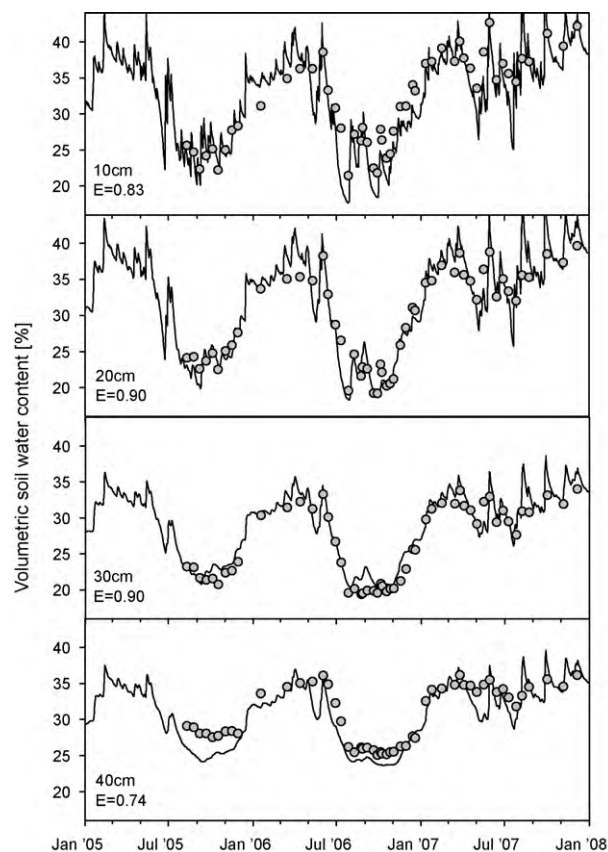

Fig. 6. Measured (dots) and simulated (lines) volumetric soil water content at 10, 20, 30 and 40 cm soil depth at DL1a.

water fluxes are reasonable. The runoff and the drainage have not been measured but the simulated values are direct results of the soil water flow simulations and were also in a plausible range. Significant amounts of runoff and drainage occurred during the wet year 2007. During the dry year 2006 and during the year 2005 with usual mean rainfall the runoff values were lower than 5% of the yearly precipitation.

The difference of the water balance components between the three stands was low in all 3 years and mostly a consequence of the higher simulated interception loss at the plot DL2c (Table 5). This higher interception led to a lower input of soil water and lower rates of simulated evapotranspiration. Despite the large interannual variation in rainfall, the simulated annual evaporation and transpiration showed only small variation. On the one hand the tree species water uptake capability decreases during periods of dry soil

Table 6
Model performance of soil water content simulations. E: model efficiency (Nash–Sutcliffe index); RMSE: root mean square error.

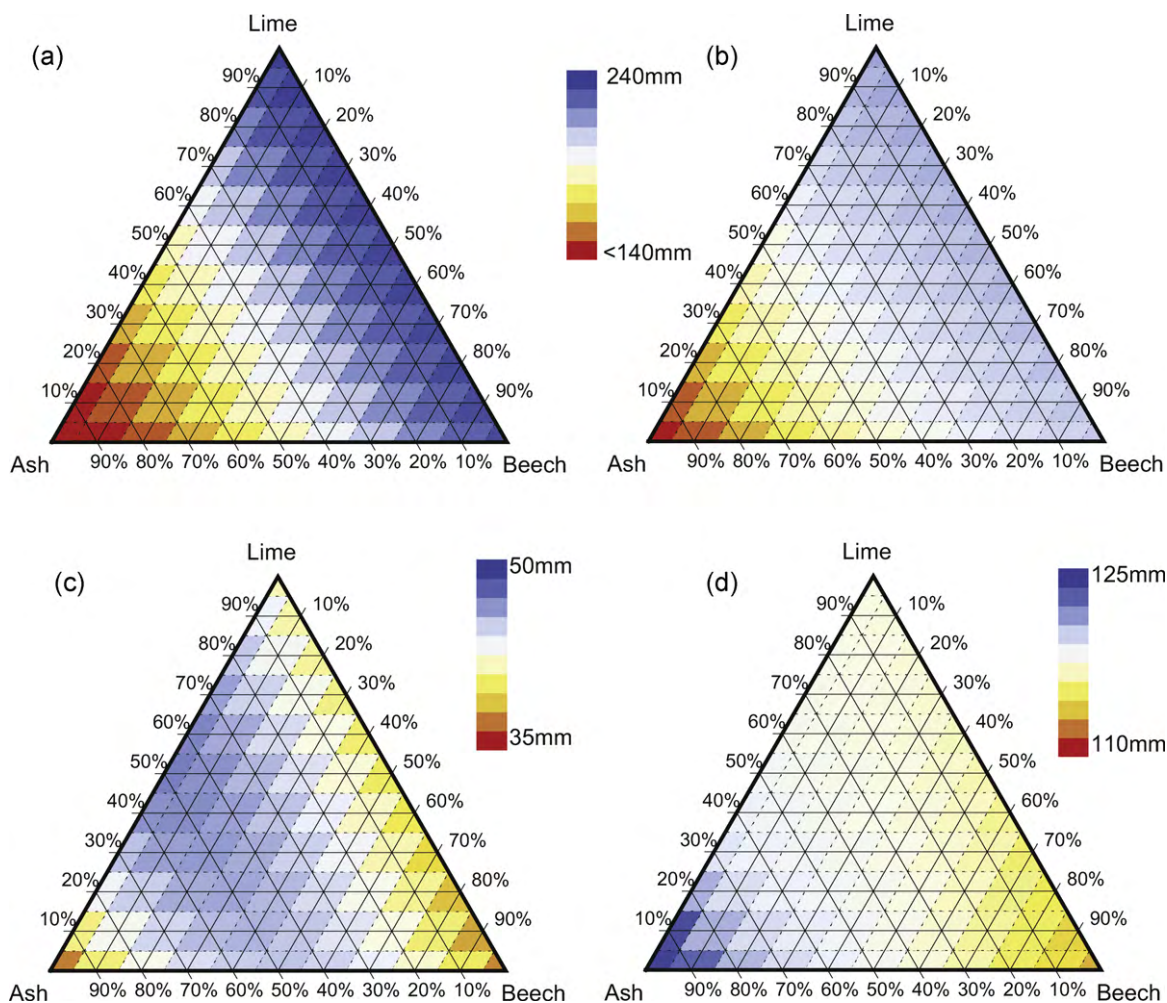| Site	Depth	E	RMSE [%]
DL1a	10 cm	0.83	2.5
	20 cm	0.90	2.0
	30 cm	0.90	1.6
	40 cm	0.74	2.0
DL2c	10 cm	0.42	5.0
	20 cm	0.80	2.8
	30 cm	0.85	2.0
	40 cm	0.56	3.3
DL3a	10 cm	0.73	4.2
	20 cm	0.80	3.7
	30 cm	0.69	3.1
	40 cm	0.84	2.0

Fig. 7. Transpiration (mm) of mixed stands of drought sensitive beech and drought tolerant lime and ash for the years 2005 (a), 2006 (b), for July 2006 (c) and for a hypothetical scenario with a 25% reduction of the precipitation of 2006 (d).

conditions in years with low annual rainfall, but on the other hand the atmospheric water demand is lower in wet years with many rainy days which also decreases the transpiration rates. Small inter-annual variability of the evapotranspiration was also observed at a broad-leaved forest in North America (Oishi et al., 2010).

3.3. Scenario of species composition

The actual water uptake was calculated for a scenario of different combinations of beech, lime and ash in mixed stands for the observed years 2005–2007 as well as for the very dry year 2003. We used the species specific water uptake functions (Fig. 2) weighted by the proportion of the species in the stand scenario. All other model input parameters such as soil characteristics and rainfall interception parameters were not changed.

The calculations show large differences of simulated yearly transpiration between the stands of different species composition (Fig. 7). This is due to the different water uptake rates of the species at optimal soil water conditions, as the diffuse-porous species lime and beech were parameterized to have twice as high transpiration rates than the ring-porous species ash at wet soil water conditions. In the wet year 2007 there was sufficient water available during the vegetation period and no water stress occurred such that the simulated differences between the transpiration rates are a direct result of the root water uptake parameterization at optimal soil water conditions.

The simulated reaction to dry soil water conditions is in accordance with observations during the rainless periods of the dry years 2003 and 2006. Thereby two contrary effects influence the tree water uptake at dry conditions. Low soil water contents lead to low leaf water potentials and therewith to stomatal closure decreasing evaporative water flow from the tree leaves to the atmosphere. In contrast dry and warm conditions lead to a higher evaporative demand and hence higher potential transpiration rates. The scenario calculations showed that depending on the tree species either one effect dominated or the effects levelled out. The ring-porous ash was the most drought tolerant species and had the lowest soil water uptake throughout all years. The total water uptake of ash monocultures was higher in dry years compared with wet years due to a higher atmospheric evaporative demand (149 mm in 2003, 123 mm in 2005, 134 mm in 2006, 117 mm in 2007). Beech monocultures on the other side showed higher yearly water uptake in the wet years (219 mm in 2003, 233 mm in 2005, 208 mm in 2006, 234 mm in 2007), because in the dry years beech reduced the xylem sap flux sensitively at low soil water contents. Lime monocultures showed the highest values of transpiration in all years, the yearly transpiration values (249 mm in 2003, 244 mm in 2005, 239 mm in 2006, 234 mm in 2007) were similar at all years.

The tree species specific water uptake strategies were also reflected in the differences between the simulated yearly actual transpiration amounts of the assumed beech, lime, and ash monocultures of the years 2003, 2005, 2006, and 2007. The difference

between beech and ash was lower in the dry years (70 mm in 2003, 74 mm in 2006) than in the wet years (110 mm in 2005, 117 mm in 2007). The difference between beech and lime disappeared in the wet year 2007 and was low in the other years (8 mm in 2003, 6 mm in 2005, 6 mm in 2006).

The model scenario showed that the minimum of the volumetric soil water content θ_V at the end of a drought period is lower in stands with drought tolerant species (unpublished data) as result of the better capability of these species to extract water at low soil matric potentials. This indicates that the exhaustion of soil water by drought tolerant species can increase water stress and may damage the drought sensitive species in mixed stands of drought tolerant and drought sensitive species under very dry conditions.

4. Conclusion

By coupling models that describe physiological and hydrological processes we were able to simulate the water balance and water dynamics of the three forest stands. In accordance with precedent observational studies (Gebauer, 2010; Krämer and Hölscher, 2009) this modelling study showed that rainfall interception and transpiration did not generally correlate with species diversity. It was not possible to trace back the differences of the interception loss to single tree species. Also the impact of different water uptake functions of the different species on soil water flow and yearly transpiration rates could not be identified due to the strong overlay by differences in soil water infiltration and soil hydrological characteristics between the tree study plots.

An analysis of the daily values of transpiration and the volumetric soil water contents showed that the low soil water contents during periods with low rainfall can lead to water stress of the trees and that these periods occurred in the years 2005 and 2006. Scenario calculations of tree species composition based on the same hydraulic characteristics showed that the simulated water exhaustion can differ between stands of different mixtures of drought tolerant and sensitive species. The exhaustion of soil water by drought tolerant species could increase the water stress for drought sensitive species and may possibly decrease ecosystem stability at sites, where the plant available soil water is low during the vegetation period.

In future studies the model should be extended to also consider the damage of trees due to water stress. Moreover, the analysis of neighbouring effects, especially between drought tolerant and drought sensitive species can lead to a better understanding of the interaction of trees in mixed forests and may be particularly useful to predict future water dynamics under the expected climate change towards warmer and drier conditions.

Acknowledgments

References

Allen, R.G., Pereira, L.S., Raes, D., Smith, M., 1998. Crop evaporation: guidelines for computing crop requirements. In: Irrigation and Drainage Paper No. 56. FAO, Rome, Italy.
Calder, I.R., 2007. Forests and water—ensuring forest benefits outweigh water costs. For. Ecol. Manage. 251, 110–120.
CarboEurope, 2009. Carbo Europe Database, Last visited: 10/01/2009 http://www.carboeurope.org.
Christiansen, J.R., Elberling, B., Jansson, P.-E., 2006. Modelling water balance and nitrate leaching in temperate Norway spruce and beech forests located on the same soil type with the CoupModel. For. Ecol. Manage. 237, 545–556.
Christiansen, J.R., Vesterdal, L., Callesen, I., Elberling, B., Schmidt, I.K., Gundersen, P., 2010. The role of six European tree species and land-use legacy for nitrogen and water budgets in forests. Global Change Biol. 16, 2224–2240.
Dalsgaard, L., 2007. Above and below ground gaps-the effects of a small canopy opening on throughfall, soil moisture and tree transpiration in Suserup Skov, Denmark. Ecol. Bull. 52, 81–102.
Deguchi, A., Hattori, S., Park, H.-T., 2006. The influence of seasonal changes in canopy structure on interception loss: application of the revised Gash model. J. Hydrol. 318, 80–102.
Droogers, P., 2000. Estimating actual evapotranspiration using a detailed agro-hydrological model. J. Hydrol. 229, 50–58.
Dünisch, O., Morais, R.R., 2002. Regulation of xylem sap flow in an evergreen, a semi-deciduous, and a deciduous Meliaceae species from the Amazon. Trees 16, 404–416.
DWD, 2009. Deutscher Wetterdienst, Last visited: 10/01/2009 http://www.dwd.de.
Engel, T., Priesack, E., 1993. Expert-N, a building block system of nitrogen models as resource for advice, research, water management and policy. In: Eijsackers, H.J.P., Hamers, T. (Eds.), Integrated Soil and Sediment Research: A Basis for Proper Protection. Kluwer Academic Publishers, Dordrecht, The Netherlands, pp. 503–507.
FAO, 2005. Global forest resources assessment 2005. In: FAO Forestry Paper 147. FAO, Rome.
Feddes, R.A., Kowalik, P.J., Zaradny, H., 1978. Simulation of field water use and crop yield. In: Simulation Monographs. Pudoc, Wageningen.
Fischer, B., Goldberg, V., Bernhofer, C., 2008. Effect of a coupled soil water-plant gas exchange on forest energy fluxes: simulations with the coupled vegetation-boundary layer model HIRVAC. Ecol. Model. 214, 75–82.
Gale, M.R., Grigal, D.F., 1987. Vertical root distributions of northern tree species in relation to successional status. Can. J. Forest Res. 17, 829–834.
Gash, J.H.C., Lloyd, C.R., Lachaud, G., 1995. Estimating sparse forest rainfall interception with an analytical model. J. Hydrol. 170, 79–86.
Gebauer, T., 2010. Water turn over in species-rich and species-poor deciduous forests: xylem sap flow and canopy transpiration. Biodiversity and Ecology Series B, vol. 4. Göttingen Centre for Biodiversity and Ecology, University of Göttingen, Göttingen.
Gebauer, T., Horna, V., Leuschner, C., 2008. Variability in radial sap flux density patterns and sapwood area among seven co-occurring temperate broad-leaved tree species. Tree Physiol. 28, 1821–1830.
Granier, A., 1985. Une nouvelle méthode pour la mesure du flux de sève brute dans le tronc des arbres. Ann. Forest Sci. 42, 193–200.
Granier, A., 1987. Evaluation of transpiration in a Douglas-fir stand by means of sap flow measurements. Tree Physiol. 3, 309–320.
Granier, A., Huc, R., Barigah, S.T., 1996. Transpiration of natural rain forest and its dependence on climatic factors. Agric. Forest. Meteorol. 78, 19–29.
Granier, A., Biron, P., Lemoine, L., 2000. Water balance, transpiration and canopy conductance in two beech stands. Agric. Forest. Meteorol. 100, 291–308.
Guckland, A., Jacob, M., Flessa, H., Thomas, F.M., Leuschner, C., 2009. Acidity, nutrient stocks and organic matter content in soils of a temperate deciduous forest with different abundance of European beech (*Fagus sylvatica* L.). J. Plant Nutr. Soil Sci. 172, 500–511.
Herbst, M., Roberts, J.M., Rosier, P.T.W., Taylor, M.E., Gowing, D.J., 2007. Edge effects and forest water use: a field study in a mixed deciduous woodland. For. Ecol. Manage. 250, 176–186.
Hoff, C., Rambal, S., Joffre, R., 2002. Simulating carbon and water flows and growth in a Mediterranean evergreen Qercus ilex coppice using the FOREST-BGC model. For. Ecol. Manage. 164, 121–136.
Hölscher, D., Koch, O., Korn, S., Leuschner, C., 2005. Sap flux of five co-occurring tree species in a temperate broad-leaved forest during seasonal soil drought. Trees 19, 628–637.
Hutson, J.L., Wagenet, R.J., 1992. LEACHM: leaching estimation and chemistry model. In: Research Series No. 92–93, Version 3. Department of Soil, Crop and Atmospheric Sciences, Ithaca, USA.
Iida, S., Ohta, T., Matsumoto, K., Nakai, T., Kuwada, T., Kononov, A.V., Maximov, T.C., van der Molen, M.K., Dolman, H., Tanaka, H., Yabuki, H., 2009. Evapotranspiration from understory vegetation in an eastern Siberian boreal larch forest. Agric. Forest. Meteorol. 149, 1129–1139.
INRA, 2009. L'Institut National de Recherche Agronomique: French National Institute for Agricultural Research, Last visited: 10/01/2009 http://www.avignon.inra.fr/can_eye/.
Jacob, M., Leuschner, C., Thomas, F.M., 2010. Productivity of temperate broad-leaved forest stands differing in tree species diversity. Ann. Forest Sci. 67, 503.
Javaux, M., Schröder, T., Vanderborght, J., Vereecken, H., 2008. Use of a three-dimensional detailed modeling approach for predicting root water uptake. Vadose Zone J. 7, 1079–1088.
Kelliher, F.M., Köstner, B.M.M., Hollinger, D.Y., Byers, J.N., Hunt, J.E., McSeveny, T.M., Meserth, R., Weir, P.L., Schulze, E.-D., 1992. Evaporation, xylem sap flow, and tree transpiration in a New Zealand broad-leaved forest. Agric. Forest. Meteorol. 62, 53–73.
Klaassen, W., Bosveld, F., de Water, E., 1998. Water storage and evaporation as constituents of rainfall interception. J. Hydrol. 212–213, 36–50.
Köcher, P., Gebauer, T., Horna, V., Leuschner, C., 2009. Leaf water status and stem xylem flux in relation to soil drought in five temperate broad-leaved tree species with contrasting water use strategies. Ann. For. Sci. 66, 101–112.
Korn, S., 2004. Experimentelle Untersuchung der Wasseraufnahme und der hydraulischen Eigenschaften des Wurzelsystems von sechs heimischen Baumarten. PhD Thesis. Georg-August-Universität Göttingen, Göttingen.

Krämer, I., Hölscher, D., 2009. Rainfall partitioning along a tree diversity gradient in a deciduous old-growth forest in Central Germany. Ecohydrology 2, 102–114.

Krämer, I., Hölscher, D., in press. Soil water dynamics along a tree diversity gradient in a deciduous forest in Central Germany. Ecohydrology, doi:10.1002/eco.103.

Lai, C.-T., Katul, G., 2000. The dynamic role of root-water uptake in coupling potential to actual transpiration. Adv. Water Resour. 23, 427–439.

Leuschner, C., Jungkunst, H.F., Fleck, S., 2009. Functional role of forest diversity: pros and cons of synthetic stands and across-site comparisons in established forests. Basic Appl. Ecol. 10, 1–9.

Lüttschwager, D., Rust, S., Wulf, M., Forkert, J., Hüttl, R.F., 1999. Tree canopy and herb layer transpiration in three Scots pine stands with different stand structures. Ann. Forest Sci. 56, 256–274.

Marin, C.T., Bouten, I.W., Dekker, S., 2000. Forest floor water dynamics and root water uptake in four forest ecosystems in northwest Amazonia. J. Hydrol. 237, 169–183.

Meinen, C., 2008. Fine root dynamics in broad-leaved deciduous forest stands differing in tree species diversity. PhD Thesis. University of Göttingen, Göttingen.

Meinen, C., Leuschner, C., Ryan, N.T., Hertel, D., 2009. No evidence of spatial root system segregation and elevated fine root biomass in multi-species temperate broad-leaved forests. Trees 23, 941–950.

Mitchell, K., 2005. The community Noah land surface model (LSM). In: User's Guide Public Release Version 2.7.1, Last visited: 10/01/2009 ftp://ftp.emc.ncep.noaa.gov/mmb/gcp/ldas/noahlsm/ver_2.7.1.

Mölder, A., Bernhardt-Römermann, M., Schmidt, W., 2008. Herb-layer diversity in deciduous forests: raised by tree richness or beaten by beech? For. Ecol. Manage. 256, 272–281.

Monteith, J.L., 1965. Evaporation and the environment. Proc. Symp. Soc. Exp. Biol. 19, 205–234.

Monteith, J.L., 1981. Evaporation and surface temperature. Q. J. R. Meteorol. Soc. 107, 1–27.

Moore, K.E., Fitzjarrald, D.R., Sakai, R.K., Goulden, M.L., Munger, J.W., Wofsy, S.C., 1996. Seasonal variation in radiative and turbulent exchange at a deciduous forest in central Massachusetts. J. Appl. Meteorol. 35, 122–134.

Nordén, U., 1991. Acid deposition and throughfall fluxes of elements as related to tree species in deciduous forests of South Sweden. Water Air Soil Pollut. 60, 209–230.

Ogée, J., Brunet, Y., 2002. A forest floor model for heat and moisture including a litter layer. J. Hydrol. 255, 212–233.

Oishi, A.C., Oren, R., Novick, K.A., Palmroth, S., Katul, G.G., 2010. Interannual invariability of forest evapotranspiration and its consequence to water flow downstream. Ecosystems 13, 421–436.

Pataki, D.E., Oren, R., 2003. Species differences in stomatal control of water loss at the canopy scale in a mature bottomland deciduous forest. Adv. Water Resour. 26, 1267–1278.

Pataki, D.E, Oren, R., Smith, W.K., 2000. Sap flux of co-occurring species in a western subalpine forest during seasonal soil drought. Ecology 81, 2557–2566.

Peck, A.K., 2004. Hydrometeorologische und mikroklimatische Kennzeichen von Buchenwäldern. Berichte des Meteorologischen Institutes der Universität Freiburg Nr. 10. University of Freiburg, Freiburg.

Perrochet, P., 1987. Water uptake by plant roots—a simulation model, I. conceptual model. J. Hydrol. 95, 55–61.

Price, A.G., Carlyle-Moses, D.E., 2003. Measurement and modelling of growing-season canopy water fluxes in a mature mixed deciduous forest stand, southern Ontario, Canada. Agric. Forest. Meteorol. 119, 69–85.

Priesack, E., Achatz, S., Stenger, R., 2001. Parameterisation of soil nitrogen transport models by use of laboratory and field data. In: Shaffer, M.J., Ma, L., Hansen, S. (Eds.), Modelling Carbon and Nitrogen Dynamics for soil Management. CRC Press, Boca Raton, USA, pp. 461–484.

Schaap, M.G., Leij, F.J., van Genuchten, M.T., 2001. ROSETTA: a computer program for estimating soil hydraulic parameters with hierarchical pedotransfer functions. J. Hydrol. 251, 163–176.

Schipka, F., Heimann, J., Leuschner, C., 2005. Regional variation in canopy transpiration of Central European beech forests. Oecologia 143, 260–270.

Schlichting, E., Blume, H.-P., Stahr, K., 1995. Bodenkundliches Praktikum, Pareys Studientexte, vol. 81. Blackwell Wissenschafts-Verlag, Wien.

Schmidt, I., Leuschner, C., Mölder, A., Schmidt, W., 2009. Structure and composition of the seed bank in monospecific and tree species-rich temperate broad-leaved forests. For. Ecol. Manage. 257, 695–702.

Schwärzel, K., Häntzschel, J., Grünwald, T., Köstner, B., Bernhofer, C., Feger, K.-H., 2007. Fundamentals of the spatially distributed simulation of the water balance of forest sites in a low-range mountain area. Adv. Geosci. 11, 43–47.

Schwärzel, K., Feger, K.-H., Häntzschel, J., Menzer, A., Spank, U., Clausnitzer, F., Köstner, B., Bernhofer, C., 2009. A novel approach in model-based mapping of soil water conditions at forest sites. For. Ecol. Manage. 258, 2163–2174.

Sen, O.L., Shuttleworth, W.J., Yang, Z.-L., 2000. Comparative Evaluation of BATS2, BATS, and SiB2 with Amazon Data. J. Hydrometeorol. 1, 135–153.

Šimunek, J., Huang, K., van Genuchten, M.T., 1998. The HYDRUS code for simulation the one-dimensional movement of water, heat, and multiple solutes in variably-saturated media. In: Version 6.0, Research Report No. 144. U.S. Salinity Laboratory, USDA, ARS, Riverside, CA, USA.

Stenger, R., Priesack, E., Engel, T., Expert, N., 1999. A tool for simulating nitrogen and carbon dynamics in the soil–plant–atmosphere system. In: Tomer, M., Robinson, M., Gielen, G. (Eds.), NZ Land Creatment Collective Proceedings Technical Session 20: Modelling of Land Treatment Systems. New Plymouth, New Zealand, pp. 19–28.

van Dijk, A.I.J.M., Keenan, R.J., 2007. Planted forests and water in perspective. For. Ecol. Manage. 251, 1–9.

van Genuchten, M.T., 1980. A closed-form equation for predicting the hydraulic conductivity of unsaturated soils. Soil Sci. Soc. Am. J. 44, 892–898.

Vincke, C., Granier, A., Bréda, N., Devillez, F., 2005a. Evapotranspiration of a declining *Quercus robur* (L.) stand from 1999 to 2001. II. Daily actual evapotranspiration and soil water reserve. Ann. Forest Sci. 62, 615–623.

Vincke, C., Breda, N., Granier, A., Devillez, F., 2005b. Evapotranspiration of a declining *Quercus robur* (L.) stand from 1999 to 2001. I. Trees and forest floor daily transpiration. Ann. Forest Sci. 62, 503–512.

Wilson, K.B., Hanson, P.J., Mulholland, P.J., Baldochhi, D.D., Wullschleger, S.D., 2001. A comparison of methods for determining forest evapotranspiration and its components: sap-flow, soil water budget, eddy covariance and catchment water balance. Agric. Forest. Meteorol. 106, 153–168.

Wullschleger, S.D., Hanson, P.J., 2006. Sensitivity of canopy transpiration to altered precipitation in an upland oak forest: evidence from a long-term field manipulation study. Global Change Biol. 12, 97–109.

Wullschleger, S.D., Hanson, P.J., Todd, D.E., 2001. Transpiration from a multi-species deciduous forest as estimated by xylem sap flow techniques. For. Ecol. Manage. 143, 205–213.

3 Using terrestrial laser scanner data for a functional-structural water flow model of three broad-leaved tree species

Sebastian Bittner, Michael Janott, Daniel Ritter, Paul Köcher, Friedrich Beese, Eckart Priesack

Abstract

A functional-structural (FS) model of tree water flow is applied for single trees in an old-growth temperate broad-leaved forest stand. Roots, stems and branches are represented by connected porous cylinder elements that are divided into the inner heartwood cylinders surrounded by xylem and phloem. Xylem water flow is simulated by applying a non-linear Darcy water flow in porous media driven by the water potential gradient according to the cohesion-tension theory. The flow model is based on physiological input parameters such as the hydraulic conductivity, stomatal response to leaf water potential and root water uptake capability and, thus, can reflect the different properties of the tree species *Fagus sylvatica*, *Tilia cordata* and *Fraxinus excelsior*. The structure of the canopy is obtained by applying an automatic tree skeleton extraction algorithm from point clouds obtained by terrestrial laser scans allowing an explicit representation of the water flow path in the stem and branches. Supported by measurements of stem sap flow, the model reveals differences among tree species in the diurnal and daily dynamics of tree water flow and shows that stored water contributes to a significant amount of the daily transpiration of single trees (mean values $20\,\% - 29\,\%$). Due to its mechanistic foundation, the model can be parametrized for many tree and plant species and is applicable to various climatic and soil water conditions.

3.1 Introduction

Diversity effects on ecological functioning are increasingly investigated, and recently forest diversity has been the focus of observational and modeling studies [Leuschner et al., 2009, Healy et al., 2008, Thompson et al., 2009, Scherer-Lorenzen et al., 2005, Nadrowski et al., 2010]. Some studies have confirmed that the number of species can increase ecosystem functions such as productivity and stability [Thompson et al., 2009] mostly because of the complementary use of resources in mixed stands. In their review of the role of tree species diversity for ecosystem functioning on stand-levels, Nadrowski et al. [2010] state that the properties of a particular tree species may have a strong influence on the ecosystem functions and may turn into biodiversity effects when adopting a multifunctional perspective. The authors conclude that studies on biodiversity can profit from information gained on the scale of individual trees. This approach was successfully applied in the modeling study of Kirwan et al. [2009], in

which the authors traced diversity effects down to the interactions of individuals.

In this study, an individual tree water uptake flow model is parametrized to three different tree species (*F. sylvatica* L., *T. cordata* Mill. and *F. excelsior* L.) in an old-growth temperate deciduous forest in Germany and coupled to the soil-plant-atmosphere system. The different tree species have been studied extensively in preceding studies and show differences not only in their physiological properties in terms of hydrology but also in their structural properties. The structure of the old-growth beech, ash and lime differ with respect the aboveground leaf distribution and canopy shape [Frech et al., 2003] as well as the radial fine root distribution in the soil [Meinen et al., 2009]. Additionally, the physiological differences and their impact on hydrological traits have been studied in the Hainich forest with respect to branch water flux densities [Gebauer et al., 2008, Köcher et al., 2009, Hölscher et al., 2005], leaf water status [Köcher et al., 2009], and radial and axial root conductivities [Korn, 2004, Coners, 2001, Rewald, 2008]. While the knowledge of single species-specific functional traits is substantial, it remains a challenge to describe the total water use strategy of the trees, i.e., the interaction of structural and physiological properties and the identification of the single traits that influence the total hydraulic behavior most.

A mechanistic approach to simulate the water flow through the tree xylem has recently been developed [Aumann and Ford, 2002, Bohrer et al., 2005, Kumagai, 2001, Arbogast et al., 1993, Früh and Kurth, 1999, Janott et al., 2011]. The approach is based on the assumption that the tree xylem is a porous medium that conducts a non-linear Darcy water flow caused by the atmospheric demand of water according to the cohesion-tension theory. The model uses an explicit architecture of the canopy branches and of the root system allowing the simulation of the soil-plant-atmosphere water exchange. The physiological characteristics of different tree species are included in the model by defining the hydrological properties of the branches and roots in the model. The input parameters are physical properties of the xylem such as the elastic modulus, the maximal axial specific hydraulic conductivity and the ratio of the xylem area to the basal area. The functional part of the FS model is thus defined by the a set of physical properties of the wood material, whereas the structure is given by the position of single cylinders representing the canopy or root parts of the tree.

This study uses terrestrial laser scanner (TLS) images to obtain the structure of the

aboveground portions of the trees. The output data of the TLS (three-dimensional point clouds) are used to automatically extract a tree skeleton [Xu et al., 2007] and to divide it into small cylinders that conduct water. In the last decade, TLS technology has become a useful tool for forest inventory and for assessing structural forest stand parameters and the properties of single trees [van Leeuwen and Nieuwenhuis, 2010]. Applications of TLS in ecological modeling, especially in functional-structural models, are still rare and have been developed only recently [Van der Zande et al., 2009, Patenaude et al., 2008].

The aim of this study is to quantify the contributions of different tree species to total stand canopy transpiration to enable the analysis of biodiversity effects on stand water use. The integration of functional and structural information by the model makes it possible to quantify the influence of single tree characteristics in the model and to describe a species-specific behavior for water use.

3.2 Materials and Methods

3.2.1 Study area

The study site is located in a deciduous forest in the Hainich National Park (Thuringia, Germany). Minimal forest management has taken place due to the military training status of the area since the 1960s. Since 1990, the site has not been managed at all due to its national park status; therefore, the forest has a near-natural state. The selected trees were located in an old-growth forest stand with a closed canopy. The parent rock of the site is Triassic limestone covered with a loess layer of variable depth. The soil type is a Luvisol that dries out strongly during the summer and shows stagnant properties in the winter and spring. The soil texture was characterized by high silt content and low sand content (silt loam to silt clay loam, Guckland et al. [2009]). The groundwater table is found far below the rooting zone.

This study analyzed five groups (cluster), each consisting of three trees of the species *F. sylvatica* (beech), *T. cordata* (lime) and *F. excelsior* (ash) of two functional wood types. Beech and lime are diffuse-porous species and differ in the xylem anatomy from the ring-porous ash. The area of the stem and branches that is hydroactive is much smaller in ring-porous species than in diffuse-porous species, and water is conducted only by few outer year rings in ash [Gebauer et al., 2008, Herbst et al.,

36

2007].

In total, five clusters were analyzed: two clusters contained one tree of each tree species, and the other three clusters were monospecific clusters of beech, lime, and ash. The three trees of each cluster formed a triangle with no other large trees inside. The areas of the triangles were between $3.7\,m^2$ and $46.8\,m^2$ (Tab. 3.1). The heights of the trees were between $23.1\,m$ and $32.1\,m$, and the diameters of the stems at a height of $1.30\,m$ (*dbh*) ranged from $24\,cm$ to $58\,cm$.

Cluster	Area m^2	Tree	dbh cm	A_{hydr} m^2	cpa[a] m^2	Height m
82	10.7	Bu54	37	12.9	43	23.9
		Li36	26	13.3	25	27.3
		Es6	37	42.5	40	25.7
83	46.8	Bu27	58	23.0	143	27.0
		Bu30	47	21.6	70	25.2
		Bu33	45	26.5	73	24.9
93	9.7	Es28	34	24.2	44	32.1
		Es22	29	37.5	11	30.3
		Es16	32	25.3	24	30.1
181	7.5	Li5	24	11.5	11.5	24.3
		Li7	32	11.8	31	25.2
		Li10	26	8.6	17	24.5
201	3.7	Es10	46	82.5	32	30.2
		Li27	26	11.5	18	23.1
		Bu97	24	5	4	30.1

cpa, crown projection area; *dbh*, diameter at breast height
[a]M. Jacob, unpublished data.

Table 3.1: Characteristics of clusters and trees.

3.2.2 Hydrological measurements

Hourly values for precipitation, global radiation, air temperature, wind speed, and relative air humidity for the year 2009 were obtained from the Weberstedt/Hainich weather station (Meteomedia GmbH), located about $2\,km$ from the study site. At the 5 clusters the volumetric soil water content was measured using a frequency domain reflectometry (FDR) probe (Diviner 2000 FDR sensors, Sentek Pty Ltd.,

Stepney, Australia) at the middle of the triangle formed by the 3 cluster trees at a depth of $20\,cm$ (M. Meißner, personal communication).

For the 15 study trees, the sap flux density in the stem was monitored with the constant-heat method as described previously [Granier, 1987]. Two $20\,mm$-long (ash: $10\,mm$) Granier type probes were inserted at a distance of $15\,cm$ from each other at lower and higher insertion points on the stem at $1.3\,m$ height. The upper probe was constantly heated ($200\,mW$), while the lower one monitored the reference temperature of the stem. The temperature difference between the heated and reference probes was recorded continuously and related to the maximum temperature difference occurring at predawn when minimum or no flow occurred. Sap flux density (J_s, $g\,m^{-2}\,s^{-1}$) was calculated according to the empirical equation given by Granier [1987] for beech and lime and according to the empirical equation given by Herbst et al. [2007] for ash. We used data from a prior study [Gebauer et al., 2008] that investigated radial patterns and changes in sapwood area with tree size for the same tree species at the same forest site to calculate the total stem sap flux of a single tree (S_s, $kg\,d^{-1}$). Sap flux data were logged every $30\,s$ and a mean value was recorded every $30\,min$ over the whole vegetation period of 2009. In the period from 22/5/2009 to 26/6/2009, the logger provided continuous reliable data for 13 of the 15 trees. Therefore, this time period was chosen as the period to compare the simulated and measured values of sap flux (observation period).

We measured the conductance [$kg\,m\,MPa^{-1}\,s^{-1}$] of 12 root segments and 12 branch segments per tree species, using the method of Sperry et al. [1988]. Additionally, the area [m^2] of the hydroactive xylem was measured to calculate the specific axial hydraulic conductivity [$kg\,m^{-1}\,MPa^{-1}\,s^{-1}$] of the elements.

3.2.3 Terrestrial Laser Scans

The *Zoller+Fröhlich Imager 5006* (Zoller+Fröhlich GmbH, Germany) terrestrial laser scanner was used to scan the canopies of the tree groups in spring 2009 before the leaves had developed at nearly windless weather conditions. The scanner has a range measurement standard deviation of $0.1\,mm$ and a beam divergence of $0.22\,mrad$. It operates on the principle of phase difference measurements of emitted and received laser beams. The angular spacing between two measurements was 0.0018° at a beam diameter at $20\,m$ distance of $5.2\,mm$. To gather a complete 3D point cloud of the tree group and to avoid shadowing effects, 7 scans were made at positions in the

center and around the cluster. All scan setup positions were referenced in a local coordinate system using reflectors and reference targets with a positional average standard deviation of less than $12\,mm$ for all coordinate axes.

The single trees had to be identified for the input of the skeleton algorithm (sec. 3.2.5). The point cloud was therefore divided into subsets of points that belonged to the canopies of the single trees by visual inspection, and points that did not belong to any tree, such as reflections of the forest floor, were removed.

3.2.4 Water flow model

3.2.4.1 Soil water flow

The soil water dynamics are strongly influenced not only by the water uptake by the tree roots but also by the other processes of the one-dimensional soil-vegetation-atmosphere water transfer (SVAT). First, the infiltration of water into the soil is determined by calculating the canopy rainfall interception using the revised Gash interception model [Gash et al., 1995] and the surface runoff. The output is given by the drainage water, the vegetation transpiration and the soil evaporation. The percolation of water inside the soil profile is determined by the Richards equation using retention curves for the soil that had been estimated from structural soil properties such as texture and bulk density. A 1D-SVAT simulation has been performed on $50\,m \times 50\,m$ size plots that contained the trees from the present study or trees that were less than $150\,m$ from the trees [Bittner et al., 2010]. This simulation was validated by soil water contents monitored from 2005 to 2007. We used the same soil water sub-model as described by Bittner et al. [2010] but substituted the simple 1D water uptake function by the single tree model described below.

3.2.4.2 Water flow within the trees

The model assumes the xylem water flow to be driven by a xylem water potential gradient, as described by the cohesion-tension theory [Tyree and Zimmermann, 2002]. A non-linear water flow is based on Darcy's law for porous media and includes a water capacity term to better account for the dynamic behavior of the hydraulic storage in trees in a way that mass conservation can be directly calculated [Aumann and Ford, 2002, Bohrer et al., 2005, Kumagai, 2001, Arbogast et al., 1993, Früh

and Kurth, 1999]. Only recently, this approach was extended to the root system by Janott et al. [2011] and will be described below.

The pathway of the water from the soil to the atmosphere is discretized into finite elements. Components of the tree architecture such as the stem, branches and roots are simulated as connected cylinders that conduct water according to Darcy's law for water flow in porous media. The water exchange between two cylinder elements depends on the hydraulic gradient between the elements and the water conductance of the single elements. Similar to the water dynamics in the soil, the volumetric xylem sapwood water content $\theta\,[mm^3\,mm^{-3}]$ depends non-linearly on the xylem matric potential $\psi\,[mm]$. For values of ψ that are larger than the air entry value $(\psi \geq a)$, no cavitation of xylem vessels occurs, and the air content of the xylem is zero. Due to the elastic expansion of the xylem, the volumetric xylem sapwood water content changes linearly with ψ

$$\theta(\psi) = (\epsilon - \theta(a))\,(\frac{a - \psi}{a}) + \theta(a),\ \psi \geq a, \tag{3.1}$$

defining the xylem sapwood porosity $\epsilon\,[mm^3\,mm^{-3}]$ as the ratio of the maximal volume of xylem water at saturation to the maximal total volume of the xylem sapwood in the tree element. Next to the porosity, the shape of this xylem water retention curve is given by the elastic modulus of the xylem sapwood $E\,[mm]$ defined by

$$\theta(a) = \epsilon + \frac{a}{E}. \tag{3.2}$$

At dry conditions and high negative xylem water potentials $(\psi < a)$ cavitations occur, and the model assumes a reversible decrease of the xylem sapwood content, according to a Brooks and Corey water retention function [Brooks and Corey, 1966]

$$\theta(h) = \theta(a)\,(\frac{\psi}{a})^{\lambda},\ \psi < a, \tag{3.3}$$

with the Brooks and Corey exponent $\lambda\,[-]$.

From the xylem water retention curve, we can derive the xylem hydraulic conductivity $k(\psi)\,mm\,s^{-1}$, based on the law of Hagen and Poiseuille for the mass flow rate of

water in a cylindrical pipe by considering bundles of such pipes

$$k(\psi) \;=\; k_{max} \begin{cases} \frac{\theta(a)}{\epsilon} + (1 - \frac{\theta(a)}{\epsilon})(\frac{a-\psi}{a})^2 & \psi \geq a \\ (\frac{\psi}{a})^{-\lambda\eta} & \psi < a, \end{cases} \tag{3.4}$$

with $\eta := 2/\lambda + 1$. The total conductance of a cylinder element $K(\psi)\ [mm^3\,s^{-1}]$ is given by multiplication of the specific conductivity with the hydroactive xylem area $A_x\ [mm^2]$ of the element. We calculated the water conducting area of the stem using the stem basal area and the ratio of xylem to basal area obtained by Gebauer et al. [2008] using a dye method. In this way, the sapwood and the hardwood are divided in the model, and the water flow occurs only in the outer hollow cylinder of the xylem sapwood. For all cylinder elements other than the stem, a pipe model [Tyree and Zimmermann, 2002] is assumed to calculate the distribution of sapwood area at branching points of the crown and the root system. The numerical calculation of the water exchange between the cylinders adapts a numerical solution for soil layer water exchange proposed by Ross [2003] to a tree graph.

The hydraulic properties of the tree cylinder elements are included through a set of four physical input parameters (k_{max} specific axial hydraulic conductivity, ϵ xylem porosity, A_x/A_{basal} fraction of sapwood to basal area, E elastic modulus) that can be measured or found in the literature for many different deciduous and coniferous tree species (sec. 3.3.1).

The model assumes that the properties are homogeneous in every cylinder element, but parameters can be easily subdivided to account for the differences between sun-exposed and shaded branches of beech. In this study, branch and root elements differ in their values of specific axial hydraulic conductivity ($k_{max,branch}$, $k_{max,root}$) according to measurements.

3.2.4.3 Atmospheric boundary condition and plant-soil interaction

The water flux is driven by the atmospheric demand for water and the transpiration at the leaves of the trees. Therefore the hourly potential transpiration ($T_{pot,PM}$, $l\,m^{-2}\,h^{-1}$) is first calculated using the standardized reference evapotranspiration Penman-Monteith equation on an hourly basis [Allen, 2005]. $T_{pot,PM}$ reflects the atmospheric demand for water including climatic input data such as wind speed,

air temperature, relative humidity, and the global radiation. The values given by the reference equation correspond to a potential evapotranspiration per square meter ground soil and have to be down-scaled to the potential transpiration of a single tree $T_{pot}\,[l\,h^{-1}]$. At this step, the question of how large the scaling factor was for a single tree (hydraulic area $A_{hydr}\,[m^2]$) arises, so that $T_{pot} = T_{pot,PM}\,A_{hydr}$ [Crosbie et al., 2007]. Different measures such as stem diameter, crown projection area [Čermák et al., 2004] and leaf area [Pereira et al., 2006] are usually used to estimate A_{hydr}. However, observations at the Hainich forest have shown that the hydraulic area to crown projection area differs for the tree species and also depends on the size of the tree [Gebauer, 2010a]. Stand-level simulations of the site [Bittner et al., 2010] assumed a hydrological area that was smaller than the actual soil surface area covered by the trees, and the standardized reference evapotranspiration Penman-Monteith method was adapted to the forest site.

We calculated A_{hydr} for every single tree using the measured sap flux of the tree. The hydraulic area A_{hydr} was adjusted so that the mean value of the simulated sap flux values equaled the mean measured values in the observation period. For the trees *Li5*, *Li27*, and *Bu97*, no sufficient measurement data were available, and A_{hydr} was estimated using similar-sized trees.

To account for the stomatal response of the leaves to low water potentials, the model considers a reduction of the potential transpiration based on the stomatal closure of the leaves. The potential tree transpiration is distributed to the k outer branches of the canopy and reduced by the stomatal closure of the leaves attached to the branches by

$$T_{act,i} = f_{stomatal,i}\,T_{pot,i}, \tag{3.5}$$

with $T_{pot} = \sum_{i=0}^{k} T_{pot,i}$.

The stomatal reduction of the leaves attached to branch i is given by

$$f_{stomatal,i} = max[0.1,\,\exp(-\left(\frac{-\psi_i}{St_b}\right)^{St_c})], \tag{3.6}$$

with the water potential of the branch $\psi_i\,[mm]$, and parameters $St_b\,[mm]$ and $St_c\,[1]$ describing the stomatal response to branch xylem water potentials following the approach of Bohrer et al. [2005]. These parameters were estimated using empirical

vulnerability curves of leaf conductance [Köcher et al., 2009].

Radial water flow between the soil-root interface is given by the volumetric flux j_r $[mm^3\,s^{-1}]$ that describes the amount of water exchanged between a root element and the one-dimensional soil layer

$$j_r = Lp_r\,s_r\,[\psi_s - \psi_r], \tag{3.7}$$

where $Lp_r\,[s^{-1}]$ is the radial conductivity between the root xylem and the soil, $s_r\,[mm^2]$ is the surface of the root element and ψ_s and $\psi_r\,[mm]$ are the water potentials of the soil and the root xylem, respectively. To get the sink term of the $1D$ soil water model, the volumetric flux has to be converted to an uptake in liter per soil surface area, and, therefore, the water uptake of a single tree was assumed to occur on the geometrical soil surface occupation given by the Voronoi cell [Voronoi, 1908] of the tree.

3.2.5 Canopy architecture model

The model can work with tree architectures that are obtained by other methods than terrestrial laser scanning (e.g., L-Systems or simple architecture models), but this study focuses on the automatic usage of TLS data as an input of the geometry of the canopy of old-growth deciduous forest stands.

The point cloud obtained by laser scans serves as the input for an automatic skeleton extraction algorithm [Verroust and Lazarus, 2000, Xu et al., 2007] that extracts the position of the trunk and the branches from a set of three-dimensional points that are located on the surface of the trees. The algorithm first generates a mathematical weighted tree graph by adding edges to the point cloud. Every point is connected by an edge to all points that have a distance lower than a critical distance in Euclidean space ($d_{min} = 0.1\,m$). Next, the path from a pre-selected source point (root point) to every point of the point cloud is calculated using Dijkstra's shortest path algorithm [Dijkstra, 1959]. The lengths of the shortest paths are used to sort the points into bins based on these lengths and graph adjacency. These bins contain a connected subset of points that have a path distance to the root point that is in the range of the particular bin. The center of mass of all points of a bin are then calculated and give the position of the cylinder element representing the canopy. The orientation and connectivity of the elements are further given by the adjacency of the single

bins.

We used scans of the unfoliated canopy to avoid shadowing of the laser by leaves and to get information not only about the stem and the main branches, but also about the position and orientation of smaller twigs of higher branching order (Fig. 3.1).
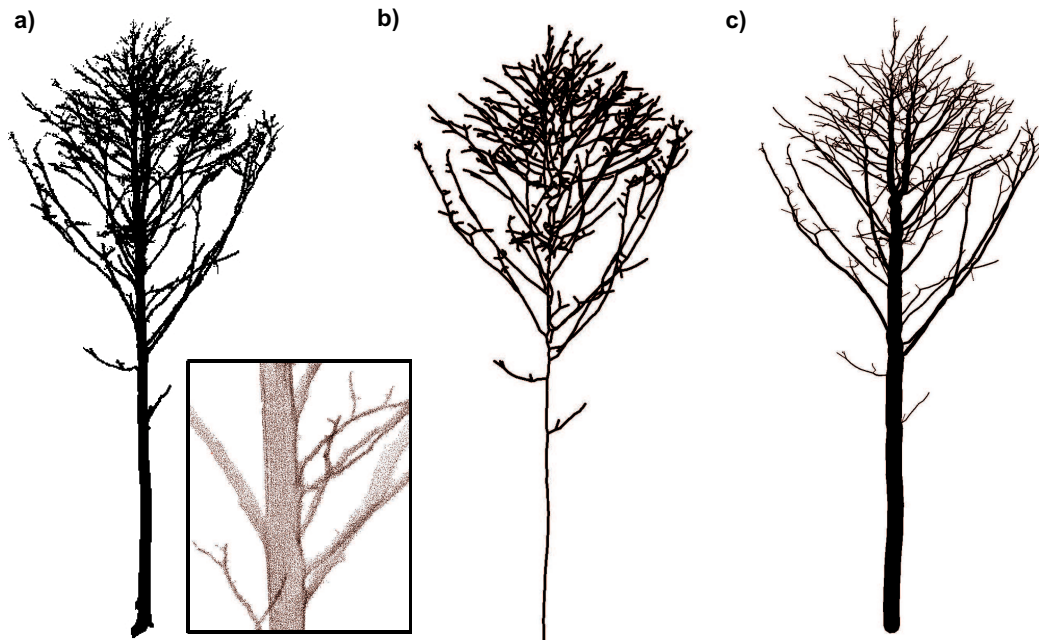

Figure 3.1: Structural representation of the tree canopy in the model. a) point cloud obtained by laser scanning, b) tree graph obtained by skeleton extraction algorithm, c) virtual canopy represented by cylinder elements

3.2.6 Root architecture model

In principle, it is also possible to use the laser scanner technique to obtain the structure of the root system [Gärtner et al., 2009]. Due to the National park status of the study site, it was not possible to excavate the root system of single trees completely. However, preceding studies [Meinen et al., 2009] have provided information on the spatial fine root distribution and total root surface area of the three tree species. We used these species-specific data to simulate the below-ground canopy using the vertical and horizontal fine root distribution, root area index and rooting depth. The root architecture is built by taproots that branch into vertical roots of second order according to the observed radial root distribution. The vertical

roots branch themselves into roots of higher branching order in a way that the observed vertical root density is reflected in the root model.

The root distribution of all three analyzed tree species is strongly influenced by the site soil conditions, leading to a narrow rooting zone with about $80\,\%$ of the fine root biomass in the upper $40\,cm$ of the soil profile. No segregation of space occupation was found at the site, and all three tree species showed a similar vertical fine root biomass distribution that could be described by an exponential distribution law [Meinen et al., 2009].

3.3 Results

3.3.1 Parametrization

Most physiological input parameters were obtained for the three tree species by own measurements at the study site (St_b, St_c, $k_{max,root}$, $k_{max,branch}$, Tab. 3.2) or could be found in other studies in the Hainich forest (Lp_r, Ax/A_b, ϵ). The parameters that described the size of the xylem water retention curve (E, a, λ) were taken from Oertli [1993] and Cochard et al. [2005].
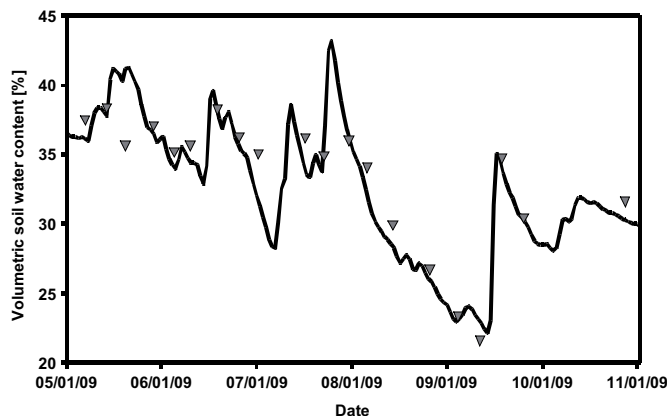
3.3.2 Simulation

Figure 3.2: Simulated (line) and measured (dots; M. Meißner, personal communication) volumetric soil water content at cluster $C83$ at a depth of $20\,cm$.

Symbol	Description	Unit	Value		
			beech	lime	ash
St_b	Stomatal response parameter	MPa	2.25	2.25	3.00
St_c	Stomatal response parameter	[-]	3.5	3.5	3.5
$k_{max,root}$	axial specific hydraulic conductivity of roots	$10^{-2}\,mm\,s^{-1}$	13.0	10.4	4.5
$k_{max,branch}$	axial specific hydraulic conductivity of branches	$10^{-2}\,mm\,s^{-1}$	1.7	0.7	1.8
Lp_r	radial root hydraulic conductivity [a]	$10^{-8}\,m\,MPa^{-1}\,s^{-1}$	4.7	28.0	7.8
ϵ	Xylem porosity[b]	$mm^3\,mm^{-3}$	0.52	0.72	0.59
A_x/A_b	Xylem area to basal area[b]	[-]	0.75	0.75	0.21
E	Elastic modulus [c]	$10^6\,mm$	3.5	3.5	3.5
a	xylem air entry value[c,d]	MPa	3.1	3.9	3.8
λ	Brooks and Corey parameter[c]	[-]	0.86	0.86	0.86

[a]Korn [2004], [b]Gebauer et al. [2008], [c]Oertli [1993],[d]Cochard et al. [2005]

Table 3.2: Physiological model input parameter values for the three tree species *F. sylvatica* (beech), *T. cordata* (lime), and *F. excelsior* (ash).

The simulated volumetric soil water contents at a depth of $20\,cm$ show dynamics that were similar to the observed values for the whole vegetation period of 2009 (Fig. 3.2). The root mean square error was below $4\,\%$ for all 5 simulated clusters.

The diurnal hourly values of tree transpiration showed a maximum around noon, and the root water uptake curve peaked two hours later. These water dynamics resulted
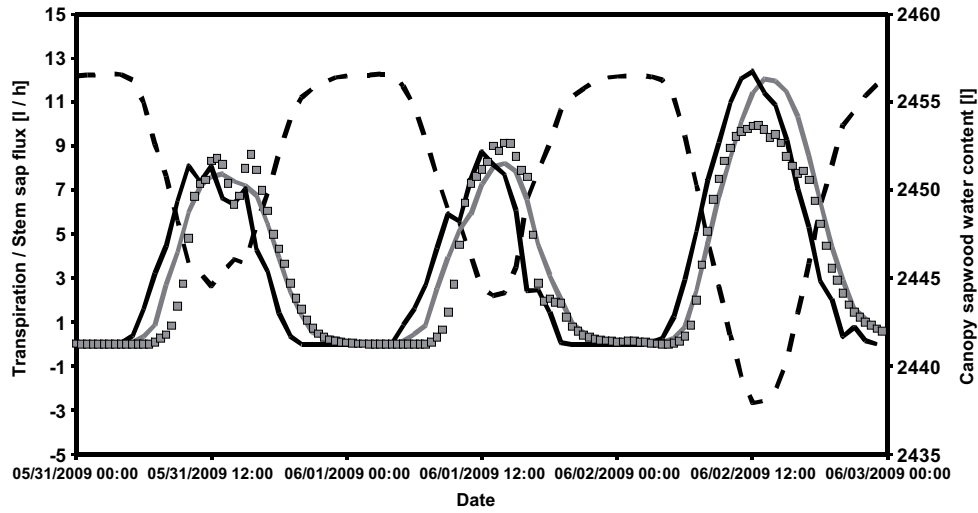

Figure 3.3: Diurnal patterns of simulated transpiration (solid black), simulated stem sap flux (solid gray), measured stem sap flux (gray dots) and simulated stored water (dashed black) in the beech tree $Bu27$.

in a depletion of the water stored in the xylem of the tree elements. For the five beech trees the water used from the canopy storage accounted for $15\,\% - 22\,\%$ (mean $20\,\%$) of the daily amount of transpiration. The values of lime ranged from $25\,\%$ to $35\,\%$ (mean $29\,\%$), and the values of ash ranged from $22\,\%$ to $26\,\%$ (mean $24\,\%$).

The simulated daily values of transpiration were similar to the simulated values of the water flux through the stem because the trees relaxated at night when the water reservoir was refilled nearly completely. The simulated values of water flux were driven by the potential transpiration of the tree, T_{pot}. T_{pot} is similar to the simulated actual transpiration, T_{act}, for the diffuse-porous species beech and lime (figure 3). The largest daily difference between T_{pot} and the simulated daily transpiration, T_{act}, during the observation period occurred on the day with the highest potential transpiration ($T_{pot,PM} = 5.2\,l\,m^2\,d^{-1}$;2/6/2009), and the ratio of T_{act}/T_{pot} was 0.93 for $Bu33$ and 0.96 for $Li10$ on that day. For the ring-porous species, ash, the
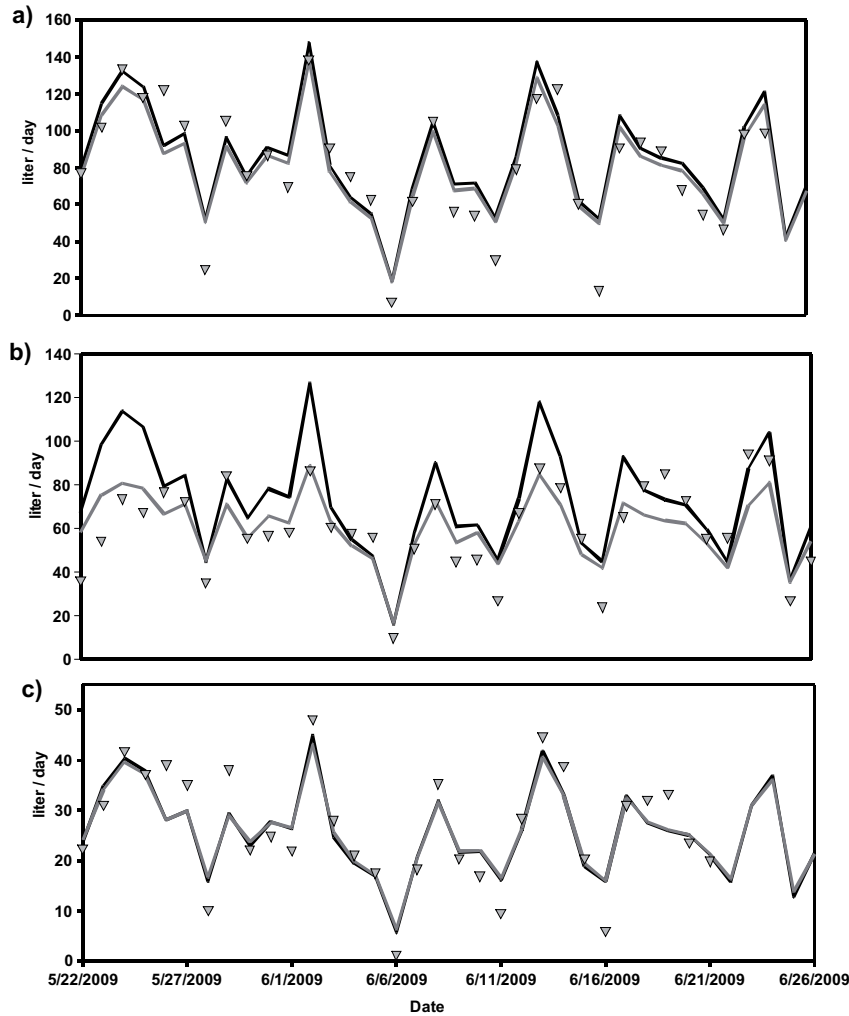
Figure 3.4: Daily values of potential transpiration (black line), simulated stem sap flux (gray line) and measured (triangles) stem sap flux. a) beech (*Bu*33), b) ash (*Es*28), c) lime (*Li*10)

differences between T_{pot} and T_{act} were higher than for the diffuse-porous species. The differences were particularly high on days with a high evaporative demand, and the minimal value was $T_{act}/T_{pot} = 0.42$ for *Es22*. The root mean square error ($RMSE$) between T_{pot} and T_{act} for all trees per species with available measurement values was $0.9\,l\,d^{-1}$ for beech, $1.4\,l\,d^{-1}$ for lime and $46.1\,l\,d^{-1}$ for ash. The normalized root mean square error ($NRMSE$), given by the ratio of the $RMSE$ and the mean value of the potential transpiration, was 0.01 for beech, 0.04 for lime and 0.64 for ash.

The values of stem sap flux calculated from heat flux measurements showed high accordance with the simulated values. The $RMSE$ and the $NRMSE$ between

measured and simulated sap flux were 9.4/0.15 for beech, 7.9/0.23 for lime and 15.4/0.21 for ash. In our model, the mean values of the simulated sap flux were calibrated to the measurement by adjusting T_{pot}; thus, the model performance with respect to the daily dynamic was of interest. The Nash-Sutcliffe model efficiency (NSE), as defined by Nash and Sutcliffe [1970] is an appropriate statistical criterion to evaluate the daily dynamic of the simulated sap flow values. The NSE values are dimensionless and can take values from $-\infty$ to 1.0. A value of $NSE = 1.0$ is given for a perfect match of simulation and observation; if $NSE \leq 0$, the model is not better than a model that uses the observed mean as a predictor. The NSE was > 0 for all trees for the observation period, and the mean NSE was 0.75 for beech, 0.59 for lime, and 0.21 for ash.

The sensitivity of the input parameters of the simulated daily values of transpiration to variation was analyzed on a day with a high potential transpiration ($T_{pot} = 5.2\,l\,m^{-2}\,d^{-1}$) for the trees *Bu33*, *Li10* and *Es28* (figure 4). The sensitivity
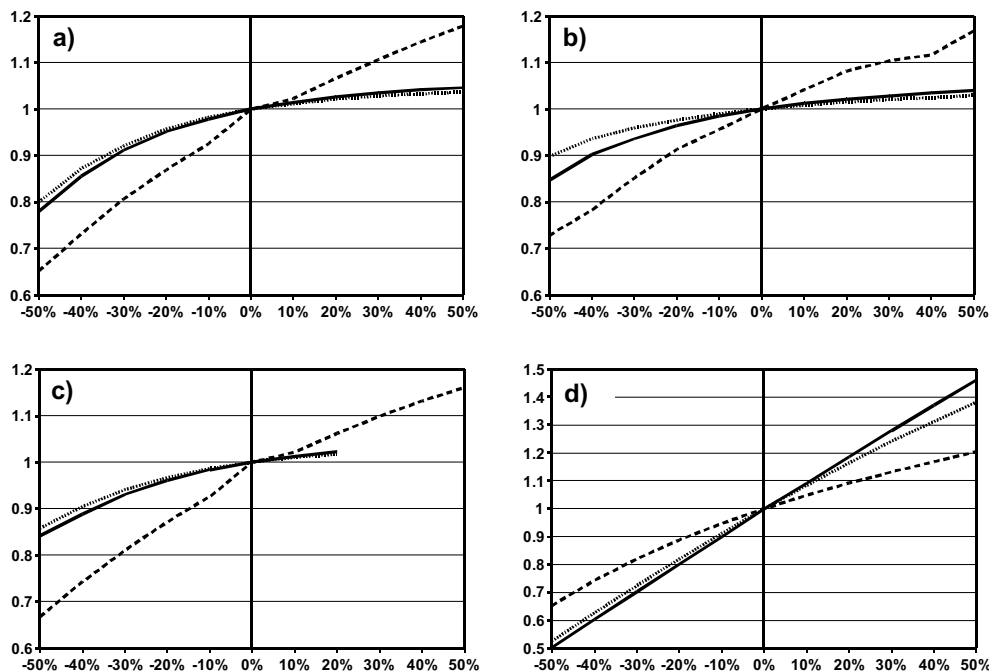

Figure 3.5: Relative change of the simulated daily transpiration when one input parameter is changed and the other input parameters are kept constant, according to table 1 and table 2. The figures show the sensibility of beech (solid), lime (dotted), and ash (dashed) on a day with $T_{pot} = 5.2\,l\,m^{-2}\,d^{-1}$. a) stomatal reaction ($St_b$), b) axial specific xylem hydraulic conductivities ($k_{max,branch}$ and $k_{max,root}$), c) xylem area to basal area ($A_x/A_b \leq 1.0$) and d) potential transpiration T_{pot}.

analysis contained parameters describing the plant-atmosphere boundary (stomatal response b, potential transpiration T_{pot}), the plant-soil boundary (root radial hydraulic conductivity Lp_r), and the total hydraulic conductance (axial maximal conductivities $k_{max,root}$ and $k_{max,branch}$, xylem area to basal area A_x/A_b). The most sensitive physiological parameter for all tree species was the parameter St_b, which described the stomatal closure with xylem water content, followed by the conductivities and the xylem to basal area. The model was not sensitive to the radial root hydraulic conductivity Lp_r for moist soil water conditions.

The diffuse-porous species beech and lime were sensible to a decrease in the the total hydraulic conductance by decreasing the axial conductivities or the xylem area fraction. In contrast, increasing these parameters by 50% led to an increase of the simulated transpiration of only about 5% because the simulated transpiration was already very close to the potential transpiration, which could not be exceeded in the model. The ring-porous ash showed a different behavior when the conductance parameters were increased. The slope of the diagram was similar for a decrease and an increase of the parameters for ash. A change of the potential transpiration led to a nearly proportional change in the simulated transpiration for beech and lime. For ash, the ratio of T_{act}/T_{pot} decreased from 0.69 to 0.55, when T_{pot} was increased by 50% and increased to 0.89 when T_{pot} was decreased by 50%.

3.4 Discussion

3.4.1 Simulation

The potential transpiration given by the Penman-Monteith equation has the most significant effect on the simulated values of daily transpiration because the model is directly driven by the potential transpiration. This behavior is supported by the observed dynamics of the measurements of the daily sap flux, which was highly correlated with T_{pot}, too. Other studies using the Granier heat flux method found a correlation between the Penman-Monteith potential transpiration and the observed sap flux [David et al., 1997, Pereira et al., 2006], but an overestimation of the flux by Penman-Monteith on days with low potential transpiration was also observed [David et al., 1997]. Our measurements (Fig. 3.3) are in agreement with this finding: the measured daily sap flux values were lower than the potential transpiration on days

with a potential transpiration lower than $2\,l\,mm^{-2}\,d^{-1}$. The simulations of the water use of ash especially showed that the simulations of tree hydrodynamics are able to enhance the model performance when compared to a simple Penman-Monteith driven model because the measured values of sap flux correlated better with our simulations than with simulation results from a model that uses the Penman-Monteith potential transpiration as a predictor of tree water use and a calculation of the actual transpiratio using the Feddes water uptake model [Bittner et al., 2010].

Daily values of the simulated transpiration revealed behaviors that were different between the ring-porous ash and the diffuse-porous species beech and lime. The ratio of T_{act}/T_{pot} was close to one for beech and lime, whereas the ratio was smaller for ash on days with medium and high T_{pot}. The different behaviors were consequences of the different physiology of the ring-porous and the diffuse-porous tree species reflected in the parameter of xylem fraction A_x/A_b. The measured specific axial hydraulic conductivity per xylem area as well as the xylem porosity are not significantly higher for ash which in combination with the lower value of A_x/A_b leads to a lower total hydraulic conductance of ash than beech and lime according to equation 3.4. The hydraulic conductance of ash was too low to supply the transpiring branches sufficiently with water extracted from soil at days of moderate and high evaporative demand. As a result, the water content of the branch element was low at mid-day, and the stomata closed according to the equation 3.5. The diffuse-porous species had a higher conductance that allowed a fast transport of soil water to the branches. The species-specific influence of conductance on the transpiration was also reflected in the sensitivity analysis (Fig. 3.4); a further increase in the conductance (directly proportional to the parameters A_x/A_b and k_{max}) increased the simulated transpiration of ash significantly but only slightly increased the simulated transpiration of beech and lime. Model uncertainties in calculating T_{pot} were a source of error because higher T_{pot} values can lead to a lower T_{act}/T_{pot} ratio. Lower values of T_{pot} can lead to higher values of T_{act}/T_{pot}, but the sensibility analysis showed that even with an increased T_{pot}, the ratio T_{act}/T_{pot} was close to 1 for beech and lime. In contrast, the atmospheric demand for water was still not satisfied in case of ash, even when T_{pot} was reduced on days with a high potential transpiration. The functional consequences of the different xylem anatomies of diffuse-porous, ring-porous, and coniferous species are observed and discussed in McCulloh et al. [2010]. The authors found the lowest conductances and lowest hydraulic efficiencies in coniferous species. Therefore, it would be interesting to apply our model also to coniferous species.

The simulated amount of water from the canopy water storage that was depleted every day was similar for all three tree species, and the values were similar to those from observational studies of the water storage of large old-growth trees. Similar values of water storage depletion were observed using sap flow measurements at different positions on the tree stem [Čermák et al., 2007, Goldstein et al., 1998] or by measuring the diurnal change of the stem diameter [Peramaki et al., 2001, Zweifel et al., 2001]. Some studies found lower values of water storage depletion [Čermák et al., 1984, Tyree and Yang, 1990] and concluded that the significance of the stored water depends on climatic and site conditions as well as tree size. Zweifel et al. [2001] calculated a fraction of 10 % on sunny days in contrast to a fraction of 65 % on cloudy days for a 6-year-old potted Norway spruce. In our calculations the variation was not as pronounced as in this observational study and the simulated amounts of water depletion in relation to the daily transpiration varied for beech between 13 % and 29 %, for lime between 16 % and 42 %, and for ash between 16 % and 33 %. The simulation showed a dependence on the climatic conditions but was more dependent on the daily pattern of potential transpiration than the total daily sum of potential transpiration. Interestingly, the values of the ring-porous ash were as high as those for the diffuse-porous species. The volumetric water content was lower in ash due to the low xylem area, but the gradients of the xylem water potential were higher in ash and resulted in larger changes in the simulated xylem water content.

3.4.2 Parametrization and sensitivity

Generally, it is possible to allocate every single tree cylinder element to a specific set of parameters to account for the inhomogeneity of the xylem anatomy in a tree [Cruiziat et al., 2002]. The hydraulic conductivity and the vulnerability to cavitation were found to differ between fine and coarse roots [Rewald, 2008] and depend on the depth of the roots at special site conditions [McElrone et al., 2004]. Above-ground parametrization of the stomatal reaction and the properties of the branches may depend on the grade of the sun exposition [Cochard et al., 1999, Lemoine et al., 2002] and the age of the woody elements [Phillips et al., 2002, Köstner et al., 2002, Tyree et al., 1998]. For the sake of simplicity and the lack of input parameters for lime and ash, the tree elements all have the same parameter values in this study, and the root and branch xylem parameters differ only by the value of the specific hydraulic conductivity.

The interaction of the tree and the soil is given by the root distribution, the root total surface, and the radial root hydraulic conductivity Lp_r. The simulations in this study revealed only a small sensitivity to the plant-soil boundary conditions because the soil water content was high in the observation period and the water uptake of the tree roots was not limited by available soil water. In this way, the uncertainties of the simulated root architecture and the root radial hydraulic conductivity Lp_r parametrization were small. In the case of limited soil water availability the model reacts with more sensitivity to the root distribution and Lp_r as was shown in simulated drying scenarios by Janott et al. [2011]. Therefore, we expect the root architecture to be more sensitive if the model is applied to simulate drought periods.

The values of the root radial hydraulic conductivity Lp_r are difficult to measure, but values for different deciduous and coniferous species are given in the literature [Korn, 2004, Coners, 2001, Steudle, 2000]. The values for beech, lime, and ash were obtained by Korn [2004] using *in situ* measurements of the root surface area and radial water flow into the roots as well as the water potential difference of the roots and the soil. The matric potential of the soil was measured using tensiometers; thus, the potential gradient also contains the rhizosphere, which is in accordance with the equation 3.7. The values for *Fagus sylvatica* were similar to the values obtained by Coners [2001] at the same forest site and by Steudle [2000] using xylem pressure probes under laboratory conditions.

Because the model is driven by the potential transpiration per tree T_{pot}, the hydraulic area A_{hydr} is an input parameter with a high sensitivity (Fig. 3.5). The sensitivity analysis shows that the difference in behaviour between ring-porous and diffuse-porous species is observed even if the values of A_{hydr} vary. Nevertheless, further studies should calculate the potential transpiration per single tree without calibration to sap flux measurements. This approach will avoid the uncertainties of the sap flux method [Bush et al., 2010, Herbst et al., 2007], and it is also advisable because sap flux measurements are often not available, especially when a large number of trees is analyzed. When laser scans of the foliated canopy are available, the up-scaling could be achieved by calculating the leaf area of the single trees [Hosoi and Omasa, 2006, Huang and Pretzsch, 2010] and then adjusting the Penman-Monteith method to the measured leaf area [Pereira et al., 2006].

3.5 Conclusion

The mechanistic single tree level approach of this study has advantages over stand level approaches, especially when species diversity effects of mixed forest stands are of interest. Combining structural and physiological information allows the model to describe the water dynamics of the soil-plant-atmosphere continuum and of single trees under moist soil water conditions. Furthermore, the contribution of the different species to the total stand transpiration can be calculated, thus enabling an analysis of the effect of biodiversity on the soil-plant atmosphere water cycle.

This study contributes to the understanding of the differences in water usage between diffuse-porous and ring-porous trees as well as the importance of the water stored in the wood material of large trees. The low area of hydroactive xylem in ash led to a water conductance that was too low to satisfy the evaporative demand and the ratio of simulated daily transpiration to potential transpiration was lower than the simulated values for the diffuse-porous beech and lime.

In future studies, the model will be used to analyze the different drought tolerance strategies of deciduous trees and to explain interactions of single trees. Aboveground, the spatial distribution of radiation and potential transpiration can be simulated by the coupling of the current model with a radiation model that simulates the light regime and, thus, the atmospheric water demand on branch scale. Belowground, interaction effects of tree species can be included below-ground using a 3D soil water flux model, keeping the root architecture in the present form.

Acknowledgments

References

R.G. Allen. *The ASCE standardized reference evapotranspiration equation.* Amer Society of Civil Engineers, 2005.

T. Arbogast, M. Obeyesekere, and M.F. Wheeler. Numerical methods for the simulation of flow in root-soil systems. *SIAM Journal on Numerical Analysis*, 30 (6):1677–1702, 1993.

C.A. Aumann and E.D. Ford. Modeling tree water flow as an unsaturated flow through a porous medium. *Journal of theoretical biology*, 219(4):415–429, 2002.

S. Bittner, U. Talkner, I. Krämer, F. Beese, D. Hölscher, and E. Priesack. Modeling stand water budgets of mixed temperate broad-leaved forest stands by considering variations in species specific drought response. *Agricultural and Forest Meteorology*, 150:1347–1357, 2010.

G. Bohrer, H. Mourad, T.A. Laursen, D. Drewry, R. Avissar, D. Poggi, R. Oren, and G.G. Katul. Finite element tree crown hydrodynamics model (FETCH) using porous media flow within branching elements: A new representation of tree hydrodynamics. *Water Resources Research*, 41(11):W11404, 2005.

RH Brooks and AT Corey. Properties of porous media affecting fluid flow. *J. Irrig. Drain. Div*, 6:61, 1966.

S.E. Bush, K.R. Hultine, J.S. Sperry, and J.R. Ehleringer. Calibration of thermal dissipation sap flow probes for ring-and diffuse-porous trees. *Tree Physiology*, 30 (12):1545, 2010.

J. Čermák, J. Jeník, J. Kučera, and V. Žídek. Xylem water flow in a crack willow tree (Salix fragilis L.) in relation to diurnal changes of environment. *Oecologia*, 64 (2):145–151, 1984.

J. Čermák, J. Kučera, and N. Nadezhdina. Sap flow measurements with some thermodynamic methods, flow integration within trees and scaling up from sample trees to entire forest stands. *Trees-Structure and Function*, 18(5):529–546, 2004.

J. Čermák, J. Kučera, W.L. Bauerle, N. Phillips, and T.M. Hinckley. Tree water storage and its diurnal dynamics related to sap flow and changes in stem volume in old-growth Douglas-fir trees. *Tree Physiology*, 27(2):181, 2007.

H. Cochard, D. Lemoine, and E. Dreyer. The effects of acclimation to sunlight on the

xylem vulnerability to embolism in Fagus sylvatica L. *Plant, Cell & Environment*, 22(1):101–108, 1999.

H. Cochard, G. Damour, C. Bodet, I. Tharwat, M. Poirier, and T. Améglio. Evaluation of a new centrifuge technique for rapid generation of xylem vulnerability curves. *Physiologia Plantarum*, 124(4):410–418, 2005.

H. Coners. *Wasseraufnahme und artspezifische hydraulische Eigenschaften der Feinwurzeln von Buche, Eiche und Fichte: In situ-Messungen an Altbäumen.* PhD thesis, Niedersächsische Staats-und Universitätsbibliothek Göttingen, 2001.

R.S. Crosbie, B. Wilson, J.D. Hughes, and C. McCulloch. The upscaling of transpiration from individual trees to areal transpiration in tree belts. *Plant and Soil*, 297(1):223–232, 2007.

P. Cruiziat, H. Cochard, and T. Améglio. Hydraulic architecture of trees: main concepts and results. *Annals of Forest Science*, 59(7):723–752, 2002.

TS David, MI Ferreira, JS David, and JS Pereira. Transpiration from a mature Eucalyptus globulus plantation in Portugal during a spring-summer period of progressively higher water deficit. *Oecologia*, 110(2):153–159, 1997.

E.W. Dijkstra. A note on two problems in connexion with graphs. *Numerische Mathematik*, 1(1):269–271, 1959.

A. Frech, C. Leuschner, M. Hagemeier, and D. Hölscher. Nachbarschaftsbezogene Analyse der Kronenraumbesetzung von Esche, Hainbuche und Winterlinde in einem artenreichen Laubmischwald (Nationalpark Hainich, Thüringen). *Forstwissenschaftliches Centralblatt*, 122(1):22–35, 2003.

T. Früh and W. Kurth. The hydraulic system of trees: Theoretical framework and numerical simulation. *Journal of Theoretical Biology*, 201(4):251–270, 1999.

H. Gärtner, B. Wagner, I. Heinrich, and C. Denier. 3D-laser scanning: a new method to analyze coarse tree root systems. *For. Snow Landsc. Res.*, 82(1):95–106, 2009.

JHC Gash, CR Lloyd, and G. Lachaud. Estimating sparse forest rainfall interception with an analytical model. *Journal of Hydrology*, 170(1-4):79–86, 1995.

T. Gebauer. *Water turnover in species-rich and species-poor deciduous forests: xylem sap flow and canopy transpiration.* PhD thesis, 2010a.

T. Gebauer, V. Horna, and C. Leuschner. Variability in radial sap flux density

patterns and sapwood area among seven co-occurring temperate broad-leaved tree species. *Tree physiology*, 28(12):1821, 2008.

G. Goldstein, JL Andrade, FC Meinzer, NM Holbrook, J. Cavelier, P. Jackson, and A. Celis. Stem water storage and diurnal patterns of water use in tropical forest canopy trees. *Plant, Cell & Environment*, 21(4):397–406, 1998.

A. Granier. Evaluation of transpiration in a Douglas-fir stand by means of sap flow measurements. *Tree Physiology*, 3(4):309, 1987.

A. Guckland, M. Jacob, H. Flessa, F.M. Thomas, and C. Leuschner. Acidity, nutrient stocks, and organic-matter content in soils of a temperate deciduous forest with different abundance of European beech (Fagus sylvatica L.). *Journal of Plant Nutrition and Soil Science*, 172(4):500–511, 2009.

C. Healy, N.J. Gotelli, and C. Potvin. Partitioning the effects of biodiversity and environmental heterogeneity for productivity and mortality in a tropical tree plantation. *Journal of Ecology*, 96(5):903–913, 2008.

M. Herbst, J.M. Roberts, P.T.W. Rosier, M.E. Taylor, and D.J. Gowing. Edge effects and forest water use: A field study in a mixed deciduous woodland. *Forest Ecology and Management*, 250(3):176–186, 2007.

D. Hölscher, O. Koch, S. Korn, and C. Leuschner. Sap flux of five co-occurring tree species in a temperate broad-leaved forest during seasonal soil drought. *Trees-Structure and Function*, 19(6):628–637, 2005.

F. Hosoi and K. Omasa. Voxel-based 3-D modeling of individual trees for estimating leaf area density using high-resolution portable scanning lidar. *IEEE Trans Geosci Remote Sens*, 44(12):3610, 2006.

P. Huang and H. Pretzsch. Using terrestrial laser scanner for estimating leaf areas of individual trees in a conifer forest. *Trees-Struct Funct*, in Press, 2010.

M. Janott, S. Gayler, A. Gessler, M. Javaux, C. Klier, and E. Priesack. A one-dimensional model of water flow in soil-plant systems based on plant architecture. *Plant and Soil*, 341:233–256, 2011.

L. Kirwan, J. Connolly, JA Finn, C. Brophy, A. Lüscher, D. Nyfeler, and MT Sebastià. Diversity-interaction modeling: estimating contributions of species identities and interactions to ecosystem function. *Ecology*, 90(8):2032–2038, 2009.

P. Köcher, T. Gebauer, V. Horna, and C. Leuschner. Leaf water status and stem xylem flux in relation to soil drought in five temperate broad-leaved tree species

with contrasting water use strategies. *Annals of Forest Science*, 66(1):101–101, 2009.

S. Korn. *Experimentelle Untersuchung der Wasseraufnahme und der hydraulischen Eigenschaften des Wurzelsystems von sechs heimischen Baumarten*. PhD thesis, Georg-August-Universität Göttingen, 2004.

B. Köstner, E. Falge, and JD Tenhunen. Age-related effects on leaf area/sapwood area relationships, canopy transpiration and carbon gain of Norway spruce stands (Picea abies) in the Fichtelgebirge, Germany. *Tree Physiology*, 22(8):567, 2002.

T. Kumagai. Modeling water transportation and storage in sapwood–model development and validation. *Agricultural and forest meteorology*, 109(2):105–115, 2001.

D. Lemoine, H. Cochard, and A. Granier. Within crown variation in hydraulic architecture in beech (Fagus sylvatica L): evidence for a stomatal control of xylem embolism. *Annals of forest science*, 59(1):19–27, 2002.

C. Leuschner, H.F. Jungkunst, and S. Fleck. Functional role of forest diversity: pros and cons of synthetic stands and across-site comparisons in established forests. *Basic and Applied Ecology*, 10(1):1–9, 2009.

K. McCulloh, J.S. Sperry, B. Lachenbruch, F.C. Meinzer, P.B. Reich, and S. Voelker. Moving water well: comparing hydraulic efficiency in twigs and trunks of coniferous, ring-porous, and diffuse-porous saplings from temperate and tropical forests. *New Phytologist*, 186(2):439–450, 2010.

A.J. McElrone, W.T. Pockman, J. Martínez-Vilalta, and R.B. Jackson. Variation in xylem structure and function in stems and roots of trees to 20 m depth. *New Phytologist*, 163(3):507–517, 2004.

C. Meinen, C. Leuschner, N.T. Ryan, and D. Hertel. No evidence of spatial root system segregation and elevated fine root biomass in multi-species temperate broad-leaved forests. *Trees-Structure and Function*, 23(5):941–950, 2009.

K. Nadrowski, C. Wirth, and M. Scherer-Lorenzen. Is forest diversity driving ecosystem function and service? *Current Opinion in Environmental Sustainability*, 2(1-2):75–79, 2010.

JE Nash and JV Sutcliffe. River flow forecasting through conceptual models part I–A discussion of principles. *J Hydrol*, 10(3):282–290, 1970.

J. J. Oertli. Effect of cavitation on the status of water in plants. In M. Borghetti, J. Grace, and A. Raschi, editors, *Water Transport in Plants Under Climatic Stress*, pages 27–40. Cambridge University Press, Cambridge, UK, 1993.

G. Patenaude, R. Milne, M. Van Oijen, C. S. Rowland, and R. A. Hill. Integrating remote sensing datasets into ecological modelling: a bayesian approach. *Int. J. Remote Sens.*, 29:1295–1315, March 2008.

M. Peramaki, E. Nikinmaa, S. Sevanto, H. Ilvesniemi, E. Siivola, P. Hari, and T. Vesala. Tree stem diameter variations and transpiration in Scots pine: an analysis using a dynamic sap flow model. *Tree Physiology*, 21(12-13):889, 2001.

A. R. Pereira, S. Green, and N. A. Villa Nova. Penman-Monteith reference evapotranspiration adapted to estimate irrigated tree transpiration. *Agricultural Water Management*, 83(1-2):153–161, 2006.

N. Phillips, B.J. Bond, N.G. McDowell, and M.G. Ryan. Canopy and hydraulic conductance in young, mature and old Douglas-fir trees. *Tree Physiology*, 22(2-3): 205, 2002.

B. Rewald. *Impact of climate change-induced drought on tree root hydraulic properties and competition belowground.* PhD thesis, Niedersächsische Staats-und Universitätsbibliothek Göttingen, 2008.

P. J. Ross. Modeling soil water and solute transport - fast, simplified numerical solutions. *Agronomy Journal*, 95:1352–1361, 2003.

M. Scherer-Lorenzen, C. Körner, and E.D. Schulze. *Forest diversity and function.* Springer-Verlag Berlin Heidelberg, 2005.

JS Sperry, JR Donnelly, and MT Tyree. A method for measuring hydraulic conductivity and embolism in xylem. *Plant, Cell and Environment*, 11(1):35–40, 1988.

E. Steudle. Water uptake by plant roots: an integration of views. *Plant and Soil*, 226(1):45–56, 2000.

I. Thompson, B. Mackey, S. McNulty, and A. Mosseler. Forest resilience, biodiversity, and climate change. In *A synthesis of the biodiversity/resilience/stability relationship in forest ecosystems. Secretariat of the Convention on Biological Diversity, Montreal. Technical Series*, pages 43–67, 2009.

M.T. Tyree and S. Yang. Water-storage capacity of Thuja, Tsuga and Acer stems measured by dehydration isotherms. *Planta*, 182(3):420–426, 1990.

M.T. Tyree and M.H. Zimmermann. *Xylem structure and the ascent of sap*. Springer Verlag, 2002.

M.T. Tyree, V. Velez, and JW Dalling. Growth dynamics of root and shoot hydraulic conductance in seedlings of five neotropical tree species: scaling to show possible adaptation to differing light regimes. *Oecologia*, 114(3):293–298, 1998.

D. Van der Zande, S. Mereu, N. Nadezhdina, J. Cermak, B. Muys, P. Coppin, and F. Manes. 3D upscaling of transpiration from leaf to tree using ground-based LiDAR: Application on a Mediterranean Holm oak (Quercus ilex L.) tree. *Agr Forest Meteorol*, 149(10):1573–1583, 2009.

M. van Leeuwen and M. Nieuwenhuis. Retrieval of forest structural parameters using lidar remote sensing. *European Journal of Forest Research*, 129:749–770, 2010.

A. Verroust and F. Lazarus. Extracting skeletal curves from 3D scattered data. *The Visual Computer*, 16(1):15–25, 2000.

G. Voronoi. Recherches sur les paralléloèdres Primitives. *J. reine angew. Math.*, 134: 198–287, 1908.

H. Xu, N. Gossett, and B. Chen. Knowledge and heuristic-based modeling of laser-scanned trees. *ACM Transactions on Graphics (TOG)*, 26(4):19, 2007.

R. Zweifel, H. Item, and R. Häsler. Link between diurnal stem radius changes and tree water relations. *Tree Physiology*, 21(12-13):869, 2001.

4 Simulating the interaction between the canopy light regime and the hydraulic architecture of single *F. sylvatica* trees

Sebastian Bittner, Nicole Legner, Friedrich Beese, Eckart Priesack

A Jarvis-type leaf stomatal conductance model was combined with a hydrological tree and soil water flow model and a spatially explicit canopy light model. The model was applied to single, old-growth *Fagus sylvatica* L. trees, and the measured daily values of stem sap flux could be reproduced with a normalized root mean square error of 0.08 for an observation period of 33 days in the summer of 2009. The high temporal resolution of the model also makes it possible to simulate the diurnal dynamics of transpiration, stem sap flux, and root water uptake. We applied new data processing algorithms to information from terrestrial laser scans to represent the canopies of the functional-structural model. The high spatial resolution of the root and branch geometry and connectivity makes the detailed modeling of the water usage of single trees possible and allows for the analysis of the interaction of single trees and the influence of the canopy light regime on the water flow inside the xylem. In addition to the laser scans of the observed trees, the model needs tree species-specific physiological input parameters, which are easy to obtain. The model can be applied at various sites and to different tree species, allowing the up-scaling of the water usage of single trees to the total transpiration of mixed stands.

Keywords   *Fagus sylvatica* L.; xylem water flow; functional-structural model; CIE standard daylight distribution; voxel ray tracing

4.1 Introduction

Modeling the water flux and transpiration at the level of a single tree with both a high temporal and spatial resolution can give insights into species-specific strategies of water usage [Früh and Kurth, 1999, Bohrer et al., 2005, Janott et al., 2011, Bittner et al., submitted a]. An adequate geometrical representation of single trees is crucial, because the competition for resources is linked to a competition for space by both, the belowground and the aboveground parts of the tree. Because the potential evaporation of water at the leaves is strongly determined by the intensity of incoming radiation, additional simulation of the canopy light regime could further improve the model's performance and allow for the analysis of the aboveground interactions of single trees [Loranty et al., 2010, Van der Zande et al., 2009]. Especially at old-growth forests, the traditional acquisition of the tree structure is laborious and may be connected with uncertainties. Therefore, the terrestrial laser scanning (*TLS)*

technique and data processing have recently been developed and used to obtain the structural properties of forests [van Leeuwen and Nieuwenhuis, 2010]. The aim of this study is to present and apply a functional-structural model of the water flow of single trees that focuses on the use of *TLS* data for the automatic generation of structural model input information. In addition to *TLS*-derived detailed information on geometry, the model uses physiological species-specific parameters of stomatal behavior as well as xylem and root hydrology.

Ecological functions concerning the water cycle are often determined by the properties of a particular tree species [Krämer and Hölscher, 2009]. Additionally to species-specific effects, interaction effects between single trees may have an additional impact on the water cycle. In general, the tree species composition of mixed forests can have a significant impact on the total stand's capacity for water storage, retention of water and groundwater recharge [FAO, 2005, Calder, 2007, van Dijk and Keenan, 2007]. The effect of forests diversity on ecological functions has been the focus of recent observational and modeling studies [Leuschner et al., 2009, Healy et al., 2008, Thompson et al., 2009, Scherer-Lorenzen et al., 2005, Nadrowski et al., 2010], and it was stated that biodiversity effects can be analyzed by up-scaling the information gained on an individual scale [Nadrowski et al., 2010, Kirwan et al., 2009].

The Hainich forest in central Germany represents an old-growth, mixed temperate deciduous forest and has been studied extensively in preceding studies. Large parts of the forest are dominated by *F. sylvatica*, but other tree species co-occur in some areas and allow for the analysis of the influence of tree species diversity on the water cycle of the entire stand. Here, differences in the hydraulic physiology and in the structure were found between the deciduous tree species. The structure of the old-growth beech, ash and lime differed with respect to the aboveground leaf distribution and canopy shape [Frech et al., 2003] as well as the radial fine root distribution in the soil [Meinen et al., 2009]. These physiological differences and their impact on hydrological traits have been analyzed for the xylem fraction of the stem cross section area [Gebauer et al., 2008], leaf stomatal conductance [Köcher et al., 2009], and root water uptake [Korn, 2004, Coners, 2001, Rewald, 2008]. Modeling studies have included these hydrological properties to simulate the soil-plant-atmosphere water cycle and quantified their influence on daily water uptake and transpiration [Bittner et al., 2010, submitted a]. Further, the interaction between the tree species could be analyzed at dry soil water conditions [Bittner et al., 2010], and the influence of the tree structure on the water flow inside the trees was revealed [Bittner et al.,

submitted a, Janott et al., 2011].

Bittner et al. [submitted a] applied a sub-model that uses a static, *TLS*-derived geometry in a model that calculates the water flow through the roots, stems, and branches of single trees. Connected cylinders that could conduct water represented the tree elements. An automatic tree skeleton extraction algorithm [Xu et al., 2007] was used to obtain the position of the canopy cylinders, and a root system model was used to calculate the position of the root cylinders. The xylem water potential of the branches could be a sensible parameter for stomatal closure and is included in a Jarvis-type total stomatal reaction model [Jarvis, 1976] in this study. In addition to the water status of the leaves, the stomatal reaction is sensitive to a set of climatic variables, of which the photosynthetically active radiation *PAR* is the most fluctuating. Therefore, a sub-model to calculate the canopy *PAR* regime that was recently tested under controlled light conditions in a greenhouse [Bittner et al., submitted b] was included in the functional-structural model.

A voxel-based ray tracing algorithm was used to calculate the intensity of *PAR* inside the canopy [Kimes, 1984, Cohen and Fuchs, 1987, Gastellu-Etchegorry et al., 2004, Perttunen et al., 2007]. Therefore, the three-dimensional space was divided into cubes of the same size (voxels) that possessed different light attenuation capabilities depending on the type of vegetation the voxel is filled with based on the information obtained by the *TLS*. The incoming hourly direct sun radiation, as well as the diffuse skylight, is attenuated on the path from the top of the canopy to the forest floor in these voxels, thereby including the self-shadowing of the vegetation. Finally, a *PAR* intensity is calculated for every voxel that contains leaves. This *PAR* value is one of the most sensitive parameters for the control of the stomatal behavior of the leaves and, therefore, the transfer of water from the plant to the atmosphere.

A Jarvis-type model of stomatal conductance combined the simulations of the leaf water status and *PAR* with meteorological measurements of the air temperature and the vapor pressure deficit to give the rate of water transfer from the leaves to the atmosphere. The model output was compared with the measured values of the stem xylem sap flux of three mature *F. sylvatica* trees and showed good agreement with respect to the daily and diurnal dynamics.

4.2 Materials and Methods

4.2.1 Study site

The study was conducted in an old-growth broad-leaved forest in the Hainich National Park in Central Germany ($51°N$ $10°E$). Three neighboring *F. sylvatica* trees (Tab. 4.1) were situated in an old-growth forest stand with a closed canopy. The parent rock of the site is Triassic limestone covered with a loess layer of variable depth. The soil type is a Luvisol that dries out strongly during summer and shows stagnant properties in winter and spring, with the groundwater table found far below the rooting zone. The soil texture was characterized by a high silt content and a low sand content (silt loam to silt clay loam).

| Tree | dbh | cpa[a] | Height | Leaf Area[b] | Max. canopy xylem |
	cm	m^2	m	m^2	water content[b], l
Bu27	58	143	28	300	2513
Bu30	47	70	26	245	1816
Bu33	45	73	25	199	1578

[a]M. Jacob, unpublished data.

[b]modeled

Table 4.1: Characteristics of studied trees. The leaf area was calibrated using the measured stem sap flux. The maximum canopy xylem water content was calculated from the modeled canopy architecture. cpa, crown projection area; dbh, diameter at breast height

4.2.2 Micro-climatic measurements

Hourly values of precipitation and wind speed were obtained from the weather station at Weberstedt/Hainich (Meteomedia GmbH, Bochum, Germany). Air temperature T [°] and relative air humidity H [%] were measured directly in the upper canopy using a Rotronic temperature and humidity probe (MP 100A Hygrometer, Rotronic GmbH, Ettlingen, Germany) and were used to calculate the vapor pressure deficit VPD [kPa] inside the canopy. Half-hourly values of global radiation r_g [$W\,m^{-2}$], the diffuse fraction of global radiation, and PAR [$\mu mol\,m^{-2}\,s^{-1}$] above the canopy were provided for the Hainich site by the *CarboEurope* research project (www.carboeurope.com, Knohl et al., 2003). The volumetric soil water content, θ [%], at the center of the

three neighboring trees was measured using a frequency domain reflectometry (FDR) probe (Diviner 2000 FDR sensors, Sentek Pty Ltd., Stepney, Australia) at a depth of $20\,cm$ (M. Meißner, personal communication).

4.2.3 Leaf conductance and xylem sap flux measurements

Leaf stomatal conductance ($g_S\,[mm\,s^{-1}]$) was measured using the *LI-6400XT portable photosynthesis system* (Li-Cor, Lincoln, Nebraska, USA) at 29 leaves from different beech trees under varying artificial intensity of PAR between 0 and $2000\,\mu mol\,m^{-2}\,s^{-1}$ keeping the Temperature and the vapor pressure deficit constant. Canopy access was accomplished via a mobile canopy lifter, which had a maximum height of $30\,m$. The maximum PAR of $2000\,\mu mol\,m^{-2}\,s^{-1}$ was reduced in eight steps. At every step, we waited approximately five minutes before the measurement of g_S to let the stomata react to the lower PAR. The resulting light curves were then used to estimate the parameters of the maximal stomatal conductance $g_{max}\,[mm\,s^{-1}]$ and the light curve parameter $a1\,[mm\,s^{-1}]$ (Tab. 4.2).

At the three study trees, the sap flux density in the stem was monitored with the constant-heat method proposed by Granier [1987]. Two $20\,mm$-long Granier type probes were inserted at a distance of $15\,cm$ from each other into the stem at $1.3\,m$ height. The upper probe was constantly heated ($200\,mW$), while the lower one served tor monitor the reference temperature of the stem. The temperature difference between the heated and the reference probe was recorded continuously and related to the maximum temperature difference occurring at predawn, when minimum or no flow occurred. Sap flux density (J_s, $g\,m^{-2}\,s^{-1}$) was calculated according to the empirical equation given by Granier [1987]. We used data from a prior study [Gebauer et al., 2008] that investigated radial patterns and changes in sapwood area with tree size of the same tree species at the same forest site to calculate the total stem sap flux of a single tree (S_s, $l\,d^{-1}$). Sap flux data were logged every $30\,s$ and a mean value was recorded every $30\,min$ over the whole vegetative period of 2009. After the leaves had developed in spring, the logger provided continuous, reliable data for the period from 5/22/2009 to 6/22/2009 (observation period) for the beech trees *Bu27, Bu30*, and *Bu33*.

4.2.4 Terrestrial laser scans and voxel representation of the canopy

The *Riegl VZ-400* (Riegl GmbH, Horn, Austria) terrestrial laser scanner was used to scan the foliated canopies of the trees in September 2010 at nearly windless weather conditions. The scanner has a range precision of $3\,mm$ and a beam divergence of $0.3\,mrad$, and the angular spacing between two laser beams was set to $0.002°$. The *Riegl VZ-400* scanner records the full waveform of multiple target echoes. The full waveform of the echos was used to filter artifacts using the *RiscanPro* (Riegl GmbH, Horn, Austria) software. Multiple target echoes were included in the final point clouds, which results in a high point density even in the deeper and higher parts of the canopy. To further decrease the effect of shadowing, 4 scans were made at positions around the tree group. All scan setup positions were then referenced in a local coordinate system using reflectors and reference targets with a positional average standard deviation of less than $8\,mm$.

A Voxel-based canopy architecture model was obtained from the TLS measurements using the cloud of three-dimensional points that resulted from reflections of the laser beam at the surface of the trees. The region of interest was divided into three-dimensional small cubes (voxels), and the canopy of each of the three trees was represented by a set of k voxels $V = \{v_1 \ldots v_k\}$ containing at least one of the TLS reflection points. The voxels were further divided voxels that contain woody material and into voxels that contain leaves (Fig. 4.1) by visual inspection. The region of interest was defined by all points that were inside a cylinder with the center of the group of the neighboring three *F. sylvatica* trees and a diameter of $51.2\,m$. In this way, edge effects could be avoided because, in addition to the three analyzed *F. sylvatica* trees, the neighboring trees were included in the model. The edge length of the voxels was set to be $0.1\,m$. The resulting voxel representation of the tree group served as the input for the light regime sub-model (sec. 4.2.8), assuming a static architecture of the old-growth trees.

4.2.5 Water exchange model of the soil-plant-atmosphere system

A hydrological model of water flow on a single tree scale has been recently developed [Bohrer et al., 2005, Aumann and Ford, 2002, Janott et al., 2011]. The water flow
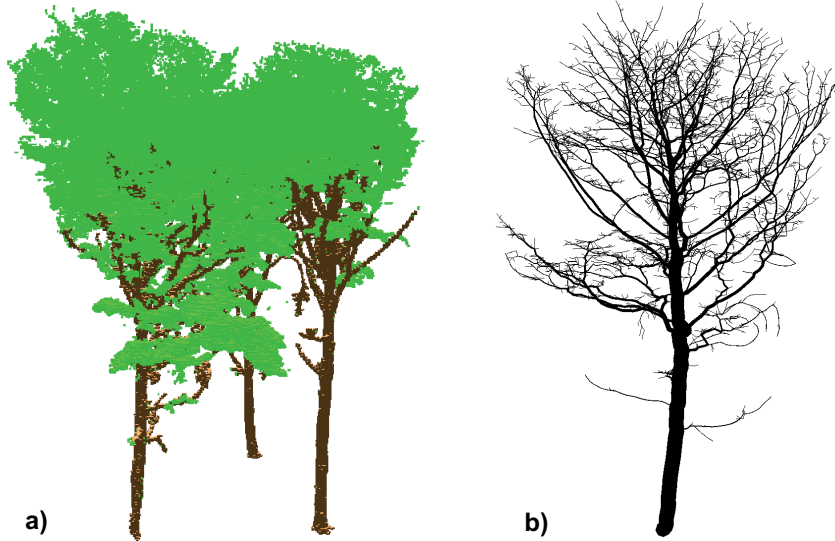
Figure 4.1: a) Voxel representation of the *F. sylvatica* trees with the distinction of woody material and leaves. b) Canopy representation of connected cylinders obtained by a skeleton extraction algorithm. The position and connectivity of the cylinders gives the potential pathway of the water flow through the tree.

inside the tree is driven by the transpiration of water at the leaves, which leads to a gradient of xylem water potential between the fine branches and the root system and results in a water uptake of available soil water by the roots. The flow of water along the hydrological pathway of the roots, stem, and branches is driven by the hydraulic gradient according to the cohesion-tension theory [Tyree and Zimmermann, 2002] and is calculated using the non-linear Darcy equation for the flow of water in a porous media. Here, the volumetric xylem water content and the xylem axial hydraulic conductivity depend non-linearly on the xylem water potential. The xylem elements have the maximal axial hydraulic conductivity at the xylem water potential $\psi_x = 0$. At higher negative values of ψ_x, the diameter of the cylinder elements is reduced, resulting in a lower area of water conducting xylem and, therefore, in a decrease in the conductance. Below the air entry value $\psi_x < a$, air enters into single xylem vessels, which leads to a strong decrease in the xylem hydraulic conductance. The resulting xylem water curves for the volumetric xylem water content, $\theta\,[mm^3\,mm^{-3}]$, and the xylem hydraulic conductivity $k(\psi)\,[mm\,s^{-1}]$ are given by

$$\theta(\psi) \quad = \quad \begin{cases} (\epsilon - \theta(a))\left(\frac{a-\psi}{a}\right) + \theta(a) & \psi \geq a \\ \theta(a)\left(\frac{\psi}{a}\right)^{\lambda_{BC}} & \psi < a, \end{cases} \tag{4.1}$$

and

$$k(\psi) \quad = \quad k_{max} \begin{cases} \frac{\theta(a)}{\epsilon} + (1 - \frac{\theta(a)}{\epsilon})(\frac{a-\psi}{a})^2 & \psi \geq a \\ (\frac{\psi}{a})^{-\lambda_{BC}\eta} & \psi < a, \end{cases} \tag{4.2}$$

with $k_{max}\,[mm\,s^{-1}]$, the specific axial hydraulic conductivity, the Brooks and Corey [Brooks and Corey, 1966] exponent $\lambda_{BC}\,[-]$, and $\eta := 2/\lambda_{BC} + 1$. Here, the xylem sapwood porosity $\epsilon\,[mm^3\,mm^{-3}]$ is defined as the ratio of the maximal volume of xylem water at saturation to the maximal total volume of the xylem sapwood in the tree element, and the elastic modulus of the xylem sapwood $E\,[mm]$ is defined by $\theta(a) = \epsilon + a/E$. The total conductance of a cylinder element $K(\psi)\,[mm^3\,s^{-1}]$ is given by multiplication of the specific conductivity with the hydroactive xylem area $A_x\,[mm^2]$ of the element. A mathematically rigorous description of the xylem water retention curve and the xylem conductance curve is given in Janott et al. [2011].

The radial volumetric flux $j_r\,[mm^3\,s^{-1}]$ between the soil-root interface that describes the amount of water exchanged between a root element and the one-dimensional soil layer is driven by the difference of the water potentials of the soil,$\psi_s\,[mm]$, and water potentials of the soil and the root xylem, $\psi_r\,[mm]$,

$$j_r = Lp_r\,s_r\,[\psi_s - \psi_r], \tag{4.3}$$

where $s_r\,[mm^2]$ is the surface of the root element, $Lp_r\,[s^{-1}]$ is the radial conductivity between the root xylem and the soil.

We used a geometrically explicit model of the potential pathway of tree water flow. Therefore, the xylem is represented by connected cylinder elements with specific hydrological properties, such as the axial conductivity and the water retention curves of the xylem. We used laser scans of the unfoliated canopy from Spring 2010 as the

input for a tree skeleton extraction algorithm [Verroust and Lazarus, 2000, Xu et al., 2007] to derive the position of the stem and branches from the three dimensional point cloud [Bittner et al., submitted a]. The algorithm could give a more detailed representation of the canopy when laser scans of the unfoliated canopy were used than the laser scans from Summer 2010 because the fine branches in the higher canopy were more shaded in the scans of the foliated canopy due to the reflection of the laser beams at the leaves. The canopies of the three trees consisted of 2255, 2754, and 6591 cylinder elements with a length of $0.25\,m$ (Fig. 4.1). The root architecture of the trees was simulated using the vertical and horizontal fine root distribution, the root area index and the rooting depth that was measured at the study site [Meinen et al., 2009]. The taproots system of beech was strongly influenced by the site soil conditions, leading to a narrow rooting zone with approximately $80\,\%$ of the fine root biomass in the upper $40\,cm$ of the soil profile.

Similar to the water flow through the tree, the soil water flow was calculated by solving Richards equation describing the soil water flow in porous media [Richards, 1931]. The coupling between the plant and the soil is achieved by the possible water exchange between the tree roots and one-dimensional soil layers by a Darcy flux driven by a possible water potential difference between the soil and the roots, which further depends on the tree hydraulic properties, such as the radial root water conductivity [Janott et al., 2011]. For a detailed description of the hydraulic properties of the soil and the calculation of the infiltration of water after rain, see Bittner et al. [2010].

The water flow in the model is driven by the transpiration at the leaf scale; therefore, the modeling of the actual transpiration is crucial. A first approach could be to use a stand-level scale to calculate the potential transpiration and then downscale this value to the single tree and the leaf scales. Downscaling to the leaf scale is especially difficult, as the micro-climate at the leaf scale shows a high spatial variation. In forests that are well coupled to the atmosphere, the spatially most heterogeneous parameter that influences the potential transpiration is the incoming PAR. Therefore, we first calculated the light regime inside the tree canopies (see sec. 4.2.8), which serves as input for the leaf stomatal conductance model (see sec. 4.2.6). In addition to the PAR, the stomatal conductance model includes the reaction of the leaves to the air temperature, T, and the VPD. By applying the calculated leaf stomatal conductance in conjunction with the simulation of the xylem water potential, the actual transpiration, i.e., the water that is exchanged between the single branch

70

elements and the atmosphere, is calculated and drives the water flux inside the tree and the uptake of the roots.

4.2.6 Stomatal conductance model

To describe the stomatal conductance of the leaves, we used an empirical model of the reaction of the stomatal conductance $g_S \, [mm \, s^{-1}]$ as proposed by Jarvis [1976]. The maximal stomatal conductance per unit leaf area $g_{Smax} \, [mm \, s^{-1}]$ is reduced by four independent reduction factors $f_x \in [0..1]$, $x \in \{PAR, VPD, T, \psi_l\}$, that each depend on a single environmental variable. The theoretical maximal value of the stomatal conductance g_{Smax} is usually not observed under field conditions and was extrapolated from porometer measurements of single leaves under controlled environmental conditions of $T = 25°C$, $VPD = 1.5 \, kPa$, and $PAR = 2000 \, \mu mol \, m^{-2} \, s^{-1}$. The model considers the vapor pressure deficit $VPD \, [kPa]$, the air temperature ($T \, [°C]$), the photosynthetic photon flux density $PAR \, [\mu mol \, m^{-2} \, s^{-1}]$, and the leaf matrix water potential $\psi_l \, [mm]$ by

$$g_S = g_{Smax} \, f_{PAR}(PAR) \, f_{VPD}(VPD) \, f_T(T) \, f_{\psi_l}(\psi_l). \tag{4.4}$$

A value for the stomatal conductance is calculated in the model for every voxel that is occupied by leaves. In this way, the spatial heterogeneity of the PAR and the xylem water potential is included. For every tree canopy that is represented by n voxels, we built an average canopy stomatal conductance per unit leaf area $g_c \, [mm \, s^{-1}]$ by

$$g_c = \frac{1}{n} \sum_{i=1}^{n} g_{,i} = \frac{1}{n} \sum_{i=1}^{n} g_{Smax} \, f_{PAR,i}(PAR_i) \, f_{VPD}(VPD) \, f_T(T) \, f_{\psi_l,i}(\psi_{l,i}). \tag{4.5}$$

The summation index, i, indicates values that are simulated as voxel-specific. The reduction factors f_{VPD} and f_T were not simulated for every voxel, but a single value was calculated describing the whole canopy assuming a homogenous VPD and T inside the whole canopy according to the microclimatic measurements.

The single reduction factors were calculated as follows.

- f_{PAR}

  The PAR light regime is the most temporal and spatial fluctuating determinant

of the stomatal conductance. A hyperbolic function can be used in modeling the dependency on the light regime [Herbst, 1995, Jarvis, 1976, Lohammar et al., 1980]

$$f_{PAR}(PAR) = \frac{PAR}{PAR + a_1}, \tag{4.6}$$

with the curvature parameter $a_1 \, [\mu mol \, m^{-2} \, s^{-1}] > 0$. The parameter a_1 was estimated using conductance curves of single leaves measured by *in situ* porometry.

- f_{VPD}

  Assuming a hyperbolic relationship between the conductivity and the vapor pressure deficit VPD [Herbst, 1995, Lohammar et al., 1980, Oren et al., 1999, Ewers et al., 2001], we calculated the vapor pressure deficit reduction factor as

$$f_{VPD}(VPD) = \frac{VPD}{VPD + a_2}. \tag{4.7}$$

  In an observational study of old-growth *F. sylvatica*, Herbst [1995] stated that the hyperbolic approach could describe the behavior of the stomata and found a value of $a_2 = 495 \, kPa$.

- f_T

  The dependency of the stomatal conductance on the temperature $T \, [°]$ was calculated as in Jarvis [1976], using

$$f_T(T) = \frac{(T - T_{min})}{(T_{opt} - T_{min})} \left(\frac{T_{max} - T}{T_{max} - T_{opt}} \right)^{\left(\frac{T_{max} - T_{opt}}{T_{max} - T_{min}} \right)}, \tag{4.8}$$

  with the further restriction of $0 \leq f_T \leq 1$. This bell-shaped function gives a value of $f_T = 1$ at the optimal temperature $T_{opt} \, [°C]$ and decreases to $f_T = 0$ at a minimum and maximum temperature, T_{min} and $T_{max} \, [°C]$.

- $f_{\psi l}$

  The stomatal reduction of the leaves to the leaf water status is given by

72

$$f_{\psi l}(\psi_l) = max[0.1 \, , \, \exp(-\left(\frac{-\psi_l}{St_b}\right)^{St_c})], \tag{4.9}$$

with the water potential of the leaf $\psi_l\,[mm]$, and parameters $St_b\,[mm]$ and $St_c\,[1]$ describing the stomatal response to branch xylem water potentials following the approach of Bohrer et al. [2005] and are estimated using empirical vulnerability curves for leaf conductance [Köcher et al., 2009, Bittner et al., submitted a]. We further assumed that the water potential of the leaf is equal to the water potential of the corresponding branch. Therefore, every voxel containing leaves was assigned to a cylinder element of the canopy using the smallest distance in the tree-dimensional space among all canopy cylinder elements.

4.2.7 Up-scaling from leaf to tree transpiration

The Penman-Monteith equation of evapotranspiration [Monteith, 1965] includes the influence of the radiative and the advective energy on the tree transpiration rate per unit leaf area $E\,[mm\,s^{-1}]$. The equation can be applied at the stand-level and at higher spatial resolutions, but in that case it requires information on the wind speed profile and the radiation profile inside the canopy. If the aerodynamic conductance highly exceeds the canopy conductance, a simplified equation to calculate the tree transpiration can be derived [Köstner et al., 1992] for vegetation showing a high coupling to the atmosphere,

$$E = \frac{VPD\,g_c}{\varrho\,G_V\,T}, \tag{4.10}$$

with the air vapor pressure deficit $VPD\,[kPa]$, the air temperature $T\,[°K]$, the density of water $\varrho\,[kg\,m^{-3}]$, the gas constant for water vapor $G_V\,[kPa\,kg^{-1}\,K^{-1}]$, and the tree canopy average of the stomatal conductance per unit are leaf area $g_c\,[mm\,s^{-1}]$. The advantage of this simplification of the Penman-Monteith equation is that g_c includes the spatial heterogeneous PAR regime and that no further information on the wind profile inside the canopy is needed.

Theoretical [Jarvis and McNaughton, 1986] and observational [McDowell et al., 2008, Gao et al., 2002] studies show that it is appropriate to assume a high coupling to the

atmosphere of the canopy of some tree species, especially in old-growth stands and coniferous forests. The degree of the coupling of the canopy to the atmosphere can be expressed by the dimensionless omega coefficient, Ω, and a value of $\Omega < 0.2$ is often chosen as a threshold for the simplified calculation of the canopy transpiration. A strong coupling is reported in the literature for mature *F. sylvatica* stands ($\Omega = 0.1$, Jarvis and McNaughton, 1986; $\Omega \in 0.05..0.2$, depending on wind speed [Granier et al., 2000]; $\Omega = 0.2$, Herbst, 1995), as well as for various other broad leaved forest stands [Granier and Bréda, 1996]. Therefore, we used eq. 4.10 to calculate E.

To quantify the tree's total water usage, the rate of water volume that is evaporated in $[mm^3\,s^{-1}]$ is given by multiplying $E\,[mm\,s^{-1}]$ with the total leaf area, $LA\,[mm^2]$, of the canopy. In sec. 4.3.2, we compared the simulated and the modeled stem sap flux of water $[mm^3\,s^{-1}]$, and we used the LA as a calibration factor for the model in such a way that the mean value of the daily modeled stem sap flux values equaled the mean value of the measured daily values of the stem sap flux. When measurements or estimations of LA are available, the model can use the LA as an input parameter and therefore calculate the transpiration rate of single trees without the need for calibration to sap flux measurements. In sec. 4.4.1, we discuss measurements and estimations of the LA using a terrestrial laser scanner.

4.2.8 Light model

Voxel ray tracer

A voxel-based representation of the canopy is a way to obtain a detailed envelope of the canopy [Kimes, 1984, Cohen and Fuchs, 1987, Gastellu-Etchegorry et al., 2004, Perttunen et al., 2007], and the use of terrestrial laser scans allows the usage of a small voxel size and therefore a high spatial resolution of the geometrical model [Van der Zande et al., 2009, Bittner et al., submitted b]. The combination of a *TLS*-derived voxel representation and a ray tracing algorithm results in low requirements for computational time and computer memory consumption and is capable of reproducing the distribution of PAR inside the canopy and at the forest floor [Bittner et al., submitted b]. We give a short description of the ray tracing algorithm; for a detailed description, see Bittner et al. [submitted b].

The incoming light is represented by line segments, R_i, which are each defined by a starting point S_i, an ending point E_i, and a starting intensity, I_0^i. The line segments

are referred to hereafter as rays in this article and may intersect voxels of the canopy. The start points of the rays were given by the position of the sun and 99 additional random positions in the hemisphere. In this way, the direct sunlight and the diffuse skylight in the field conditions were included. The center of all voxels that contained leaves of the three observed *F. sylvatica* trees, were the end points of the rays, which resulted in a number of $N = 100\,n_l$ rays per time step (time step of one hour), with n_l being the number of leaf voxels. The intensity of the ray that represents the direct sunlight is calculated by using the measured fraction of the direct radiation multiplied by the measured total incoming PAR. The initial intensities of the diffuse rays were calculated using the *CIE* standard general sky model, which is described below.

To couple the voxel representation with the rays, we applied the Amanatides-Woo algorithm [Amanatides and Woo, 1987] to calculate the set of n_i voxels $A^i = \{a^i_j\}$ with $j \in \{1, \ldots, n_i\}$ and $a^i_j \in \{v_1 \ldots v_m\}$ that intersect as well as the intersection length d^i_j of the ray R_i and every intersected voxel j. The attenuation of light can then be calculated at every position in the canopy by using Beer's law

$$I(d) = I^i_o \exp(-\lambda\,d), \tag{4.11}$$

with the incoming light intensity above the canopy $I^i_0\,[\mu mol\,m^{-2}\,s^{-1}]$, the attenuation coefficient, $\lambda\,[m^{-1}]$, and the the attenuation length, $d\,[m]$, which is the sum of the intersection length of the intersected voxels between the starting point of the ray and the regarded position. Thus, the light intensity $I^i_{j,}\,[\mu mol\,m^{-2}\,s^{-1}]$ after intersecting the voxel, a^i_j, is given by

$$I^i_j = I^i_o \exp(-k \sum_{c=1}^{j} d^i_c). \tag{4.12}$$

The attenuation coefficient of voxels that contained leaves was calibrated to the fraction of PAR that reaches the forest floor. At the Hainich forest, about $2 - 3\,\%$ of the incoming PAR reaches the forest floor on clear days [Frech et al., 2003]. Voxels, that contained woody material, such as the stem or coarse branches, could not transmit any light and the intensity of a ray that intersected such was completely attenuated in the model.

CIE standard general sky

The diffuse part of the PAR is distributed over the sky hemisphere according to the standard general sky as defined by the *Commission Internationale de l'Eclairage* [CIE, 2003a]. This standard defines 15 luminance distributions (sky types) that depend on weather and climate and change during the course of a day with the position of the sun. The aim of this standard is to model the the sky under a wide range of climatic conditions ranging from an overcast sky to cloudless weather. The 15 sky types can be divided into lumination distributions of overcast skies (CIE types $1 - 5$), transitional skies (CIE types $6 - 10$), and clear skies (CIE types $11 - 15$). In this study, the hourly CIE sky types were derived from the measured total global radiation and diffuse global radiation according to Kittler and Danda [2000].

4.3 Results

4.3.1 Parameterization

The model parameter values that were used in the sub-models of the light regime and the stomatal conductance are listed in Tab. 4.2. Additional model parameters were needed for the sub-models of the water flow inside the trees and in the soil. Values for the soil water retention curves can be found in Bittner et al. [2010], and the parameters describing the hydraulic properties of the xylem can be found in Bittner et al. [submitted a].

4.3.2 Simulation results

4.3.2.1 Sky luminance and canopy light regime

The measured daily maxima of above-canopy PAR ranged from $430-1920\,\mu mol\,m^{-2}\,s^{-1}$ during the observation period, and the direct fraction of global radiation was 0.6. All 15 CIE sky types were observed during the vegetative period of 2009 in the model. The most frequent CIE sky types were type 12 (*CIE standard clear sky*) and type 9 (*partly cloudy, with the obscured sun*) with a proportion of $24\,\%$, followed by sky type 10 (*partly cloudy, with brighter circumsolar region*, $19\,\%$). The five CIE overcast sky

Table 4.2: Model input parameters of the light regime sub-model and the stomatal conductance sub-model.

Symbol	Description	Unit	Value
λ	light attenuation factor	m^{-1}	2.5
g_{max}	maximal stomatal conductance per unit leaf area	$mm\,s^{-1}$	0.8
St_b	Parameter of stomatal response to leaf water potential[b]	MPa	2.25
St_c	Parameter of stomatal response to leaf water potential[b]	[-]	3.5
a_1	Parameter of stomatal response to PAR	$\mu mol\,m^{-2}\,s^{-1}$	255
a_2	Parameter of stomatal response to VPD [a]	kPa	495
T_{min}	Parameter of stomatal response to T	°C	-5.0
T_{max}	Parameter of stomatal response to T	°C	43.0
T_{opt}	Parameter of stomatal response to T	°C	25.0
$k_{max,root}$	axial specific hydraulic conductivity of roots	$10^{-2}\,mm\,s^{-1}$	13.0
$k_{max,branch}$	axial specific hydraulic conductivity of branches	$10^{-2}\,mm\,s^{-1}$	1.7
Lp_r	radial root hydraulic conductivity [e]	$10^{-8}\,m\,MPa^{-1}\,s^{-1}$	4.7
ϵ	Xylem porosity[b]	$mm^3\,mm^{-3}$	0.52
A_x/A_b	Xylem area to basal area[d]	[-]	0.75
E	Elastic modulus [c]	$10^6\,mm$	3.5
a	xylem air entry value[c]	MPa	3.1
λ_{BC}	Brooks and Corey parameter[c]	[-]	0.86

[a]Herbst [1995], [b]Bittner et al. [submitted a],[c]Oertli [1993],[d]Gebauer et al. [2008],[e]Korn [2004]

types had a proportion of 11 %, the five transitional sky types had a proportion of 46 %, and the five clear sky types had a proportion of 43 %.

The vertical distribution profiles inside the canopy can be derived by building the mean values of the PAR intensity of all voxels with the same height (Fig. 4.2). Approximately 80 % of the incoming PAR is attenuated at the highest $5\,m$ of the canopies. Below the onset of the canopy, more than 95 % of the incoming PAR was attenuated.

4.3.2.2 Volumetric soil water content

During the observation period, the measured volumetric soil water content at a depth of $20\,cm$ varied between 35 % and 38 %, indicating wet soil water conditions with
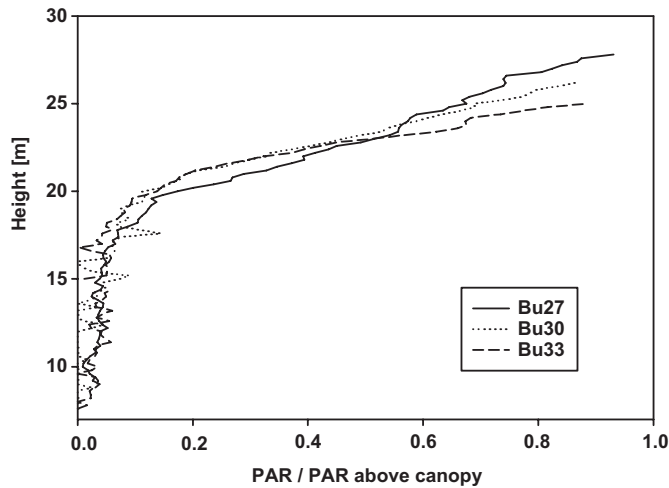
Figure 4.2: Vertical distribution of PAR in the canopies of the three beech trees.

enough soil water available to the plants. The simulated values of the volumetric soil water content were similar to the measured values, and the root mean square error of the observation period was below 2%.

4.3.2.3 Xylem water potential

An important model state variable is the xylem water potential, which is calculated for every cylinder element at every time step. The gradient of lower values of the xylem water potential in the fine branches and higher values in the root system is a result of the gravitation gradient and the depletion of branch xylem water caused by the daily transpiration. Following the the diurnal changes in transpiration, the highest gradient of xylem water potential is observed in the afternoon. During the night, the tree takes up water from the soil and after filling only a xylem water potential difference between the cylinder elements due to the gravity potential is observed.

4.3.2.4 Daily and diurnal stem sap flux

During the observation period the mean value of the measured daily stem sap flux was $69\,l\,d^{-1}$ for *Bu27*, $65\,l\,d^{-1}$ for *Bu30*, and $80\,l\,d^{-1}$ for *Bu33*. The highest value of $138\,l\,d^{-1}$ was measured for *Bu33* on 6/2/2009. The calculated root mean square error $RMSE\,[l\,d^{-1}]$ between the measured and the simulated stem sap flux was $6.3\,l\,d^{-1}$ for *Bu27*, $4.5\,l\,d^{-1}$ for *Bu30*, and $6.3\,l\,d^{-1}$ for *Bu33* (Fig. 4.4). The normalized root

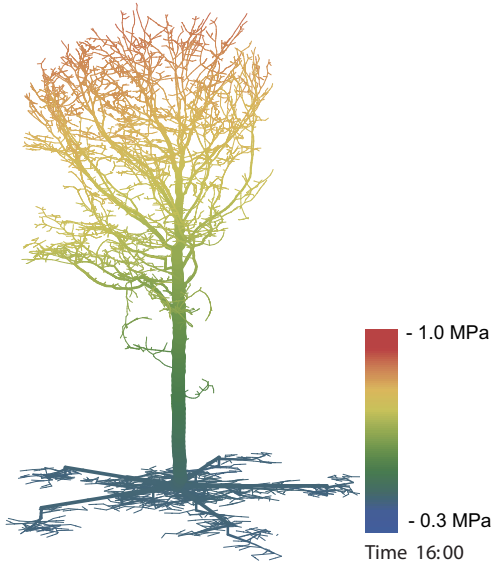**- 1.0 MPa**

- 0.3 MPa

Time 16:00

Figure 4.3: Xylem water potential of the model xylem cylinder elements at the observation day 6/2/2009 16:00 at the tree *Bu27*. The visualization shows a simplified root system with less elements than are actually used in the model.

mean square error $NRMSE = \frac{RMSE}{\overline{S}}$ was 0.09 for *Bu27*, 0.07 for *Bu30*, and 0.08 for *Bu33*. The *NRMSE* was $20 - 40\%$ lower than the error of a model simulation that was driven by the stand-level Penman-Monteith reference evapotranspiration. The Nash-Sutcliffe model efficiency [Nash and Sutcliffe, 1970] was 0.89 for *Bu27*, 0.96 for *Bu30*, and 0.94 for *Bu33* and was lower than a model simulation driven by the stand-level Penman-Monteith reference evapotranspiration (0.83 *Bu27*, 0.88 *Bu30*, and 0.82 *Bu33*).

As a result of the high availability of soil water during the whole observation period, the water status of the leaves was high and only restricted by the hydraulic conductivity of the roots and branches and the resulting capability to supply the fine branches at the top of the canopy with enough water at noon, when the transpiration rates were highest. On 6/2/2009, the restriction of transpiration described by the factor $f_{\psi l}(\psi_l)$ was 0.96 for *Bu27*, 0.98 for *Bu30*, and 0.95 for *Bu33*.

The simulated diurnal dynamics of stem sap flow were similar to the measured half-hourly values (Fig. 4.5). The simulated values of stem sap flux of the Jarvis-type stomatal reaction model were different compared to the stand-level simulations of transpiration using the Penman-Monteith reference method, although both simulations were calibrated to the mean value of the sap flux. The onset of the simulated sap flux in the morning hours was up to one hour later when using the stomatal
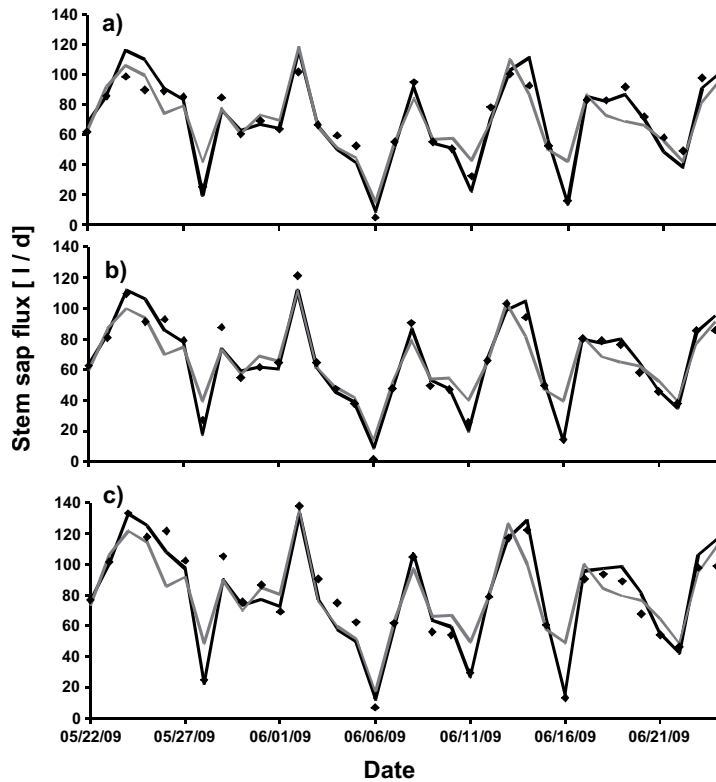
Figure 4.4: Daily values of measured (dots) and simulated (black solid line) stem
sap flux. The gray solid line gives the simulated values of sap flux using the
Penman-Monteith reference evapotranspiration model instead of the Jarvis-type
model of stomatal reaction. a) Bu27 b) Bu30 c) Bu33

reaction model compared to the Penman-Monteith approach. This was because the
Jarvis model included the incoming light, which was low inside the canopy of the
three *F. sylvatica* trees because the angle between the direct sunlight and the horizon
was low in the morning hours, which resulted in a high shadowing of the canopy.
Another difference was observed on days with a low VPD. For example, on the rainy
day of 5/28/2009, the Penman-Monteith approach overestimated the transpiration
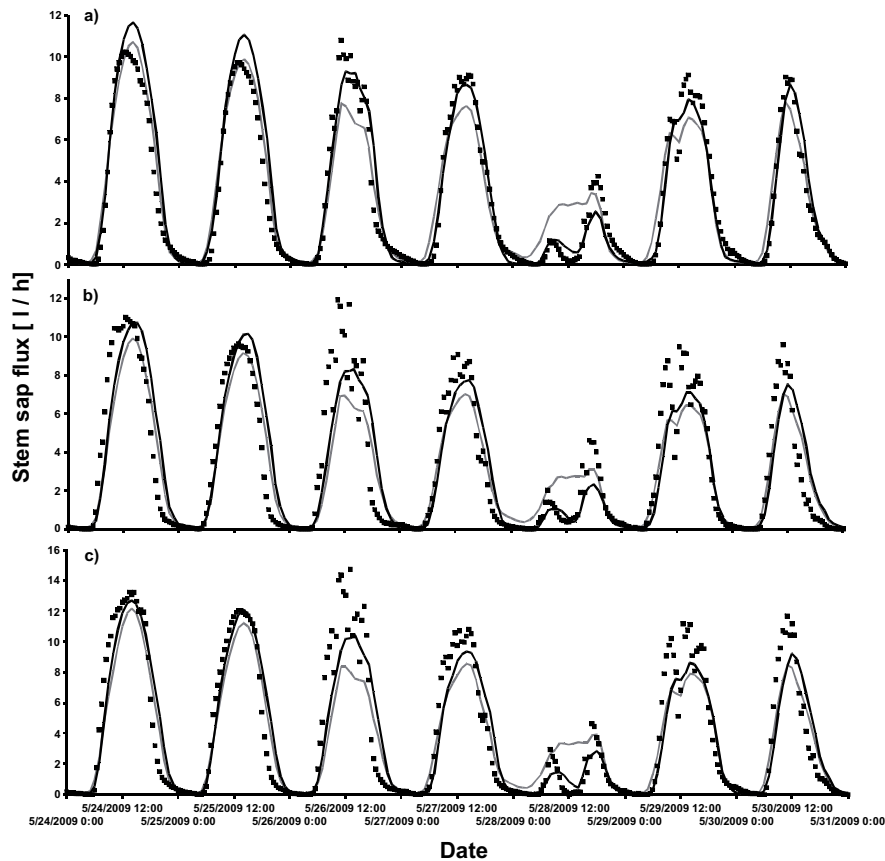rate of all three trees.

Figure 4.5: Diurnal values of measured (dots) and simulated (black solid line) stem sap flux. The gray solid line gives the simulated values of sap flux using the Penman-Monteith reference evapotranspiration model instead of the Jarvis-type model of stomatal reaction. a) Bu27 b) Bu30 c) Bu33

4.4 Discussion

4.4.1 Parameterization

The maximal stomatal conductance g_{max} is one of the most crucial model input parameters because the tree transpiration is proportional to g_{max}. We could estimate the value using *in situ* porometer measurements; the values were similar to other observational studies of *F. sylvatica* [Köcher et al., 2009, Herbst, 1995]. When measurements are not available, Kelliher et al. [1995] give values for a range of species and sites.

The most variable parameter for calculating the stomatal conductance g_S was the intensity of PAR. The sub-model to calculate the PAR regime inside the canopy

needs the light attenuation factor, λ, as a single input when the size of the voxels is fixed. Usually no measurements of the PAR profiles are available to calibrate λ, but it is possible to estimate the value in different ways. In this study, we used the fraction of PAR that reaches the forest floor to obtain a value of $\lambda = 2.5\,m^{-1}$. A preceding model analysis by Bittner et al. [submitted b] of the light regime sub-model at an artificial stand of young *F. sylvatica* trees in a green house found a best value of $\lambda = 2.7\,m^{-1}$ for a voxel size of $0.1\,m$, which is similar to the value used in the present study on an old-growth stand. Thus, species-specific values of λ may be found, but the analysis of more sites is needed to test this assumption. A third way to obtain λ is to vary the value in a certain range and analyze the model performance. By doing this, we found an optimal value of $\lambda_{opt} = 2.1\,m^{-1}$, which resulted in a modeled stem sap flux that was closest to the measured sap flux. Therefore, the estimation of λ using a model performance optimization strategy might be appropriate when no other parameterization is possible.

Next to the canopy conductance, the LA is the most crucial value for calculating the total tree transpiration. In this study, we calibrated the LA using the measured stem sap flux in such a way that the mean value of the daily modeled stem sap flux values equals the mean value of the measured daily values of the stem sap flux. The calibrated value of the LA of all three trees ($LA = 744\,m^2$) was similar to the value that was calculated using the litter that was collected at the center of the tree group using a litter collector with an area of $28\,cm^2$ in Autumn of 2008 ($LA = 684\,m^2$, D. Hertel, personal communication). Because of the uncertainties of the litter collection method, we did not use the observed LA as the model input. Methods to derive the LA from TLS measurements have been recently proposed for coniferous and broad-leaved forests. We tested the voxel-based method of Hosoi and Omasa [2006] at our site, but the calculated LA was not invariant when voxel size changed, which is sign that the resolution of our laser scans is too low for this method. In our case, a voxel-size of $< 1\,cm$ could not be achieved because of the angular step width of the laser beams, $0.002°$, and the large distance to the tree canopies. Nevertheless, the use of an estimation of the LA has advantages compared to the calibration to stem sap flux measurements because the measurements are often not available for a large number of trees and require a careful calibration to the stand and the tree species [Bush et al., 2010].

4.4.2 Simulation results

4.4.2.1 Sky luminance and canopy light regime

A database of daylight information such as the half-hourly CIE sky types has been made available for Western and Central Europe via the $Satel-light$ project (www.satel-light.com; Fontoynont et al., 1999). The daylight information within this framework is completely derived from *Meteosat* satellite imagery of the years $1996-2000$. The proportions of the derived CIE types for the Hainich site are 24% overcast sky types, 40% transitional sky types, and 36% clear sky types. These are similar to the CIE type frequencies that we have derived from micro-meteorological measurements for the year 2009.

The modeled vertical distribution of PAR is similar to the vertical PAR regime that were observed at *F. sylvatica* forests with a similar structure [Leuchner et al., 2005, Hansen et al., 2002].

4.4.2.2 Xylem water potential

The simulated diurnal change of the xylem water potential is observed in field measurement. Values of the daily leaf water potential, ψ_l, ranged from -2.5 to $-1.4\,MPa$ at sun-exposed leaves at noon and from -1.8 to $-0.3\,MPa$ at predawn [Köcher et al., 2009]. The observed fine root xylem water potential ranged from -1.5 to $-0.5\,MPa$ [Korn, 2004]. The values are similar to observations of broad-leaved old-growth trees at other temperate sites; for an overview over the observed values, see Korn [2004].

4.4.2.3 Daily and diurnal stem sap flux

The stomatal conductance model could increase the model performance of the simulated daily sap flux compared to the Penman-Monteith calculation of the potential transpiration. This is in accordance with Loranty et al. [2010], who achieved a similar model error using a simpler representation of the canopy and light attenuation. Therefore, the good performance of the functional-structural model presented in this study has to be compared to the performance of other simpler models. Here we observed that a stand-level estimation of the potential transpiration using the Penman-Monteith reference evapotranspiration method in combination with

a geometrically explicit tree water flow model could already adequately reproduce the measured values of stem sap flux [Bittner et al., submitted a]. The Jarvis-type model of stomatal reaction performed better than the Penman-Monteith approach, especially on days with a low Penman-Monteith potential transpiration, because the Penman-Monteith approach tends to overestimate the potential transpiration under these weather conditions at forest sites [David et al., 1997, Bittner et al., submitted a].

This raises the question of, whether the voxel-based light model and the Jarvis-type model of stomatal response are an adequate way (with respect to the model complexity) to describe the water use of single trees. First, it has to be stated that the additional model input parameters, such as the light attenuation factor or the parameters for the stomatal reaction, are easily estimated (see sec. 4.4.1) and can be found in the literature for many species. If laser scans of the canopy are available, the algorithms to extract the voxel and the cylinder element representations work automatically and require little user interaction. In this way, TLS is an elegant way to provide the functional-structural model of single tree water flow with detailed structural information on the aboveground part of the trees, as was suggested by Loranty et al. [2010]. Second, the simulation of tree water flux at high temporal and spatial resolutions allows the analysis of the influence of the light regime on the water usage, the interaction of the light regime and the hydraulic architecture, and the interaction with single neighboring trees.

The influence of low leaf water status at noon on the closure of the stomata was low during the observation period, with a maximal daily decrease of 5%. The inclusion of a detailed tree hydraulic model and root water uptake model is nevertheless crucial because the impact of the leaf water status could be higher under different climatic and site conditions. The sensitivity of the stomatal conductance to the leaf water status is highly determined by the structure and height of the stand [Novick et al., 2009, Janott et al., 2011], and is significantly higher for ring-porous species [Bittner et al., submitted a]. Furthermore, the Hainich site shows dry soil water conditions and long drought periods in some years, leading to a significant decrease in transpiration at non-optimal soil water conditions [Hölscher et al., 2005, Köcher et al., 2009, Gebauer, 2010].

Using measurements of radiation and vegetation-atmosphere energy fluxes at the Hainich forest, Knohl and Baldocchi [2008] analyzed the influence of the fraction of

diffuse skylight of total incoming radiation on photosynthesis and tree transpiration. They found a sensitive dependency of the total stand-atmosphere gas exchange on the fraction of diffuse radiation at forests with a heterogeneous canopy as a result of a higher penetration into the canopy of diffuse radiation than direct radiation [Leuchner et al., 2005]. Therefore, a detailed simulation of the skylight using the *CIE* model is adequate, especially for heterogeneous canopies of mixed or uneven-aged forests.

The effect of radiation on the diurnal dynamics of transpiration and sap flux has been observed at forest edges [Herbst et al., 2007], tree belts [Crosbie et al., 2007], and sites with a high aspect [Mayer et al., 2002]. In this study, the effect could be observed at the three observation trees situated in the middle of a forest with a closed canopy via the delay of the onset of the simulated sap flux in the morning hours in comparison to the Penman-Monteith approach, which does not include the inclination angle of the light. In general, the interaction of the light regime and the hydraulic properties and structure has been the focus of research [Loranty et al., 2010, Campanello et al., 2008].

This study focused on the simulation of *F. sylvatica* trees, but the application on other tree species is possible. A preceding study had applied the soil-plant water flow model to *F. sylvatica*, *T. cordata*, and *F. excelsior* species and was able to simulate the species specific water balances. Thus, an up-scaling of the simulations of the single trees to a mixed stand is possible by applying the model on tree groups that consist of different species.

4.5 Conclusion

A functional-structural model that is capable of simulating the water flux in single trees at a high temporal and spatial resolution was presented. Using the information of the TLS combined with a root architecture model, it is possible to analyze the water flux through single root elements and branches. The model combines physiological tree properties with the structure of the trees and allows us to describe the interaction of function and structure and to quantify the influence of single species-specific hydraulic traits. In its present form, the model may be useful for analyzing the interactions of neighboring trees and their competition for available soil water and sunlight. By up-scaling the hydrological properties of different tree

species of a mixed forest, this model can be used to analyze the effect of biodiversity on the water cycles of the entire stand.

The geometrical input was derived from point clouds provided by terrestrial laser scans. The data processing algorithms to convert the point clouds into voxels and into cylinder elements require minimal user input and are applicable for various tree sizes and species. A good estimation of the leaf area is crucial for simulating the use of water per tree.

Acknowledgments

References

J. Amanatides and A. Woo. A fast voxel traversal algorithm for ray tracing. In *Eurographics*, volume 87, page 9. Citeseer, 1987.

C.A. Aumann and E.D. Ford. Modeling tree water flow as an unsaturated flow through a porous medium. *Journal of theoretical biology*, 219(4):415–429, 2002.

S. Bittner, U. Talkner, I. Krämer, F. Beese, D. Hölscher, and E. Priesack. Modeling stand water budgets of mixed temperate broad-leaved forest stands by considering variations in species specific drought response. *Agricultural and Forest Meteorology*, 150:1347–1357, 2010.

S. Bittner, M. Janott, D. Ritter, P. Köcher, F. Beese, and E. Priesack. Using terrestrial laser scanner data for a functional-structural water flow model of three broad-leaved tree species. *Agricultural and Forest Meteorology*, submitted a.

S. Bittner, S. Gayler, J. B. Winkler, S. Seifert, and E. Priesack. Using a voxel-based representation of tree canopies for a 3D light regime model. *Trees*, submitted b.

G. Bohrer, H. Mourad, T.A. Laursen, D. Drewry, R. Avissar, D. Poggi, R. Oren, and G.G. Katul. Finite element tree crown hydrodynamics model (FETCH) using porous media flow within branching elements: A new representation of tree hydrodynamics. *Water Resources Research*, 41(11):W11404, 2005.

RH Brooks and AT Corey. Properties of porous media affecting fluid flow. *J. Irrig. Drain. Div*, 6:61, 1966.

S.E. Bush, K.R. Hultine, J.S. Sperry, and J.R. Ehleringer. Calibration of thermal dissipation sap flow probes for ring-and diffuse-porous trees. *Tree Physiology*, 30 (12):1545, 2010.

I.R. Calder. Forests and water–ensuring forest benefits outweigh water costs. *Forest Ecology and Management*, 251(1-2):110–120, 2007.

P.I. Campanello, M.G. Gatti, and G. Goldstein. Coordination between water-transport efficiency and photosynthetic capacity in canopy tree species at different growth irradiances. *Tree physiology*, 28(1):85, 2008.

CIE. Spatial distribution of daylight-CIE standard general sky (CIE ISO15469/CIE S011/E-2003, http://www.cie.co.at). 2003a.

S. Cohen and M. Fuchs. The distribution of leaf area, radiation, photosynthesis and transpiration in a Shamouti orange hedgerow orchard. Part I. Leaf area and radiation. *Agricultural and Forest Meteorology*, 40(2):123–144, 1987.

H. Coners. *Wasseraufnahme und artspezifische hydraulische Eigenschaften der Feinwurzeln von Buche, Eiche und Fichte: In situ-Messungen an Altbäumen.* PhD thesis, Niedersächsische Staats-und Universitätsbibliothek Göttingen, 2001.

R.S. Crosbie, B. Wilson, J.D. Hughes, and C. McCulloch. The upscaling of transpiration from individual trees to areal transpiration in tree belts. *Plant and Soil*, 297(1):223–232, 2007.

TS David, MI Ferreira, JS David, and JS Pereira. Transpiration from a mature Eucalyptus globulus plantation in Portugal during a spring-summer period of progressively higher water deficit. *Oecologia*, 110(2):153–159, 1997.

BE Ewers, R. Oren, KH Johnsen, and JJ Landsberg. Estimating maximum mean canopy stomatal conductance for use in models. *Canadian Journal of Forest Research*, 31(2):198–207, 2001.

FAO. Global forest resources assessment 2005. *FAO Forestry Paper*, 147, 2005.

M. Fontoynont, D. Dumortier, D. Heinemann, A. Hammer, J. Olseth, A. Skartveit, P. Ineichen, C. Reise, J. Page, and L. Roche. Satellight- A WWW server which provides high quality daylight and solar radiation data for Western and Central Europe. In *Conference on Satellite Meteorology and Oceanography, 9 th, Paris, France*, pages 434–437, 1999.

A. Frech, C. Leuschner, M. Hagemeier, and D. Hölscher. Nachbarschaftsbezogene Analyse der Kronenraumbesetzung von Esche, Hainbuche und Winterlinde in einem artenreichen Laubmischwald (Nationalpark Hainich, Thüringen). *Forstwissenschaftliches Centralblatt*, 122(1):22–35, 2003.

T. Früh and W. Kurth. The hydraulic system of trees: Theoretical framework and numerical simulation. *Journal of Theoretical Biology*, 201(4):251–270, 1999.

Q. Gao, P. Zhao, X. Zeng, X. Cai, and W. Shen. A model of stomatal conductance to quantify the relationship between leaf transpiration, microclimate and soil water stress. *Plant, Cell & Environment*, 25(11):1373–1381, 2002.

JP Gastellu-Etchegorry, E. Martin, and F. Gascon. DART: a 3D model for simulating satellite images and studying surface radiation budget. *International Journal of Remote Sensing*, 25(2):73, 2004.

T. Gebauer. *Water turnover in species-rich and species-poor deciduous forests: Xylem sap flow and canopy transpiration.* PhD thesis, Georg-August-Universität Göttingen, 2010.

T. Gebauer, V. Horna, and C. Leuschner. Variability in radial sap flux density patterns and sapwood area among seven co-occurring temperate broad-leaved tree species. *Tree physiology*, 28(12):1821, 2008.

A. Granier. Evaluation of transpiration in a Douglas-fir stand by means of sap flow measurements. *Tree Physiology*, 3(4):309, 1987.

A. Granier and N. Bréda. Modelling canopy conductance and stand transpiration of an oak forest from sap flow measurements. In *Annales des Sciences Forestieres*, volume 53, pages 537–546. edpsciences. org, 1996.

A. Granier, P. Biron, and D. Lemoine. Water balance, transpiration and canopy conductance in two beech stands. *Agricultural and Forest Meteorology*, 100(4): 291–308, 2000.

U. Hansen, B. Fiedler, and B. Rank. Variation of pigment composition and antioxidative systems along the canopy light gradient in a mixed beech/oak forest: a comparative study on deciduous tree species differing in shade tolerance. *Trees-Structure and Function*, 16(4):354–364, 2002.

C. Healy, N.J. Gotelli, and C. Potvin. Partitioning the effects of biodiversity and environmental heterogeneity for productivity and mortality in a tropical tree plantation. *Journal of Ecology*, 96(5):903–913, 2008.

M. Herbst. Stomatal behaviour in a beech canopy: an analysis of Bowen ratio measurements compared with porometer data. *Plant, Cell & Environment*, 18(9): 1010–1018, 1995.

M. Herbst, J.M. Roberts, P.T.W. Rosier, M.E. Taylor, and D.J. Gowing. Edge effects and forest water use: A field study in a mixed deciduous woodland. *Forest Ecology and Management*, 250(3):176–186, 2007.

D. Hölscher, O. Koch, S. Korn, and C. Leuschner. Sap flux of five co-occurring tree species in a temperate broad-leaved forest during seasonal soil drought. *Trees-Structure and Function*, 19(6):628–637, 2005.

F. Hosoi and K. Omasa. Voxel-based 3-D modeling of individual trees for estimating leaf area density using high-resolution portable scanning lidar. *IEEE transactions on geoscience and remote sensing*, 44(12):3610, 2006.

M. Janott, S. Gayler, A. Gessler, M. Javaux, C. Klier, and E. Priesack. A one-dimensional model of water flow in soil-plant systems based on plant architecture. *Plant and Soil*, 341:233–256, 2011.

PG Jarvis. The interpretation of the variations in leaf water potential and stomatal conductance found in canopies in the field. *Philosophical Transactions of the Royal Society of London. Series B, Biological Sciences*, 273(927):593–610, 1976.

PG Jarvis and KG McNaughton. Stomatal control of transpiration: scaling up from leaf to region. *Advances in ecological research*, 15(1):49, 1986.

FM Kelliher, R. Leuning, MR Raupach, and E.D. Schulze. Maximum conductances for evaporation from global vegetation types. *Agricultural and Forest Meteorology*, 73(1-2):1–16, 1995.

DS Kimes. Modeling the directional reflectance from complete homogeneous vegetation canopies with various leaf-orientation distributions. *Journal of the Optical Society of America A*, 1(7):725–737, 1984.

L. Kirwan, J. Connolly, JA Finn, C. Brophy, A. Lüscher, D. Nyfeler, and MT Sebastià. Diversity-interaction modeling: estimating contributions of species identities and interactions to ecosystem function. *Ecology*, 90(8):2032–2038, 2009.

R. Kittler and S. Danda. Determination of sky types from global illuminance. *Lighting Research and Technology*, 32(4):187, 2000.

A. Knohl and D.D. Baldocchi. Effects of diffuse radiation on canopy gas exchange processes in a forest ecosystem. *Journal of Geophysical Research*, 113(G2):G02023, 2008.

A. Knohl, E.D. Schulze, O. Kolle, and N. Buchmann. Large carbon uptake by an unmanaged 250-year-old deciduous forest in Central Germany. *Agricultural and Forest Meteorology*, 118(3-4):151–167, 2003.

P. Köcher, T. Gebauer, V. Horna, and C. Leuschner. Leaf water status and stem xylem flux in relation to soil drought in five temperate broad-leaved tree species with contrasting water use strategies. *Annals of Forest Science*, 66(1):101–101, 2009.

S. Korn. *Experimentelle Untersuchung der Wasseraufnahme und der hydraulischen Eigenschaften des Wurzelsystems von sechs heimischen Baumarten*. PhD thesis, Georg-August-Universität Göttingen, 2004.

BMM Köstner, E.D. Schulze, FM Kelliher, DY Hollinger, JN Byers, JE Hunt, TM McSeveny, R. Meserth, and PL Weir. Transpiration and canopy conductance in a pristine broad-leaved forest of Nothofagus: an analysis of xylem sap flow and eddy correlation measurements. *Oecologia*, 91(3):350–359, 1992.

I. Krämer and D. Hölscher. Rainfall partitioning along a tree diversity gradient in a deciduous old-growth forest in central germany. *Ecohydrology*, 2(1):102–114, 2009.

M. Leuchner, P. Fabian, and H. Werner. Spectral multichannel monitoring of radiation within a mature mixed forest. *Plant Biology*, 7(6):619–627, 2005.

C. Leuschner, H.F. Jungkunst, and S. Fleck. Functional role of forest diversity: pros and cons of synthetic stands and across-site comparisons in established forests. *Basic and Applied Ecology*, 10(1):1–9, 2009.

T. Lohammar, S. Larsson, S. Linder, and SO Falk. FAST: Simulation Models of Gaseous Exchange in Scots Pine. *Ecological Bulletins*, pages 505–523, 1980.

M.M. Loranty, D.S. Mackay, B.E. Ewers, E. Traver, and E.L. Kruger. Competition for light between individual trees lowers reference canopy stomatal conductance: Results from a model. *Journal of Geophysical Research*, 115(G4):G04019, 2010.

H. Mayer, T. Holst, and D. Schindler. Microclimate within beech stands–part I: photosynthetically active radiation. *Forstwissenschaftliches Centralblatt*, 121(6): 301–321, 2002.

N.G. McDowell, S. White, and W.T. Pockman. Transpiration and stomatal conductance across a steep climate gradient in the southern Rocky Mountains. *Ecohydrology*, 1(3):193–204, 2008.

C. Meinen, C. Leuschner, N.T. Ryan, and D. Hertel. No evidence of spatial root system segregation and elevated fine root biomass in multi-species temperate broad-leaved forests. *Trees-Structure and Function*, 23(5):941–950, 2009.

JL Monteith. Evaporation and environment. In *Symp. Soc. Exp. Biol*, volume 19, pages 205–234, 1965.

K. Nadrowski, C. Wirth, and M. Scherer-Lorenzen. Is forest diversity driving ecosystem function and service? *Current Opinion in Environmental Sustainability*, 2(1-2):75–79, 2010.

JE Nash and JV Sutcliffe. River flow forecasting through conceptual models part I–A discussion of principles. *J Hydrol*, 10(3):282–290, 1970.

K. Novick, R. Oren, P. Stoy, J.Y. Juang, M. Siqueira, and G. Katul. The relationship between reference canopy conductance and simplified hydraulic architecture. *Advances in Water Resources*, 32(6):809–819, 2009.

J. J. Oertli. Effect of cavitation on the status of water in plants. In M. Borghetti, J. Grace, and A. Raschi, editors, *Water Transport in Plants Under Climatic Stress*, pages 27–40. Cambridge University Press, Cambridge, UK, 1993.

R. Oren, JS Sperry, GG Katul, DE Pataki, BE Ewers, N. Phillips, and KVR Schäfer. Survey and synthesis of intra-and interspecific variation in stomatal sensitivity to vapour pressure deficit. *Plant, Cell & Environment*, 22(12):1515–1526, 1999.

J. Perttunen, R. Sievänen, and E. Nikinmaa. Assessing the light environment for scots pine in the functional-structural tree model LIGNUM. In *Proceedings of the 5th International Workshop on Functional-Structural Plant Models. Napier, New Zealand*, pages 59–1, 2007.

B. Rewald. *Impact of climate change-induced drought on tree root hydraulic properties and competition belowground.* PhD thesis, Niedersächsische Staats-und Universitätsbibliothek Göttingen, 2008.

L.A. Richards. Capillary conduction of liquids through porous mediums. *Physics*, 1 (5):318–333, 1931.

M. Scherer-Lorenzen, C. Körner, and E.D. Schulze. *Forest diversity and function.* Springer-Verlag Berlin Heidelberg, 2005.

I. Thompson, B. Mackey, S. McNulty, and A. Mosseler. Forest resilience, biodiversity, and climate change. In *A synthesis of the biodiversity/resilience/stability relationship in forest ecosystems. Secretariat of the Convention on Biological Diversity, Montreal. Technical Series*, pages 43–67, 2009.

M.T. Tyree and M.H. Zimmermann. *Xylem structure and the ascent of sap.* Springer Verlag, 2002.

D. Van der Zande, S. Mereu, N. Nadezhdina, J. Cermak, B. Muys, P. Coppin, and F. Manes. 3D upscaling of transpiration from leaf to tree using ground-based LiDAR: Application on a Mediterranean Holm oak (Quercus ilex L.) tree. *Agricultural and Forest Meteorology*, 149(10):1573–1583, 2009.

A.I.J.M. van Dijk and R.J. Keenan. Planted forests and water in perspective. *Forest Ecology and Management*, 251(1-2):1–9, 2007.

M. van Leeuwen and M. Nieuwenhuis. Retrieval of forest structural parameters using lidar remote sensing. *European Journal of Forest Research*, 129:749–770, 2010.

A. Verroust and F. Lazarus. Extracting skeletal curves from 3D scattered data. *The Visual Computer*, 16(1):15–25, 2000.

H. Xu, N. Gossett, and B. Chen. Knowledge and heuristic-based modeling of laser-scanned trees. *ACM Transactions on Graphics (TOG)*, 26(4):19, 2007.

5 The performance of a voxel-based canopy light model based on terrestrial laser scans

Sebastian Bittner, Sebastian Gayler, Christian Biernath, Jana Barbro Winkler, Stefan Seifert, Eckart Priesack

Abstract

The local light regime within the tree canopy is a crucial information for modeling the cycles of water, carbon and nutrients and of the interaction between vegetation and atmosphere. The objective of this study is to test the performance of an approach for the simulation of the light environment in the canopy given by an experimental juvenile beech (*Fagus sylvatica* L.) stand under controlled light conditions in a greenhouse. The model is based on a representation of the canopy as three-dimensional cells (voxels) in combination with a fast ray tracing algorithm that calculates the absorbed fraction of incoming photosynthetically active radiation (PAR). Terrestrial laser scanner data provide the input data for the explicit geometrical representation of the above-ground part of the trees. The simulated light regime of the stand was compared with measurements of the PAR regime inside the canopy (model efficiency $NSE = 0.88$, $RMSE = 124\,\mu mol\,m^{-2}\,s^{-1}$) and at the surface of the soil ($NSE = 0.65$ and a $RMSE$ of $22\,\mu mol\,m^{-2}\,s^{-1}$). The model needs two input parameters, the edge length of the voxels and the light attenuation coefficient of the voxels. A sensitivity analysis of these input parameters shows that best results can be achieved with a medium spatial resolution of the 3D-representation of the canopy at a voxel size of ca. 3 cm. For the calibration of the model only measurements of the fraction of light reaching the soil surface are needed. The good agreement of the simulated light regime with PAR measurements together with the low computational time needed for the ray tracing algorithm suggest that the presented modeling approach may also be applicable to simulate the light regime of natural old-growth forests under variable light conditions.

5.1 Introduction

A good estimation of the local light regime within tree canopies is a crucial information needed in models of the cycles of water, carbon and nutrients in forest ecosystems and of the interaction between the vegetation and the atmosphere. In these models, interception and absorption of light are sensible input variables to simulate functions such as transpiration and photosynthesis. Several models are based on a stand level approach and neglect local inhomogeneity of the canopy like gaps or leaf clusters [Bossel, 1996, Hoffmann, 1995] or include an up-scaling from individual trees to consider light inhomogeneities in a parametric way [Oker-Blom et al., 1989, Larsen

96

et al., 1996]. However, as inhomogeneities can have large effects on the local light regime [Castro and Fetcher, 1999, Whitehead et al., 1990] more advanced models use explicit 3D representations of the canopy.

Explicit geometrical models have approached the representation of the canopy in different levels of complexity. The use of three-dimensional virtual trees generated from growth simulation rules such as L-Systems [Allen et al., 2005, Da Silva et al., 2008, Disney et al., 2006, Roupsard et al., 2008, Lamanda et al., 2008, Sinoquet et al., 2007, Parveaud et al., 2008, Hemmerling et al., 2008] provides information on the position and orientation of leaves and can be used for ray tracing algorithms, for example by using the leaf orientation for the calculation of scattered light. The disadvantage of complex canopy models is the high demand of input data that are often difficult to obtain.

Therefore, some models approximate the shape of the canopy by simple geometrical bodies (such as ellipsoids, frustrums or cylinders [Widlowski et al., 2006, Brunner, 1998, Green et al., 2003, Kobayashi and Iwabuchi, 2008, Courbaud et al., 2003, Gayler et al., 2006]) or hulls [Cescatti, 1997a, Da Silva et al., 2008]. In these models, the leaf area is distributed inside the bodies either constantly or based on physiological observations. The light distribution within the canopy can then be calculated by the radiative transfer equation [Ross, 1981] with the scattering being often neglected leading to a Beer's law of light attenuation [Monsi and Saeki, 1953]. An alternative approach to represent the structure of a canopy in a model is to use a discretization of the space into cubical volume elements, called voxels [Kimes, 1984, Cohen and Fuchs, 1987, Gastellu-Etchegorry et al., 2004, Perttunen et al., 2007, Van der Zande et al., 2009], which are either filled by elements of the vegetation or not. Light attenuation within the canopy can then be calculated by tracing the light rays that penetrate the canopy and applying Beer's law for each filled voxel. By decreasing the size of the voxels a more precise determination of the space occupied by the vegetation can be achieved. But on the other hand the question arises if the originally assumptions leading to the Beer's law of light attenuation are still valid, because the assumption of infinitesimal small phytoelements randomly distributed inside the single voxels does not hold if the voxel size is similar to the leaf size of the plant [Knyazikhin et al., 1997, Myneni et al., 1989, Govaerts and Verstraete, 1998]. In this case, the extinction coefficient of the simple exponential formula of light attenuation cannot be refered to physical or geometrical properties of the vegetation. In this study the light attenuation coefficient can be interpreted as a voxel-based model input parameter

that has to be calibrated to the specific stand.

Due to the improvement of the light detection and ranging (LiDAR) technique in recent years, terrestrial laser scanner (TLS) make it possible to retrieve the structural data of forests in high detail. Moorthy et al. [2008] were able to retrieve the structural parameters leaf area index (LAI), gap fraction and clumping index from laser scans in a laboratory experiment with a tree of similar height as the beeches used in our experiment. Structural parameters such as the total LAI and foliage profile have also been retrieved in natural forest stands using TLS [van Leeuwen and Nieuwenhuis, 2010]. Estimations of the directional canopy gap probability, the probability that a beam will not intercept a canopy element in a given direction, can be retrieved from TLS data and are used as a measure of the spatial light regime [Jupp et al., 2009, Ni-Meister et al., 2008, Danson et al., 2007, Huang and Pretzsch, 2010]. Advances in the interpretation of the TLS data and algorithms for the computing of the retrieved data offer possibilities for applications in functional-structural modeling of the water and nutrient cycle of trees [Van der Zande et al., 2009, Todd et al., 2003, Van der Zande et al., 2010]. Todd et al. [2003] showed that laser scanning is a promising technique for the estimation of light regime by testing the simulations with measurements of PAR at the forest surface of a sugar maple (*Acer saccharum* L.) stand.

The aim of the present study is to evaluate the performance of an modeling approach which is based on a voxel representation of the canopy based on TLS measurements of trees in combination with a fast ray tracing algorithm that calculates the attenuation of incoming photosynthetically active radiation (PAR). In this approach, the space containing the trees is divided into voxels and every voxel, that contains at least one point of the TLS point cloud, is assumed to be part of the canopy. The ray tracing algorithm represents the incoming light rays as lines, which decrease in intensity according to Beer's law every time an occupied voxel is intersected. To evaluate the accuracy of the simulated light regime, we measured the light distribution in a juvenile beech stand (*Fagus sylvatica* L.) under controlled light conditions in a greenhouse and use our model to simulate the special situation of this experimental setup. The deviation between simulated and measured light regime in the stand is assessed by different statistical criteria. In a next step, we analyze the sensitivity of the model with respect to the input parameters of the model, the edge length of the voxels and the light absorption coefficient. Finally, we analyze the computational performance of the model and discuss the question if the model is transferable to

natural adult forests under variable light conditions.

5.2 Material and Methods

5.2.1 Experimental Setup

Experimental beech stand

Nine containers each planted with eight 4-years-old beech trees were set up in a greenhouse in a way that a dense canopy was achieved. The total number of 72 trees occupied a ground area of about $1.25\,m \times 1.45\,m$. The highest tree was $1.07\,m$ high, the mean height of the stand was $0.58\,m$. The stem diameters $5\,cm$ above the ground varied between $3.6\,mm$ and $11.3\,mm$. Subsequent to the TLS measurements (see sec. 5.2.1) the leaves were collected and the total LAI was determined to be 2.5. Measurements of the leaf angle distribution allowed an estimation of the vertical projection of the leaf area per square meter of $2.2\,[m^2 m^{-2}]$.
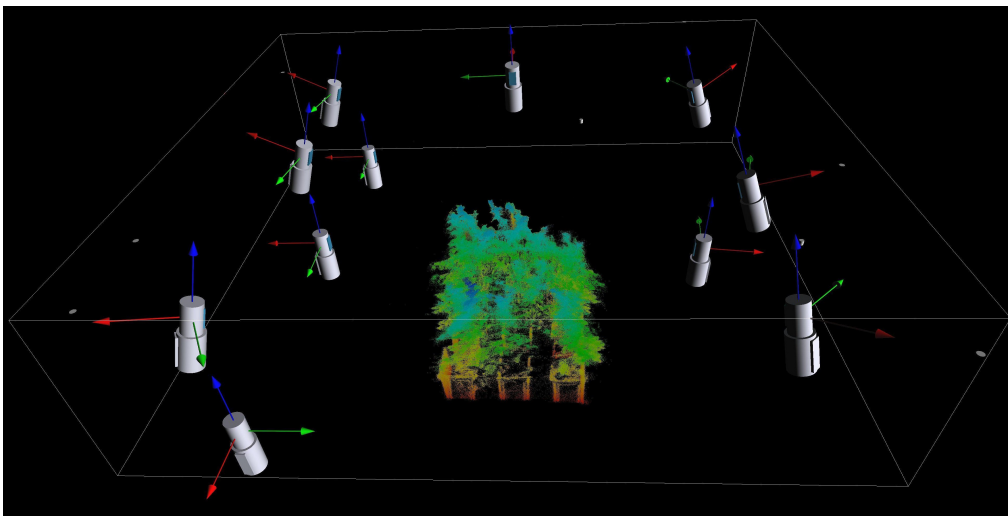

Figure 5.1: Scanner setup to measure the trees. Multiple positions were used to minimize shadow areas.

Lighting and PAR measurements

A grid of nine $400\,W$ metal halide lamps (Osram HQI-TS 400 W/D, Osram GmbH, München, Germany) in combination with projectors (Lightstream Box-type Maxi

721091.784, RZB GmbH, Bamberg, Germany) was installed above the canopy to provide a constant incoming light intensity. The distance of the lamps to the soil surface of the beech stand was $1.35\,m$.

Under these light conditions, PAR was measured using the Li-190 Quantum Sensor (LI-COR Biosciences, Lincoln, Nebr., USA) for measuring light intensity of the electromagnetic spectrum ranging from $400 - 700\,nm$. On the soil surface beneath the canopy we measured the PAR values at $n = 783$ positions on a grid layout with a distance between two measurement positions of $5\,cm$. At a three-dimensional grid layout with $20\,cm$ distance between the measurement points, PAR was also measured at layers at a distance of 0, 20, 40, and 60 cm from the surface of the soil ($n = 224$).

Terrestrial laser scanner setup

To get information about the shape and spatial distribution of leaves and twigs of the sample trees we used a Riegl Z420i terrestrial laser scanner. This scanner has a range measurement standard deviation of 1 cm and a beam divergence of 0.25 mrad. It operates on the principle of time-of-flight measurements, which means it counts the time between sending out a laser impulse and the detection of the returned echo. The scanner is able to scan a panoramic 360° by 80° field with one setup. The angular spacing between two measurements was set to about 0.06° at a resolution of 0.002°, which resulted in an average point distance of 2 mm in 2 m distance. To gather a complete 3D point cloud of the beech group scans where made from 4 positions at ground level and 7 from about 1 m above ground level (Fig. 5.1). The setup positions were distributed around the tree groups to scan from many directions with a distance of approximately 2 to 3 meters to the center of the tree group. The size of the greenhouse and the minimal distance of the laser scanner to the scene did not allow a perfectly symmetric layout of the scan positions. All scan setup positions were referenced in a local coordinate system by using reflectors and reference targets with a positional average standard deviation of less than 4 mm for all coordinate axes. As the scanner is able to detect first or last returning pulse, the first pulse was used to ensure that also small twigs were detected by the scanner. Additional to the distance measurements, photographic images with a digital camera attached to the scanner were made. To be able to simulate the light conditions adequately, the coordinates of the lamps were extracted manually from the laser scans.

5.2.2 Canopy and light model

The canopy model architecture is solely retrieved from TLS measurements using the cloud of three-dimensional points that result from reflections of the laser beam at the surface of the trees. The virtual space is divided into three-dimensional small cubes (voxels) and the canopy was represented by a set of m voxels $V = \{v_1 \ldots v_m\}$ containing at least one point of the TLS reflection points. The number n of the voxels that the space is divided into will further be referred as the resolution of the voxel representation. For reasons of optimizing the memory usage and the computational time (see sec. 5.3.3), the implementation is based on the octree division of space [Wilhelms and Van Gelder, 1992]. The space is represented by a three dimensional cube and is recursively subdivided into eight octants of the same size. The number of voxels equals the number of the smallest cubes that result from the partitioning and is given by

$$n = (2^p)^3, \ p \in \mathbb{N}. \tag{5.1}$$

where p is the number of subdivisions of the space by the octree algorithm.

The octree division of space optimizes the use of memory by dividing the space into voxels of different size. A 3D region that does not contain any biomass is represented by a large cube with one parameter set and regions containing biomass are represented by smaller voxels according to the defined resolution.

The incoming light is represented by line segments R_i each defined by a starting point S_i, an ending point E_i, and a starting intensity I_0^i. The line segments are referred as rays further in this article. Assuming the greenhouse lamps to behave as point light sources, the starting points of the rays are the positions of the lamps. The end points of the rays are the middle of the m voxels the canopy consists of resulting in a total number of $9 \cdot m$ rays. Further the light regime was simulated at the positions of the PAR sensors that could be located at voxels not obtained by the canopy. The starting intensity I_0^i was calculated by setting the position of the lamp into the origin of a coordinate system and then using the solid angle that the voxel i subtended. Further the azimuth and elevation of the ray are used considering a non-homogeneous spatial light distribution of the lamps in combination with the projectors given by the retailer in the EULUMDAT format (RZB GmbH, Bamberg, Germany).

The coupling with the canopy model is done in a first step by the calculation of the set of voxels $A^i = \{a^i_j\}$ with $j \in [1 \dots n_i]$ and $a^i_j \in \{v_1 \dots v_m\}$ that intersect with an arbitrary ray R_i. We applied the Amanatides-Woo algorithm [Amanatides and Woo, 1987] for three dimensions for this step. In a second step the intersection length d^i_j of the ray R_i and every intersected voxel a^i_j is calculated analytically. The attenuation of light can then be calculated at every position in the canopy by using Beer's law

$$I(d) = I^i_o \exp(-k\,d), \tag{5.2}$$

with the incoming light intensity above the canopy $I^i_0\,[\mu mol\,m^{-2}\,s^{-1}]$, the attenuation coefficient $k\,[m^{-1}]$, and the the attenuation length $d\,[m]$ that is the sum of the intersection length of the intersected voxels between the starting point of the ray and the regarded position. Thus, the light intensity $I^i_{j,}\,[\mu mol\,m^{-2}\,s^{-1}]$ after intersecting the voxel a^i_j is given by

$$I^i_j = I^i_o \exp(-k \sum_{c=1}^{j} d^i_c). \tag{5.3}$$

The value for the attenuation coefficient k is kept constant for all voxels in this study. However, the model would be capable of dealing with voxels that are unequaly parametrized allowing a division into sun and shade leaves for example.

We further included an optional first-order isotopic scattering of light on leaves and other plant structures. For every canopy voxel, we use eq. 5.3 to calculate the light that does not transmit the voxel freely and is either absorbed or scattered. The partitioning into absorption and scattering is given by the scattering coefficient. In that way every illuminated voxel acts as a secondary light source in the scattering model. The targets of the secondary light sources are every voxels of the canopy and of the layers that are interesting for the light regime comparison to measurements. The intensity of these secondary light rays are given by the total amount of scattered light by the source multiplied with the solid angle of the target in relation to the voxel scattering the light.

5.2.3 Calibration criteria

Three statistical criteria were used to compare the simulated values of PAR m_i with the n measured values o_i.

Deviations from the measurements are estimated by the root mean square error RMSE in total values $[\mu mol\, m^{-2}\, s^{-1}]$ with

$$RMSE = \sqrt{\frac{1}{n}\sum_{i=1}^{n}(o_i - m_i)^2}. \tag{5.4}$$

The Nash-Sutcliffe efficiency (NSE) is related to the RMSE and defined by Nash and Sutcliffe [1970]

$$NSE = 1 - \frac{\sum_{i=1}^{n}(o_i - m_i)^2}{\sum_{i=1}^{n}(o_i - \bar{o})^2} \tag{5.5}$$

where $\bar{o}$ is the mean value and σ_0 is the standard deviation of the observed values. The NSE values are dimensionless and can take values from $-\infty$ to 1.0. A value of $NSE = 1.0$ is given for a perfect match of simulation and observation, if $NSE \leq 0$, the model is not better than a model that uses the observed mean as a predictor.

The third criterion is the normalized root mean square error. It is given as the ratio of the RMSE to the data range

$$NRMSE = \frac{RMSE}{o_{max} - o_{min}}, \tag{5.6}$$

with o_{max} and o_{min} the largest and lowest observed values.

5.3 Results and Discussion

5.3.1 Measured and simulated PAR

The measured PAR intensities at the surface ranged from 6 to $296\,\mu mol\, m^{-2}\, s^{-1}$. The relative error of the PAR measurements was estimated statistically to be 0.10 and was based primarily on errors of the positioning of the quantum sensor at the grid nodes. Additional errors occurred at positions where the sensor was close to the tree stem, branches or leaves. At these locations small variations of the sensor position of some millimeters lead to sensible variations of the measured value up to 25%. To elicit effects of data noise due to measurement errors, the measured values have been smoothed before the comparison with the simulated values. A

Gaussian kernel was used for the smoothing of the values at the ground according to a Gaussian semivariogram model of the measured data. The data was not smoothed for the three dimensional $20\,cm$ grid, as the distance between two measurement points was too large with respect to the covariation length of the local light regime.
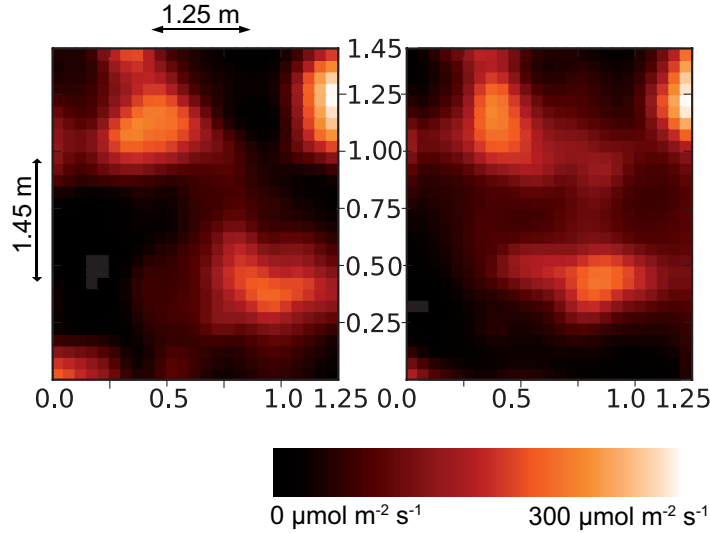

Figure 5.2: Smoothed measured (left) and simulated PAR values at soil surface beneath the canopy of the artificial beech stand.

The voxel ray tracer was able to reproduce the light regime with respect to the position of bright spots and shadowed areas (Fig. 5.2) as well as the total values of light intensity. The attenuation coefficient was calibrated to $k = 2.1\,m^{-1}$. For the 783 measurement points at the soil surface the model performed with $NSE = 0.65$, $RMSE = 22\,\mu mol\,m^{-2}\,s^{-1}$, $NRMSE = 0.11$. Without smoothing the NSE was 0.56. The values at the three-dimensional grid were $NSE = 0.88$, $RMSE = 124\,\mu mol\,m^{-2}\,s^{-1}$, $NRMSE = 0.10$. Separated into the single layers the NSE values were 0.25 for the layer at soil surface, 0.31 for the layer at $20\,cm$ height, 0.50 for the layer at $40\,cm$, and 0.55 for the layer at $60\,cm$. We interpret the values as a good match of the simulation and the measurement, because in addition to the intrinsic simplifications of the voxel ray tracer approach several factors contribute to a deviation of simulation and measurement: *a*) PAR measurement errors occurred as discussed above. *b*) Woody compartments such as stem or branches also contribute points to the laser scan and to the voxel representation of the tree.

The quality of the model could be further increased by separating non-green voxels from leaf voxels to exclude a transmission of light through woody parts. Applying

this correction, Moorthy et al. [2008] were able to improve the estimation of LAI from laser scanned data at an experimental setup.

We also analyzed the influence of first order scattering by keeping the transmissibility of the voxels constant and assume a scattering of the light that does not transmit the voxel freely. First order isotropic scattering increases the simulated light regime at the sensor positions when the transmissibility is kept constant. Using a scattering coefficient of 0.10 [De Pury and Farquhar, 1997] and not changing the value of k the PAR intensity is increased by 4.3% at the surface in comparison with the calculations without scattering. The $RMSE$ is decreased only marginally at all canopy layers even if k was re-calibrated. Because of the minor impact of the isotropic first-order scattering on the modeled light regime as a result of the low PAR scattering coefficient of leaves we conclude that the simulation of the light regime can be simplified by neglecting the scattering of PAR at the voxels. This is in consistence with a study which states that neglecting light scattering is an acceptable simplification for modeling the distribution of PAR within plant canopies. By comparing three different canopy radiation models Wang [2003] concluded that a simple Beer's absorption law can be used to estimate the absorbed visible radiation. However, the situation may be different for old-growth forest stands at days with a high fraction of diffuse sky radiation. It was observed that the relative light intensity below the canopy was higher below the canopy under these conditions because of the effects of scattering. Scattering effects will have a higher impact on the simulated light regime, when wavelengths at near infra-red or ultra-violett are simulated, because their reflection coefficient is higher than the reflection coefficient for PAR [De Pury and Farquhar, 1997].

5.3.2 Sensitivity analysis

The input parameters of the model are the spatial resolution of the scene, given by the total number of voxels n or the edge length $l\,[cm]$ of the voxels, and the light attenuation coefficient $k\,[m^{-1}]$. Fig. 5.3 shows the visualization of the experimental canopy for different resolutions of the voxel space. The sensitivity of the model to the spatial resolution was analyzed by computing NSE between measured and simulated PAR at the soil surface for different values of n (Fig. 5.4).

The model shows an optimum NSE for an edge length of $3.1\,cm$. The decrease for higher l can be explained by an insufficient representation of the canopy by large
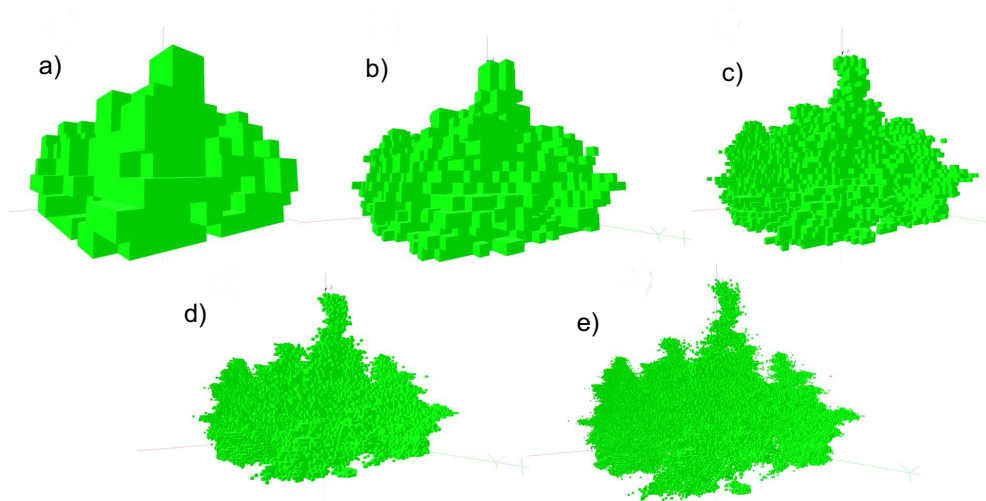
Figure 5.3: Voxel representation of the artificial beech stand with different resolutions (n number of voxels representing the space containing the canopy; l edge length of a single voxel). Visualization with use of the PlantGL framework [Pradal et al., 2009]. a) $n = 16^3$, $l = 12.4cm$ b) $n = 32^3$, $l = 6.2cm$ c) $n = 64^3$, $l = 3.1cm$ d) $n = 128^3$, $l = 1.6cm$ e) $n = 256^3$, $l = 0.8cm$.

voxels. Also for a higher resolution, the model efficiency decreased which is due to the errors of the input data of the laser scanner. Regions inside the canopy were shadowed by outer trees and so the point density was larger in the edge regions of the beech stand, where the shadowing of the laser rays was low. These differences of the point cloud density resulted in a different density of voxels in the model only for high resolutions. For low resolutions with larger voxels, the effect was leveled out, because a voxel was defined to be part of the canopy if at least one point of the laser scan was inside. The total number of laser scanned points lying inside of a voxel was not included in the model and did not effect the absorption coefficient of the voxel. This simple approach may be improved by the possibility of the model to assign every voxel a distinct absorption coefficient that may be correlated to density of laser scanned points lying in that voxel.

An interesting outcome of the sensitivity analysis of the voxel size was the behavior of the model for values of l in the region of the optimal value. The slope of the model efficiency curve was low indicating a robust reaction of the model to changes of l. For values between $0.8\,cm$ and $3.1\,cm$ the model efficiency was larger than 0.4. This behavior is a good indication for the transferability of the light model to further applications in natural and adult forests. Obviously the geometry of the canopy can
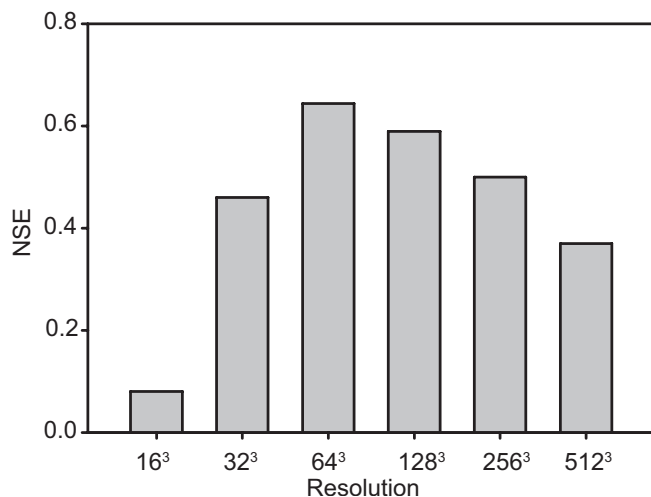
Figure 5.4: Model efficiency (NSE Nash-Sutcliffe efficiency) for the PAR measurements at the soil surface (783 measurement points) for different resolutions of the voxel representation.

be represented adequately if the intrinsic resolution of the TLS data is not exceeded by the voxel size and, on the other side, if l is small enough to represent the canopy structure with respect to leaf clustering and gaps. A more accurate calibration of l to laborious and expensive field measurements that are not easily to obtain may be not necessary.

For the second input parameter, the attenuation coefficient k, the situation is different. We use k as a calibration parameter of the model and do not give a physical or geometrical description for the calculation of k. The values of k are also dependent on the voxel size l. The calibrated values of k were smaller for large voxels. This can be explained geometrically by the space occupation factor of the canopy in voxel space for different resolutions. For applications of the light model, the parameter k has to be calibrated to the fraction of light reaching the forest soil surface or measurements of other variables related to light regime.

5.3.3 Performance

At a resolution of $n = 512^3$ the canopy occupied about $m \approx 10^6$ voxels. For every voxel the incoming direct light originating from the nine lamps was calculating resulting in a total number of $9 \cdot 10^6$ rays. On a single processor machine ($2.3\,Ghz$,

$2\,GB\,RAM$) the computational time was about 4 minutes. At a resolution of $n = 64^3$ the canopy occupied about $3.3 \cdot 10^4$ voxels and the computational time was about two seconds. The algorithm is therefore fast enough to simulate a large amount of incoming rays allowing to simulate a variable light regime in time, where the light source changes and therefore more incoming rays have to be considered to describe the light regime correctly. The change of the sun position during the day or the change of meteorological conditions such as cloudiness are examples for a variable light regime in sky luminance models CIE [2003]. Moreover, a parallelization of the algorithm can be easily achieved because the calculation of the intersection of a ray and the canopy is independent for individual rays. Including a first-order scattering increases the amount of rays to be of $\mathcal{O}(m^2)$ and thus reaching the limit of computational resources when no further simplifications are assumed [Kimes, 1984]. In our simulations of first-order scattering we just simulated the scattered rays that end at sensor positions to compare the simulations with the measurements.

The largest amount of system memory is occupied by the position and parameters of the voxels occupied by the trees. For each voxel information such as the absorbed light intensity and the absorption coefficient have to be stored in memory for a fast computation. A high spatial resolution of the voxel space leads to a high amount of voxels representing the space. The fraction of voxels, that are occupied by a tree to the total amount of voxels representing the scene is low in forest stands as shown in our experimental setup. A typical tree architecture also shows large empty regions with no occupied voxels for example between ground and crown onset or above the canopy. The octree division of space optimizes the use of memory by dividing the space into voxels of different size. A 3D region that does not contain any element of the plant structure is represented by a large cube with one parameter set. Regions containing biomass are represented by smaller voxels according to the defined resolution. Using the octree memory structure, a parametrization is possible for high resolutions that allow to describe old-growth forest trees or stands. The ray tracing algorithm itself could be further optimized by an adaption to non uniform voxels as discussed in Revelles et al. [2000].

5.3.4 Possible application of the model to old-growth forest stands

Our future goal is to apply the model to old-growth single deciduous trees to natural light conditions. For the application to natural large trees several further steps must be included in the model. Firstly the distinction between wood and leave material must be included. This can be done manually [Van der Zande et al., 2006, Huang and Pretzsch, 2010] or automatically if the laser scanner hardware provides additionally the information on the reflectivity of the surfaces that reflect the laser beam. Voxels containing woody material will be parametrized to have no transmissivity, the transmissivity of the leaf voxels can be set on a value that reproduces the mean PAR intensity that reaches the forest floor.

No laborious light measurements are therefore needed to apply the model in the field. The total intensity of incoming PAR can be provided by meteorological observation stations and the spatial distribution in the hemisphere can be calculated using daylight distribution models [CIE, 2003]. In contrast to the greenhouse light conditions the diffuse radiation of the sky will have to be included next to the direct light from the sun. At this, the hemisphere is typically fragmented into some hundred parcels and the light rays start at every parcel. This will increase the number of rays in comparison with the nine direct light sources in the greenhouse but a fast computation on a single processor computer will still be possible.

This study shows that the voxel ray tracing is capable to simulate the PAR distribution in the canopy and the absorption of PAR at every voxel. In functional-structural models of forests this information is important for the calculation of the stomatal conductance of the leaves that depends sensibly on the incoming PAR. Also in photosynthesis calculations the PAR regime is the most important model input. For the estimation of energy fluxes inside the canopy and between vegetation and soil this light model has to be tested and extended to handle the full electromagnetic spectrum of incoming radiation.

5.4 Conclusion

Although the model includes a rather complex representation of the canopy retrieved from TLS data, the approach of the ray tracing algorithm is simply based on

absorption and transmission of radiation. Despite those simplifications the model was able to reproduce the measured regime of the visible spectrum of light of an experimental greenhouse setup of juvenile beeches. It is shown that a voxel ray tracing algorithm is a promising approach to the simulation of PAR environments in tree canopies.

In comparison with other models, that include a detailed geometrical representation of the canopy, the input parameters are easy to retrieve from laser scans of the canopy. A sensitivity analysis showed that the voxel size should be adjusted in a way that the intrinsic resolution of the TLS data are not exceeded and on the other side should be small enough to represent the canopy structure with respect to leaf clustering and gaps. The light absorption coefficient can be calibrated by using non-spatial input data like the mean fraction of incoming light that reaches the forest floor. The absorption constant is attached to every voxel and it is easily possible to include an absorption behavior of the leaves that is variable in space. This allows the distinction of sun leaves and shade leaves, which is often related to different physiology or nutrient status, if measurement values for the parametrization are available.

The advantage of a more complex light model such as used in our approach compared to well known one-dimensional models is given by the the spatial resolution of the light distribution within the canopy. Therefore competition effects of neighboring trees for light or stomatal reactions of single branches and leaves can be simulated in detail by including the spatial heterogenities of the canopy. Performance tests showed that the model is able to deal with variable light input that depends on the time of the day and on meteorological conditions such as clear sky or overcast sky. The algorithm is capable to handle the amount of voxels that is necessary to represent the canopy in a sufficient way. Consequently, the coupling of our approach to a functional-structural tree model that uses the information of the light regime for the estimation of photosynthesis rates and canopy transpiration rates can be directly achieved.

However, as our approach in its present form handles scattering of rays on leaves and other plant structures in a very simple way, the applicability of the model is restricted to PAR simulations. If the model should be used for the simulation of the total spectral intensity of the light including UV and IR, scattering effects have to be analyzed in more detail. The total wavelength spectrum is typically

110

needed for the calculation of the energy balance in a stand as it is required in soil-atmosphere-vegetation transfer (SVAT) models, or for simulating the distribution of UV radiation within a stand, which is the most biological reactant radiation and could have influence to the space occupation of trees.

Acknowledgments

References

MT Allen, P. Prusinkiewicz, and TM DeJong. Using L-systems for modeling source-sink interactions, architecture and physiology of growing trees: the L-PEACH model. *New Phytologist*, 166(3):869–880, 2005.

J. Amanatides and A. Woo. A fast voxel traversal algorithm for ray tracing. In *Eurographics*, volume 87, page 9. Citeseer, 1987.

H. Bossel. TREEDYN3 forest simulation model. *Ecological modelling*, 90(3):187–227, 1996.

A. Brunner. A light model for spatially explicit forest stand models. *Forest Ecology and Management*, 107(1-3):19–46, 1998.

F. Castro and N. Fetcher. The effect of leaf clustering in the interception of light in vegetal canopies: theoretical considerations. *Ecological Modelling*, 116(2-3): 125–134, 1999.

A. Cescatti. Modelling the radiative transfer in discontinuous canopies of asymmetric crowns. I. Model structure and algorithms. *Ecological Modelling*, 101(2-3):263–274, 1997a.

CIE. Spatial distribution of daylight-CIE standard general sky (CIE ISO15469/CIE S011/E-2003, http://www.cie.co.at). 2003.

S. Cohen and M. Fuchs. The distribution of leaf area, radiation, photosynthesis and transpiration in a Shamouti orange hedgerow orchard. Part I. Leaf area and radiation. *Agricultural and Forest Meteorology*, 40(2):123–144, 1987.

B. Courbaud, F. de Coligny, and T. Cordonnier. Simulating radiation distribution in a heterogeneous Norway spruce forest on a slope. *Agricultural and Forest Meteorology*, 116(1-2):1–18, 2003.

D. Da Silva, F. Boudon, C. Godin, and H. Sinoquet. Multiscale Framework for Modeling and Analyzing Light Interception by Trees. *Multiscale Modeling & Simulation*, 7:910, 2008.

F.M. Danson, D. Hetherington, F. Morsdorf, B. Koetz, and B. Allgower. Forest canopy gap fraction from terrestrial laser scanning. *IEEE Geoscience and Remote Sensing Letters*, 4(1):157, 2007.

DGG De Pury and GD Farquhar. Simple scaling of photosynthesis from leaves to canopies without the errors of big-leaf models. *Plant Cell and Environment*, 20(5): 537–557, 1997.

M. Disney, P. Lewis, and P. Saich. 3D modelling of forest canopy structure for remote sensing simulations in the optical and microwave domains. *Remote sensing of environment*, 100(1):114–132, 2006.

JP Gastellu-Etchegorry, E. Martin, and F. Gascon. DART: a 3D model for simulating satellite images and studying surface radiation budget. *International Journal of Remote Sensing*, 25(2):73, 2004.

S. Gayler, TEE Grams, AR Kozovits, JB Winkler, G. Luedemann, and E. Priesack. Analysis of Competition Effects in Mono-and Mixed Cultures of Juvenile Beech and Spruce by Means of the Plant Growth Simulation Model PLATHO. *Plant Biology*, 8(4):503–514, 2006.

Y.M. Govaerts and M.M. Verstraete. Raytran: A Monte Carlo ray-tracing model to compute light scattering in three-dimensional heterogeneous media. *Geoscience and Remote Sensing, IEEE Transactions on*, 36(2):493–505, 1998.

S. Green, K. McNaughton, JN Wunsche, and B. Clothier. Modeling light interception and transpiration of apple tree canopies. *Agronomy Journal*, 95(6):1380, 2003.

R. Hemmerling, O. Kniemeyer, D. Lanwert, W. Kurth, and G. Buck-Sorlin. The rule-based language XL and the modelling environment GroIMP illustrated with simulated tree competition. *Functional plant biology*, 35(10):739–750, 2008.

F. Hoffmann. FAGUS, a model for growth and development of beech. *Ecological modelling*, 83(3):327–348, 1995.

P. Huang and H. Pretzsch. Using terrestrial laser scanner for estimating leaf areas of individual trees in a conifer forest. *Trees-Structure and Function*, accepted, 2010.

D.L.B. Jupp, DS Culvenor, JL Lovell, GJ Newnham, AH Strahler, and CE Woodcock. Estimating forest LAI profiles and structural parameters using a ground-based laser called'Echidna (R). *Tree Physiology*, 29(2):171, 2009.

DS Kimes. Modeling the directional reflectance from complete homogeneous vegetation canopies with various leaf-orientation distributions. *Journal of the Optical Society of America A*, 1(7):725–737, 1984.

Y. Knyazikhin et al. Small-sclae study of three-dimensional distribution of photo-synthetically active radiation in a forest. *Agricultural and Forest Meteorology*, 88 (1-4):215–239, 1997.

H. Kobayashi and H. Iwabuchi. A coupled 1-D atmosphere and 3-D canopy radiative transfer model for canopy reflectance, light environment, and photosynthesis simulation in a heterogeneous landscape. *Remote Sensing of Environment*, 112(1): 173–185, 2008.

N. Lamanda, J. Dauzat, C. Jourdan, P. Martin, and E. Malézieux. Using 3D architectural models to assess light availability and root bulkiness in coconut agroforestry systems. *Agroforestry Systems*, 72(1):63–74, 2008.

D.R. Larsen, J.A. Kershaw, et al. Influence of canopy structure assumptions on pre-dictions from Beer's law. A comparison of deterministic and stochastic simulations. *Agricultural and Forest Meteorology*, 81(1-2):61–77, 1996.

M. Monsi and T. Saeki. Über den Lichtfaktor in den Pflanzengesellschaften und seine Bedeutung für die Stoffproduktion. *Japanese Journal of Botany*, 15:22–52, 1953.

I. Moorthy, J.R. Miller, B. Hu, J. Chen, and Q. Li. Retrieving crown leaf area index from an individual tree using ground-based lidar data. *Can. J. Remote Sensing*, 34(3):320–332, 2008.

RB Myneni, J. Ross, and G. Asrar. A review on the theory of photon transport in leaf canopies. *Agricultural and Forest Meteorology*, 45(1-2):1–153, 1989.

JE Nash and JV Sutcliffe. River flow forecasting through conceptual models part I–A discussion of principles. *Journal of hydrology*, 10(3):282–290, 1970.

W. Ni-Meister, A.H. Strahler, C.E. Woodcock, C.B. Schaaf, D.L.B. Jupp, T. Yao, F. Zhao, and X. Yang. Modeling the hemispherical scanning, below-canopy lidar and vegetation structure characteristics with a geometric-optical and radiative-transfer model. *Can. J. Remote Sensing*, 34(2):S385–S397, 2008.

P. Oker-Blom, T. Pukkala, and T. Kuuluvainen. Relationship between radiation interception and photosynthesis in forest canopies: effect of stand structure and latitude. *Ecological Modelling*, 49(1-2):73–87, 1989.

C.E. Parveaud, J. Chopard, J. Dauzat, B. Courbaud, and D. Auclair. Modelling foliage characteristics in 3D tree crowns: influence on light interception and leaf irradiance. *Trees-Structure and Function*, 22(1):87–104, 2008.

J. Perttunen, R. Sievänen, and E. Nikinmaa. Assessing the light environment for scots pine in the functional-structural tree model LIGNUM. In *Proceedings of the 5th International Workshop on Functional-Structural Plant Models. Napier, New Zealand*, pages 59–1, 2007.

C. Pradal, F. Boudon, C. Nouguier, J. Chopard, and C. Godin. Plantgl: a python-based geometric library for 3d plant modelling at different scales. *Graphical Models*, 71(1):1–21, 2009.

J. Revelles, C. Urena, and M. Lastra. An efficient parametric algorithm for octree traversal. *Journal of WSCG*, 8(2):212–219, 2000.

J. Ross. *The radiation regime and architecture of plant stands*. Dr. W. Junk Publ., 1981.

O. Roupsard, J. Dauzat, Y. Nouvellon, A. Deveau, L. Feintrenie, L. Saint-André, I. Mialet-Serra, S. Braconnier, J.M. Bonnefond, P. Berbigier, et al. Cross-validating Sun-shade and 3D models of light absorption by a tree-crop canopy. *Agricultural and Forest Meteorology*, 148(4):549–564, 2008.

H. Sinoquet, J. Stephan, G. Sonohat, PE Lauri, and P. Monney. Simple equations to estimate light interception by isolated trees from canopy structure features: assessment with three-dimensional digitized apple trees. *New Phytologist*, 175(1): 94–106, 2007.

K.W. Todd, F. Csillag, and P.M. Atkinson. Three-dimensional mapping of light transmittance and foliage distribution using lidar. *Canadian Journal of Remote Sensing*, 29(5):544–555, 2003.

D. Van der Zande, W. Hoet, I. Jonckheere, J. van Aardt, and P. Coppin. Influence of measurement set-up of ground-based LiDAR for derivation of tree structure. *Agricultural and Forest Meteorology*, 141(2-4):147–160, 2006.

D. Van der Zande, S. Mereu, N. Nadezhdina, J. Cermak, B. Muys, P. Coppin, and F. Manes. 3D upscaling of transpiration from leaf to tree using ground-based LiDAR: Application on a Mediterranean Holm oak (Quercus ilex L.) tree. *Agricultural and Forest Meteorology*, 149(10):1573–1583, 2009.

D. Van der Zande, J. Stuckens, W.W. Verstraeten, B. Muys, and P. Coppin. Assessment of Light Environment Variability in Broadleaved Forest Canopies Using Terrestrial Laser Scanning. *Remote Sensing*, 2(6):1564–1574, 2010.

M. van Leeuwen and M. Nieuwenhuis. Retrieval of forest structural parameters using lidar remote sensing. *European Journal of Forest Research*, 129:749–770, 2010.

Y.P. Wang. A comparison of three different canopy radiation models commonly used in plant modelling. *Functional plant biology*, 30(2):143–152, 2003.

D. Whitehead, J.C. Grace, and M.J.S. Godfrey. Architectural distribution of foliage in individual Pinus radiata D. Don crowns and the effects of clumping on radiation interception. *Tree Physiology*, 7(1):135–155, 1990.

J.L. Widlowski, B. Pinty, T. Lavergne, M.M. Verstraete, and N. Gobron. Horizontal radiation transport in 3-D forest canopies at multiple spatial resolutions: Simulated impact on canopy absorption. *Remote sensing of environment*, 103(4):379–397, 2006.

J. Wilhelms and A. Van Gelder. Octrees for faster isosurface generation. *ACM Transactions on Graphics (TOG)*, 11(3):201–227, 1992.

6 Diskussion

Diese Diskussion erörtert drei Fragen. Konnte in den Modellen ein Baumartenunterschied abgebildet und Biodiversitätseffekte festgestellt und generalisiert werden? Sind die entwickelten Einzelbaummodelle geeignet, Wechselwirkungen zwischen Bäumen verschiedener Baumarten abzubilden? Welche Teilmodelle und Datenaufbereitungsalgorithmen benötigen eine weitere Entwicklung? Eine tief gehende Diskussion der Einzelergebnisse sowie eine Übersicht über vorhandene Literatur findet sich in den jeweiligen Unterkapiteln der Kapitel 2-5.

6.1 Modellparametrisierung und Modelltest

Um die Entwicklung und den Test neuer Modellansätze mittels Sensibilitäts- und Ungenauigkeitsanalysen zu überprüfen, werden genaue standortspezifische Messungen von Modelleingangsparametern und Modellzustandsvariablen benötigt. Eine Vielzahl von vorhandenen Studien am Standort Hainich gewährleisten eine hohe Verfügbarkeit von Informationen über den Wasserkreislauf. Insbesondere die Arbeiten der anderen Teilprojekte des DFG Graduiertenkollegs 1086 ermöglichten eine zuverlässige Parametrisierung und Tests der Modelle. Zusätzlich konnten Modelleingangsparameter und Testvariablen aus Feldmessungen und Laborversuchen in dieser Studie selbst ermittelt werden.

Die verfügbaren hydraulischen Messdaten am Standort Hainich umfassten alle drei Teilbereiche des Boden-Pflanze-Atmosphäre Systems. Während sich beobachtende Studien meist auf einen Bereich und oftmals auf die Messung einzelner hydraulischer Baumeigenschaften oder Komponenten des Wasserkreislaufs beschränken, ist es möglich, die Gesamtheit der verfügbaren Informationen in Computermodellen zu integrieren. Die Stärke der nichtlinearen Computermodellierung von Ökosystemen ist die implizite Berücksichtigung von Wechselwirkungen und Rückkopplungen einzelner Teilprozesse des Stoffkreislaufs [Engel and Priesack, 1993, Stenger et al., 1999]. Der Einfluss einzelner Boden- und Baumarteigenschaften kann somit quantifiziert werden und mittels Modellszenarios extrapoliert und bestenfalls generalisiert werden. So wurde in dieser Arbeit das Wissen über Baumartenunterschiede in den hydraulischen Eigenschaften verwendet, um den Einfluss dieser Eigenschaften auf die Bestandestranspiration zu quantifizieren und Baumartendiversitätseffekte auf Bestandesebene aufzudecken. Der simulierte Wasserfluss im Boden als auch innerhalb der Pflanze basiert auf der Beschreibung des nichtlinearen Wasserflusses nach Darcy und auch

der Wasserfluss zwischen den Wurzeln und dem Boden wird mittels physikalischen Modellen beschrieben. Diese physikalische Beschreibung des Boden-Pflanze Systems bietet prinzipiell eine größere Möglichkeit, Simulationsergebnisse zu verallgemeinern und letztendlich das Wissen über Ökosysteme zu erweitern, als eine Beschreibung der Modellprozesse, die auf empirischen Befunden beruht.

6.2 Simulierte Baumartendiversitätseffekte

Messungen stellten signifikante Unterschiede zwischen den Hainichbaumarten in den täglichen Saftflussraten und der Reaktion der Pflanzenwasseraufnahme auf einen geringen Bodenwassergehalt fest [Gebauer et al., 2008]. Die Simulationen der Wasserbilanzen dreier Bestände unterschiedlicher Baumartenzusammensetzung in Kapitel 1 konnten die Auswirkung dieser Unterschiede auf den Wasserkreislauf des Bestandes quantifizieren. Eschen reduzierten unter den beobachteten geringen Bodenwassergehalten im Sommer 2006 ihre tägliche Transpiration im Vergleich zu optimalen Bodenwasserverhältnissen nicht und reduzierten das vorhandene Bodenwasser durch ihre Wasseraufnahme weiter. Es zeigt sich, dass die Anteile der trockenheitsresistenten Baumart Esche und der weniger trockenheitstoleranten Baumarten Linde und Buche die Bestandestranspiration während Trockenphasen am Standort Hainich stark beeinflusst. Der Standort Hainich zeigt geringe jährliche Niederschläge und Phasen mit einem geringen Bodenwassergehalt. Es ist davon auszugehen, dass trockenheitssensible Baumarten wie die Buche, die am Standort Hainich in Jahren mit geringem Niederschlag schon gegenwärtig an ihrem Trockenheitsresistenzlimit sind [Meier and Leuschner, 2008], stark auf eine mögliche zukünftige Veränderung der Niederschlagsmengen und -verteilungen [Bates et al., 2008] reagieren werden.

Die höhere Erschöpfung des Bodenwassers durch Eschen stellt einen Prozess im Modell dar, der den Wasserstress von Buche erhöhen kann, wenn sich Buchen in Nachbarschaft zu Eschen befinden [Rust and Savill, 2000]. Eine Quantifizierung des Trockenstresses der Buche aufgrund der gemeinsamen Bodenwassernutzung mit trockenheitstoleranten Spezies ist mittels eindimensionalen Bestandsmodellen aber nur begrenzt möglich. Um genauer zu untersuchen, ob geringere Bodenwassergehalte der Wurzelzonen der Eschen auch die umliegenden Buchen beeinflussen, ist aber eine mehrdimensionale Beschreibung der lateralen Bodenwasserdynamik und die Einbeziehung der Einzelbaumpositionen nötig.

In Kapitel 3 wurde der Wasserfluss innerhalb 15 Einzelbäumen der drei Spezies *F. sylvatica*, *F. excelsior* und *T. cordata* simuliert. Durch die Integration der Physiologie des Xylems, der Blattstomata und der Feinwurzeln (Tabelle 3.2) konnte der tägliche Verlauf und die täglichen Werte der Transpiration und des Stammsaftflusses simuliert werden. In einem Simulationszeitraum mit hohem Bodenwassergehalten konnten insbesondere Unterschiede im Wasserverbrauch zwischen den diffusporigen Arten (*F. sylvatica, T. cordata*) und der ringporigen *F. excelsior* gezeigt werden. Die täglichen Werte der potentiellen Transpiration, berechnet mit der Grasreferenzverdunstung nach Penman-Monteith [Allen et al., 1998], wurden im Modellansatz in Kapitel 3 durch die stomatäre Reaktion der Blätter auf geringe Wassergehalte des Blattes und des verbundenen Astelements gegebenenfalls verringert. Basierend auf *in situ* Messungen im Hainich wurden hierbei die diffusporigen Arten als am meisten sensibel parametrisiert (Modellparameter St_b: *F. sylvatica* $-2.25\,MPa$, *T. cordata* $-2.25\,MPa$, *F. excelsior* $-3.0\,MPa$). Trotzdem waren alle simulierten tatsächlichen Tageswerte der Transpiration der diffusporigen Bäume nur um wenige Prozent ($<5\%$) gegenüber der potentiellen Transpiration reduziert. Die simulierten tatsächlichen Tageswerte der Transpiration der ringporigen *F. excelsior* waren dagegen an Tagen mit einer hohen potentiellen Transpiration um bis zu $50\,\%$ gegenüber der potentiellen Transpiration reduziert. Der Unterschied konnte auch in den Messwerten des Stammsaftflusses der 15 Bäume beobachtet werden. Die Ursache des hohen Verhältnisses der tatsächlichen zur potentiellen Transpiration der Diffusporer liegt an den höheren Werten des Parameters der hydraulischen axialen Leitfähigkeit der Xylemzylinderelemente. Während Messungen der spezifischen Xylemleitfähigkeit (Leitfähigkeit bezogen auf die Xylemfläche) geringe Unterschiede zwischen den Baumarten zeigte, so unterschieden sich die Ringporer durch einen geringeren Anteil der Xylemfläche an der Gesamtdurchschnittsfläche von nur $15\,\%$. Dieser Anteil des zum Wasserfluss beitragenden Xylems liegt bei den Diffusporern signifikant höher ($70-80\,\%$). Die höheren Leitfähigkeit der Xylemzylinderelemente der Diffusporer führt somit im Modell dazu, dass die laubtragenden Äste ausreichend mit Wasser versorgt werden und die Wasserpotentiale auch an Tagen mit hoher Transpiration keine hohe Reduktion der Transpiration durch stomatäre Reaktion zur Folge haben.

Mischbestände können sich am Standort Hainich in der Bestandsstruktur von stark Reinbeständen der beteiligten Baumarten unterscheiden [Seidel, 2011, Frech et al., 2003]. Der Einfluss der Struktur auf die hydraulischen Eigenschaften wurde in den Kapiteln 3 und 4 untersucht, und es zeigt sich, dass die Tagestranspiration stark von der

Baumgröße und der Architektur bestimmt wird. Der Vergleich zu einer Anwendung des Einzelbaummodells des Baumwasserflusses auf junge Buchen [Janott et al., 2011] zeigt, dass die Xylemwasserspeicherkapazität junger Buchen vernachlässigbar ist, aber in Gegensatz dazu das gespeicherte Xylemwasser der adulten Bäume am Standort Hainich zu ca. 20% der täglichen Transpiration beiträgt. Auch die tägliche Dynamik des Xylemwasserpotentials und die Trockenheitstoleranz unterscheiden sich zwischen jungen und adulten Buchen, da sich in jungen Bäumen die großen negativen Werte des Wasserpotentials aufgrund der geringeren Xylemwasserspeicherkapazität schneller von den Blättern bis zum Wurzelsystem ausweiten. Unterschiedliche Beobachtungen der baumartenspezifischen Xylemwasserspeicherkapazität [Čermák et al., 2007] und der Reaktion auf trockene Bodenverhältnisse kann durch die Berücksichtigung der Struktur im Modell überprüft werden.

6.3 Modellierung von Einzelbaumwechselwirkungen

Bestandsmodelle können die Wechselwirkung der Baumarten abbilden, wenn die Baumarten auf eine gemeinsame Ressource zugreifen, wie beispielsweise das Bodenwasser (Kapitel 2), oder wenn Wechselwirkungsprozesse explizit in den Modellen beispielsweise durch empirische Einflussfaktoren beinhaltet werden. Oftmals lassen sich aber in vergleichenden Studien beobachtete Artenmischungseffekte nicht generalisieren und auf andere Standorte übertragen. Wenn das Ziel der Computermodellierung die Aufdeckung und Analyse von nicht vollständig bekannten Wechselwirkungen ist, so ist eine physikalische Prozessbeschreibung im Modell meist zielführender als empirische Ansätze und oft zudem prinzipiell notwendig. Am Beispiel des Wasserkreislaufs in Wäldern zeigt sich dies an der Simulation der Einzelbaumwechselwirkung aufgrund des Wettbewerbs der Bäume um die natürlichen Ressourcen. Sowohl das Bodenwasser als auch das Sonnenlicht als bestimmende Variable der Transpiration auf Blattebene, erfordern eine Erschließung des Raumes durch die Bäume, da das verfügbare Bodenwasser im der gesamten Wurzelzone verteilt ist und auch das Tageslicht über die Beschattung räumlich inhomogen verteilt ist. Die Position und Geometrie der einzelnen Bäume wird in Bestandesmodellen definitionsgemäß nicht berücksichtigt. Ein Großteil der vorliegenden Arbeit beschreibt die Entwicklung und Anwendung eines Einzelbaummodells, das die Wechselwirkung einzelner Bäume einer Baumgruppe abbilden kann und hierbei detaillierte Informationen der räumlichen Wurzelverteilung und der Baumkrone enthält.

In Kapitel 4 wurde ein Modell der Lichtverteilung in der Krone über die Beschreibung der stomatären Reaktion an das Boden-Pflanze Wasserflussmodell (Kapitel 3) gekoppelt. Der Einsatz eines komplexen Lichtmodells wurde durch die Beobachtungen an Waldrändern [Herbst et al., 2007], Hängen [Mayer et al., 2002] und Baumgürteln [Crosbie et al., 2007] motiviert, in denen signifikante Unterschiede zu geschlossenen Beständen im Wasserverbrauch gemessen und auf die speziellen Lichtsituationen zurückgeführt wurden. Auch am Standort Hainich wurde beobachtet, dass die Kronenstruktur einzelner Bäume von den Nachbarbaumarten abhängt und somit unterschiedliche Lichtverteilungen zu erwarten sind [Frech et al., 2003, Seidel, 2011]. Die Simulationen in Kapitel 4 beschränkten sich aufgrund der vorhandenen Laserscanneraufnahmen auf drei Buchen und konnten einen starken Einfluss des Lichts auf die tägliche Dynamik des Stammsaftflusses zeigen. Die Kopplung des Lichtregimes mit der Geometrie der Bäume im Modell kann die täglichen gemessenen Werte des Stammsaftflusses für alle drei Bäume sehr genau wiedergeben. Das Verhältnis des *root mean square error* zu dem Mittelwert der Messwerte liegt bei 0.07 im Vergleich zu dem Wert von ca. 0.15 bei Verwendung eines Modelles, das die Penman-Monteith Bestandetranspiration anstelle des Lichtmodells verwendet.

Die Annahme eindimensionaler Bodenwasserschichten mit jeweils homogenen Schichtwassergehalten im Modell ist eine Vereinfachung der inhomogenen dreidimensionalen Wasserverteilung im Boden aufgrund der inhomogenen Verteilung des Bestandesniederschlags [Krämer and Hölscher, 2009], der inhomogenen Verteilung der Bodenwasseraufnahme aufgrund der Wurzelausbreitung und den räumlich variablen Bodeneigenschaften [Guckland, 2009]. Insbesondere kann die Untersuchung der Austrocknung des Bodenwassers in Mischbeständen von trockenheitstoleranten und -intoleranten Baumarten mehrdimensionale Bodenmodelle erfordern, wenn die Verteilung Bodenwassererschöpfung und der laterale Bodenwasserfluss berücksichtigt werden sollen. Das Wurzelmodell (Kapitel 3 und 4, Janott et al., 2011) berücksichtigt sowohl die Konnektivität der Wurzelelemente, als auch deren räumliche Position und somit die räumliche Verteilung der Bodenwasseraufnahme. Das Wurzelmodell kann wie in Kapitel 3 und 4 mit einem eindimensionalen Bodenwassermodell gekoppelt werden, aber auch die Kopplung mit einem zwei- oder höher-dimensionalen Bodenwassermodell [Vrugt et al., 2001] ist prinzipiell möglich.

122

6.4 Schlussfolgerung und Ausblick

Der Einsatz von Einzelbaummodellen ermöglicht es, Biodiversitätseffekte im Mischwäldern in Computermodellen zu untersuchen. Die Berücksichtigung der Kronen- und Wurzelstruktur führt zwar zu einer höheren Komplexität der Modelle, die Modellanalysen und Tests in dieser Arbeit konnten aber zeigen, das der Komplexitätsgrad angemessen ist, um Wechselwirkungen der einzelnen Bäume beschreiben zu können. Sensitivitätsanalysen der Eingangsparameter und Unsicherheitsanalysen der Zustandsvariablen konnten zeigen, dass die Modelle zuverlässige Aussagen über den Wasserfluss geben können. Vergleiche mit Messwerten des Stammsaftflusses und des volumetrischen Bodenwassergehalts konnten darlegen, dass die Berücksichtigung der geometrischen Baumstruktur eine signifikante Auswirkung auf die simulierten täglichen Werte und Tageswerte des Stammsaftflusses hat und die Abweichung der simulierten Werte von den Messwerten verringert.

Die Ergebnisse und Modellanalysen der Kapitel 4 und 5 motivieren eine weitere Anwendung des Lichtmodells auf Einzelbäume am Standort Hainich. Die Optimierungen der von den Simulationen benötigten Computerrechenzeit ermöglicht die Berechnung des Lichtregimes und der Transpiration einer großen Anzahl von Bäumen über eine Vegetationsperiode. Auch die Datenaufbereitung der Laserscans geschieht weitgehend softwaregestützt automatisiert und benötigt einen geringen Arbeitsaufwand nach der Laserscanneraufnahme der Bäume. Durch die Analyse weiterer Baumarten neben *F. sylvatica* und einer größeren Anzahl der simulierten Einzelbäume kann im Modell die Auswirkung der Baumartenspezifischen Lichtnutzung und -beschattung untersucht werden. Es kann die Hypothese untersucht werden, ob sich Unterschiede in der Baumkronengeometrie zwischen schattentoleranten Arten und schattenintoleranten Arten [Frech et al., 2003, Seidel, 2011] auch auf die Wassernutzung auswirken.

Wasserstressmodelle beschreiben die Boden-Pflanze Wechselwirkungen oft durch eine explizite, standortabhängige Parametrisierung der Stressbedingungen [Feddes et al., 1978, Li et al., 2001]. Der Vorteil des Boden-Wurzelmodells (Kapitel 3 und 4, Janott et al., 2011) liegt darin, dass der Austausch von Wasser zwischen der Wurzel und dem Boden aus der Differenz des Wasserpotentials des Bodens und des Wurzelxylemwassers und somit durch Modellzustandsvariablen berechnet wird. Hierdurch ist die Reaktion der Wurzelwasseraufnahme auf trockene Bodenwasserverhältnisse im Modell implizit enthalten. Auch sind Kompensationsmechanismen, d.h. die Aufnahme von Wasser vermehrt aus durchwurzelten Bodenschichten, die einen

höheren Wassergehalt haben, in der Modellbeschreibung eingeschlossen. Darüber hinaus kann das Modell die Umverteilung des Bodenwassers mittels der Baumwurzeln von Bodenschichten mit höherem Bodenwassergehalt in Schichten mit einem niedrigeren Bodenwassergehalt abbilden [Janott et al., 2011]. Beobachtungen zeigen, dass dieser Umverteilungsmechanismus in Mischbeständen die Bestandestranspiration stark beeinflussen kann [Domec et al., 2010]. Zum Zeitpunkt der Fertigstellung dieser Arbeit ermöglicht das Einzelbaummodell die Untersuchung des Wasseraustauschs in Trockenperioden. Sofern die Wurzelarchitektur selbst modelliert wird, ist aber eine vorherige genaue Senitivitäts- und Unsicherheitsanalyse der Modellarchitekturparameter zu empfehlen und das Wurzelarchitekturmodel gegebenenfalls an den Untersuchungsstandort anzupassen und zu verbessern [Lynch et al., 1997].

Literaturverzeichnis

R.G. Allen, L.S. Pereira, D. Raes, M. Smith, et al. Crop evapotranspiration-guidelines for computing crop water requirements-fao irrigation and drainage paper 56. *Irrigation and Drainage Paper No. 56. FAO, Rome, Italy*, 300, 1998.

B. Bates, Z.W. Kundzewicz, S. Wu, and J. Palutikof. Climate change and water. In *IPCC Technical Paper VI*. Intergovernmental Panel on Climate Change (IPCC), 2008.

J. Čermák, J. Kučera, W.L. Bauerle, N. Phillips, and T.M. Hinckley. Tree water storage and its diurnal dynamics related to sap flow and changes in stem volume in old-growth douglas-fir trees. *Tree Physiology*, 27(2):181, 2007.

R.S. Crosbie, B. Wilson, J.D. Hughes, and C. McCulloch. The upscaling of transpiration from individual trees to areal transpiration in tree belts. *Plant and Soil*, 297(1):223–232, 2007.

J.-C. Domec, J. S. King, A. Noormets, E. Treasure, M. J. Gavazzi, G. Sun, and S. G. McNulty. Hydraulic redistribution of soil water by roots affects whole-stand evapotranspiration and net ecosystem carbon exchange. *New Phytologist*, 187(1): 171–183, 2010. doi: 10.1111/j.1469-8137.2010.03245.x. URL http://dx.doi.org/10.1111/j.1469-8137.2010.03245.x.

T. Engel and E. Priesack. Expert-N, a building block system of nitrogen models as a resource for advice, research, water management and policy. In *Integrated soil and sediment research: A basis for proper protection*, pages 503–507. Kluwer Academic Publishers, Dodrecht, The Netherlands, 1993.

R.A. Feddes, PJ Kowalik, and H. Zaradny. *Simulation of field water use and crop yield.* Pudoc, Wageningen, 1978.

A. Frech, C. Leuschner, M. Hagemeier, and D. Hölscher. Nachbarschaftsbezogene Analyse der Kronenraumbesetzung von Esche, Hainbuche und Winterlinde in einem artenreichen Laubmischwald (Nationalpark Hainich, Thüringen). *Forstwissenschaftliches Centralblatt*, 122(1):22–35, 2003.

T. Gebauer, V. Horna, and C. Leuschner. Variability in radial sap flux density patterns and sapwood area among seven co-occurring temperate broad-leaved tree species. *Tree physiology*, 28(12):1821, 2008.

A. Guckland. *Nutrient stocks, acidity, processes of N transformation and net uptake of methane in soils of a temperate deciduous forest with different abundance of beech (Fagus sylvatica L.)*. PhD thesis, Georg-August-Universität Göttingen, Göttingen, 2009.

M. Herbst, J.M. Roberts, P.T.W. Rosier, M.E. Taylor, and D.J. Gowing. Edge effects and forest water use: A field study in a mixed deciduous woodland. *Forest Ecology and Management*, 250(3):176–186, 2007.

M. Janott, S. Gayler, A. Gessler, M. Javaux, C. Klier, and E. Priesack. A one-dimensional model of water flow in soil-plant systems based on plant architecture. *Plant and Soil*, 341:233–256, 2011. doi: 10.1016/j.asr.2007.08.007.

I. Krämer and D. Hölscher. Rainfall partitioning along a tree diversity gradient in a deciduous old-growth forest in central germany. *Ecohydrology*, 2(1):102–114, 2009.

KY Li, R. De Jong, and JB Boisvert. An exponential root-water-uptake model with water stress compensation. *Journal of Hydrology*, 252(1-4):189–204, 2001.

J.P. Lynch, K.L. Nielsen, R.D. Davis, and A.G. Jablokow. Simroot: modelling and visualization of root systems. *Plant and Soil*, 188(1):139–151, 1997.

H. Mayer, T. Holst, and D. Schindler. Microclimate within beech stands–part I: photosynthetically active radiation. *Forstwissenschaftliches Centralblatt*, 121(6): 301–321, 2002.

I.C. Meier and C. Leuschner. Belowground drought response of european beech: fine root biomass and carbon partitioning in 14 mature stands across a precipitation gradient. *Global Change Biology*, 14(9):2081–2095, 2008.

S. Rust and PS Savill. The root systems of fraxinus excelsior and fagus sylvatica and their competitive relationships. *Forestry*, 73(5):499, 2000.

D. Seidel. *Terrestrial laser scanning - Appications in forest ecological research*. PhD thesis, Georg-August-Universität Göttingen, Göttingen, 2011.

R. Stenger, E. Priesack, G. Barkle, and C. Sperr. Expert-N, A tool for simulating nitrogen and carbon dynamics in the soil-plant-atmosphere system. In *NZ Land Treatment Collective Proceedings Technical Session 20: Modelling of Land Treatment Systems*, pages 19–28, New Plymouth, New Zealand, 1999.

JA Vrugt, MT Van Wijk, J.W. Hopmans, and J. Simunek. One-, two-, and three-dimensional root water uptake functions for transient modeling. *Water Resources Research*, 37(10):2457–2470, 2001.

Danksagung

Viele Menschen haben mich während meiner Doktorabeit begleitet und ich danke allen sehr herzlich. Besonders möchte ich mich bei Herrn PD Dr. Eckart Priesack für die sehr gute Betreuung bedanken. Ich bin für die vielen guten Ideen, die Freiheiten, die er seinen Mitarbeitern lässt und die gute Arbeitsatmosphäre, die er verbreitet, sehr dankbar. Herrn Professor Munch danke ich für die Betreuung meines Promotionsstudiums. Bei Herrn Professor Beese bedanke ich mich für die gute Betreuung und die Hilfe bei der Erstellung der Veröffentlichungen.

Finanziert wurde diese Arbeit von der Deutschen Forschungsgesellschaft im Rahmen des Graduiertenkollegs 1086. Ich möchte mich bei allen Teilnehmern des Graduiertenkollegs für die gute Zusammenarbeit bedanken. Für die Zusammenarbeit und die Unterstützung der Feldmessungen danke ich sehr herzlich Dirk Böttger, Meik Meißner, Dominik Seidel und Paul Köcher.

Vielen Dank an die Kollegen vom Lehrstuhl für Systemsimulation der Universität Erlangen-Nürnberg für die Kooperation und die Mithilfe bei der Optimierung der Algorithmen, insbesondere an Professor Ulrich Rüde und an Daniel Ritter. Meiner Arbeitsgruppe am Institut für Bodenökologie am Helmholtz Zentrum München danke ich für die gute Arbeitsatmosphäre und die guten Ideen und Inspirationen. Besonders möchte ich mich bei Dr. Sebastian Gayler für die vielen Hilfen und die gute Zusammenarbeit bedanken.

Lebenslauf

Sebastian Bittner

Geburtsdatum: 15.01.1982
Geburtsort: Forchheim
Adresse: Siegfriedstraße 41
                  90461 Nürnberg

Ausbildung

2002   Abitur, Marie-Therese-Gymnasium Erlangen

2002 – 2008   Studium der Physik (Diplom) an der Universität Erlangen-Nürnberg

2008 – 2011   Promotion an der Technischen Universität München, Institut für Bodenökologie